九州大学学術情報リポジトリ
Kyushu University Institutional Repository

EVALUATION OF HYDRAULIC PROPERTIES OF UNSATURATED STRUCTURAL SOILS WITH INNER POROSITY

劉, 士雨

https://doi.org/10.15017/1398339

出版情報：九州大学, 2013, 博士（工学）, 課程博士
バージョン：
権利関係：全文ファイル公表済

KYUSHU UNIVERSITY

EVALUATION OF HYDRAULIC PROPERTIES OF UNSATURATED STRUCTURAL SOILS WITH INNER POROSITY

Shiyu Liu

EVALUATION OF HYDRAULIC PROPERTIES OF UNSATURATED STRUCTURAL SOILS WITH INNER POROSITY

A Thesis Submitted

In Partial Fulfillment of the Requirements

For the Degree of

Doctor of Engineering

By

Shiyu Liu

to the

DEPARTMENT OF CIVIL AND STRUCTURAL ENGINEERING

GRADUATE SCHOOL OF ENGINEERING

KYUSHU UNIVERSITY

Fukuoka, Japan

August, 2013

DEPARTMENT OF CIVIL AND STRUCTURAL ENGINEERING
GRADUATE SCHOOL OF ENGINEERING
KYUSHU UNIVERSITY
Fukuoka, Japan

CERTIFICATE

The undersigned hereby certify that they have read and recommended to the Graduate School of Engineering for the acceptance of this thesis entitled, ‘‘***Evaluation of hydraulic properties of unsaturated structural soils with inner porosity***” by **Shiyu Liu** in partial fulfillment of the requirements for the degree of **Doctor of Engineering**.

Dated: August, 2013

Thesis Supervisor:

_____
Prof. Noriyuki Yasufuku, Dr. Eng.

Examining Committee:

_____
Prof. Guangqi Chen, Dr. Eng.

_____
Prof. Noriaki Hashimoto, Dr. Eng.

_____
Prof. Noriyuki Yasufuku, Dr. Eng.

ACKNOWLEDGEMENT

First and foremost, I would like to express my sincere appreciation to my supervisor, Prof. Noriyuki Yasufuku for his constructive guidance and supervision throughout the whole period of my Ph.D. study.

Secondly, special thanks go to Prof. Guangqi Chen, Prof. Noriaki Hashimoto, Prof. Hamenda Hazarika, Assistant Prof. Ryohei Ishikura, and Associate Prof. Kiyonobu Kasama in Kyushu University, Prof. Kiyoshi Omine in Nagasaki University, Associate Prof. Taizo Kobayashi in Fukushima University, Prof. Xinrong Liu, Prof. Yongxing Zhang, Associate Prof. Zhongping Yang, Associate Prof. Zuliang Zhong and Associate Prof. Peng Li in Chongqing University, Prof. Xinhong Diao in East China Jiaotong University, Associate Prof. Ming Huang in Fuzhou University, Associate Prof. Jin Yu in Huaqiao University. It must not be forgotten that all the tests conducted in this study would not be possible without the technical support of Mr. Michio Nakashima in the Geotechnical Engineering Research Laboratory of Kyushu University. Administrative assistance from Ms. Aki Ito during my research is also greatly appreciated.

I would like to extend my sincere gratitude to my research colleague Dr. Qiang Liu, Dr. Jun Tong, Dr. Kohei Araki, Dr. Manandhar Suman, Mr. Jidong Teng, Ms. Jiali Miao, Mr. Handoko Luky, Mr. Zentaro Furukawa, Mr. Zhenbo Jiang, Mr. Yi He, Mr. Mahmoud Fawzy, Mr. Mohd Khaidir Abu Talib, Mr. Vilayvong, Mr. Shintaro Miyamoto, Mr. Kazuo Kishimoto, Mr. Masafumi Yoshida, Ms. Haruka Kiyotomo, Mr. Atsushi Shinkai, Mr. Keita Murayama, Mr. Fumio Niiya, Mr. Masataka Iwasaki, Mr. Keisuke Aotani, Mr. Hiroyuki Okada, Mr. Kenichirou Okumura, Mr. Satoshi Suenaga, Mr. Guojun Liu as well as many other students in our research group for their kind help both in the research and life. Life would be half as nice without the support and understanding from them over the 3 years.

I would like to extend my grateful acknowledgement to China Scholarship Council (CSC) for providing me the opportunity and scholarship to pursue my Ph.D. at Kyushu University.

Finally, I would like to thank my wife and parents for their continuous encouragement and support in the past years. I appreciate all the things they have done for me.

ABSTRACT

Drylands cover about 41% of Earth's land surface and are home to more than 38% of the total global population of 6.5 billion. Some form of severe land degradation is present on 10 to 20% of these lands, the consequences of which are estimated to affect directly some 250 million people in the developing world, an estimate likely to expand substantially in the face of climate change and population growth. The United Nations has periodically focused on desertification and drylands, notably adopting the Convention to Combat Desertification in 1992 and designating 2006 as the International Year of the Desert and Desertification.

Because of the serious situation of desertification, prevention of the degradation of land becomes key issue. Among existed countermeasures, greening is considered to be one of the most effective methodologies which can protect the biodiversity threaten by desertification. The conventional revegetation practice has had little or no success primarily due to the limited soil moisture. Low and sporadic precipitation that occurs in the arid regions is either not sufficient to support seed germination and plant development or it comes too late for plants or seeds to survive. In the arid regions where the groundwater table is relatively shallow, the groundwater can be used as a main water resource for the plants surviving. However, the water holding capacity and capillary rise of original soils (single-porosity soils) are limited, which leads to water stresses in the root zone. It's one of problems for vegetation restoration to overcome or mitigate desertification. Diatomite and zeolite can be used as soil amendment to retain water and plant nutrients in root zone. The high porosity associated with the inner structure of these materials allows them to retain much water, which can be released slowly during dry periods. A promising method to reestablish plants could be effective to use these materials, which have inner porosity, as a material to wick shallow groundwater to the root zone of the plants. This method could allow for the reestablishment and sustainability of vegetation in arid areas where the groundwater table is shallow but not easily accessible by young plants. In order to evaluate amended effect, the knowledge of hydraulic behavior of original soils and inner

porosity soils is the foundation of seepage analysis in the vadose zone. Although hydraulic properties may be obtained by direct measurements, it is time-consuming, labour intensive and expensive. In this study, alternative theoretical approaches are used to estimate hydraulic properties through the use of more easily measured data. The dissertation made some original contributions as mainly described in Chapeter 3, Chapeter 5 and Chapeter 6.

In Chapter 1, the research background, sets the research objectives and defines the research scope are introduced. The layout of the thesis is also comprehensively presented.

In Chapter 2, the existing studies are reviewed, including the experimental techniques on hydraulic properties and the pore geometry, and the analytical models for hydraulic properties.

In Chapter 3, the physically based scaling technique was extended to the Arya and Paris model (AP model) to predict soil water characteristic curves for single-porosity soils. AP model used to estimate the soil water characteristic curve from particle-size distribution curve. The basis for this approach is mainly on the shape similarity of the two curves. An empirical parameter α was introduced in AP model which used to scale pore attributes from hypothetical formations to natural structures. The parameter α sensitively affect the predicted results. However, original method to calculate α was quite complicated. The scaling technique is used to characterize hydraulic properties of field scale, using measurement scales that are typically much smaller. Kosugi and Hopmans presented an elegant physically based scaling technique which provides convenient way to coalesce multiple soil water characteristic curves into a single reference soil water characteristic curve. In this chapter, the physically based scaling technique was extended to the AP model to calculate parameter α. Comparing with original method, this approach simplifies the calculation process. Experimental soil data which selected from the Unsaturated Soil hydraulic Database are used to verify proposed approach. Results showed that the physically based scaling technique improved the AP model accuracy.

In Chapter 4, the basic properties of the dual-porosity soils used in the laboratory experiments are presented. Four commercial materials are used in this study, two diatomaceous earth pellets and two zeolites. Particle-size distribution, chemical compositions, inner structure and soil water characteristic of materials were investigated and the results were compared with a single-porosity sandy soil. Results show that the shapes of soil water characteristic curves for dual-porosity soils are bimodal. And the water holding capacity of raw diatomaceous earth and zeolites are higher than sandy soil, even though the particle size of these materials is coarser. The results suggest that raw diatomaceous earth and zeolite could be as sand amendments for revegetation in drylands.

In Chapter 5, a bimodal soil water characteristic curve model is proposed for dual-porosity structural soils. In the last decades, several models have been proposed to describe bimodal soil water characteristic curve. Although these approaches were successfully applied to dual-porosity structural soils, they are lack of a physical basis for their parameters due to the fact that the unimodal SWCC functions which they extended were known as empirical equations. To encounter this problem, a bimodal lognormal soil water characteristic curve model has been proposed in this chapter. It was derived by assuming a lognormal pore size distribution for each pore domains and using weighting factors combined individual functions. The proposed model is defined by parameters that have physical significances which can be related to the distribution of pore morphology of the soil. Experimental data fitting and parametric analyses were used to illustrate the fitting capability of the proposed modle. The proposed approach resulted in good agreement between measurement and simulation.

In Chapter 6, a new function is proposed for predicting unsaturated hydraulic conductivity of dual-porosity structural soils. Simulation of flow and contaminant transport through the vadose zone requires knowledge of the soil hydraulic conductivity. Although hydraulic conductivity may be obtained by direct measurements, it is time-consuming, labour intensive and expensive. In this chapter, a new function was proposed for predicting unsaturated hydraulic conductivity of

dual-porosity structural soils based on the bimodal soil water characteristic curve model proposed in Chapter 5. Experimental data verification and parametric analysis are undertaken to demonstrate the fitting and predicting capability of the proposed equations. Results demonstrate that the proposed model improved capability of representations of the hydraulic curves to simulate water flow in structural soils. These functions can potentially be used as an effective tool for identifying hydraulic properties in structural soils.

Finally, a summary of conclusions and recommendations for further research are given in Chapter 7.

TABLE OF CONTENTS

LIST OF FIGURES

LIST OF TABLES

NOTATION

w	gravimetric water content
h	matric suction head
K	hydraulic conductivity
θ	volumetric water content
S_e	effective degree of saturation
u_a	pore-air pressure
u_w	pore-water pressure
ψ	soil suction
ψ_a	matric suction at which air first enters the largest pores of the soil during a drying process
θ_r	residual water content
ψ_r	residual soil suction
ψ_w	matric suction at which the water content of the soil starts to increase significantly during the wetting process
θ_s	saturated water content
a	fitting parameter
n	fitting parameter
m	fitting parameter
e	void ratio
K_s	saturated permeability
$C(\psi)$	correction factor
v	average flow velocity
i	hydraulic gradient
r	pore radius
η	kinematic coefficient of viscosity
C	shape constant of the flow system
g	gravitational acceleration
T_s	surface tension force

P	applied pressure
G_s	specific gravity
ϕ	total soil porosity
S_w	ratio of measured saturated water content to theoretical porosity
ρ_b	soil bulk density
ρ_s	soil particle density
α	empirical parameter
δ_j	scaling factor
λ_j	characteristic length
λ_{ref}	characteristic length of a reference soil
r_m	median pore radius
σ	standard deviation of the pore frequency distribution
h_m	median suction head related to the median pore radius
$S_{e,r}$	reference SWCC function
$\alpha_{potential}$	potential α values
$S_{e,R_{measured}}$	measured reference SWCC function
$S_{e,R_{predicted}}$	alculate the predicted reference SWCC function according potential α value
$\rho_{d,\max}$	maximum dry density
$\rho_{d,\max}$	minimum dry density
$n_{\max}$	maximum total porosity
$g(r)$	pore probability density function for pore radii
$F_n(x)$	complementary normal distribution function
t	dummy variable
ϕ_i	volumetric percentage of the soil components with the *i*th pore series
r_{m_i}	the median pore radius (cm) for the *i*th pore series
σ_i	standard deviation of ln(r) associated with the *i*th pore series
h_{m_i}	median matric head components with the *i*th pore series

R^2	coefficients of determination
K_r	relative hydraulic conductivity
λ	tortuosity parameter
β	tortuosity parameter
γ	pores connectivity parameter

CHAPTER 1

1. INTRODUCTION

1.1 Research background

Drylands cover about 41% of Earth's land surface and are home to more than 38% of the total global population of 6.5 billion (MEA, 2005). Some form of severe land degradation is present on 10 to 20% of these lands, the consequences of which are estimated to affect directly some 250 million people in the developing world, an estimate likely to expand substantially in the face of climate change and population growth. The United Nations has periodically focused on desertification and drylands, notably adopting the Convention to Combat Desertification (CCD) in 1992 and designating 2006 as the International Year of the Desert and Desertification.

As defined by the CCD, desertification is land degradation in arid, semi-arid and dry sub-humid areas resulting from various factors, including climatic variations and human activities. Desertification endangers the livelihoods of rural people in drylands, particularly the poor, who depend on livestock, crops and fuelwood. Conversion of rangelands to croplands without significant new inputs brings about a significant, persistent loss of productivity and biodiversity, accompanied by erosion, nutrient depletion, salinity and water scarcity. In 2000, the average availability of freshwater for each person in drylands was 1300 m^3/year, far below the estimated minimum of 2000 m^3/year needed for human well-being, and it is likely to be further reduced (Millennium Ecosystem Assessment, 2005). Measured by indicators of human well-being and development, dryland developing countries lag far behind the rest of the world. For instance, the average infant mortality rate (54 per thousand) is 23 percent higher than in non-dryland developing countries and 10 times that of

industrialized countries.

The seriousness of the issue is recognized by the CCD, the Convention on Biological Diversity (CBD) and the United Nations Framework Convention on Climate Change (UNFCCC). The New Partnership for Africa's Development also stresses the need to combat desertification as an essential component of poverty-reduction strategies. However, investment and action to combat desertification have been held back by the isolation of drylands from mainstream development, and even by controversy over the use of the term. Debate about desertification has been fuelled by alarming articles in the popular media about "encroaching deserts", reinforced by a series of droughts from the 1960s through the 1980s (Reynolds and Stafford Smith, 2002).

Because of the serious situation of desertification, prevention of the degradation of land becomes key issue. Among existed countermeasures, greening is considered to be one of the most effective methodology which can protect the biodiversity threaten by desertification, minimizing cost and providing positive multifunction. In the application of the methodology, the vegetation is the core. However, in order to fulfill the requirement of the growth of the plants, available water resource is the one of the important limitation. In the most of desertification area, there is usually not enough water resource. Limited precipitation and dew, as water resource are obviously not sufficient for the growth of the plant. Therefore, available water becomes the key limitation to the recovery of ecosystem in such areas. The groundwater can be used as a main water resource for the plants, since it has the advantage of large quantity and relative sustainability. Based on these considerations, the capillarity of water in the soils is considered as one of the possible methodologies. However, sandy soils with big particle size and only have pores between particles (single-porosity) cause low water holding capacities, which leads to water stresses in the root zone. It's one of problem for vegetation restoration to overcome or mitigate desertification. Dual-porosity soils such as diatomaceous earths and zeolites not only have pores between particles also have pores inner particles. These structural soils have been identified as soil amendment materials in high sand content root zones (Waltz et al.

2003). The knowledge of hydraulic behavior of such single- and dual-porosity soils is the foundation of seepage analysis in the root zone.

1.2 Scope and objectives

Simulation of flow and contaminant transport through the vadose zone requires knowledge of the soil hydraulic properties. These properties are the soil water characteristic curve (SWCC) relating the volumetric water content, θ (cm^3cm^{-3}), to the matric head, h (cm), and the hydraulic conductivity curve giving the hydraulic conductivity K (cm/s) as a function of θ or h (Coppola, 2000). Although hydraulic properties may be obtained by direct measurements, it is still time-consuming, labour intensive and expensive. In this study, alternative theoretical approaches used to estimate hydraulic properties through the use of more easily measured data.

The principal objects of the research are

(1) To propose a new model which used to predict the soil water characteristic curve based on the soil basic properties for single-porosity soils.

(2) To investigate the basic properties and hydraulic properties of the dual-porosity soils.

(3) To propose a bimodal soil water characteristic curve model for dual-porosity soils.

(4) To propose a closed-form function used to predict unsaturated hydraulic conductivity for dual-porosity soils.

1.3 Layout of thesis

The structure of this thesis is as follows:

(1) Chapter 1 introduces the research background, sets the research objectives and defines the research scope. The layout of the thesis is also comprehensively presented.

(2) Existing studies are reviewed in Chapter 2, the experimental techniques on hydraulic properties and the pore geometry, and the analytical models for hydraulic properties.

(3) In Chapter 3, developed a soil water characteristic curve model for single-porosity

soils used to predict the soil water characteristic curve based on the particle-size distribution. Experimental soil data that representing wide range of textures are used to verify the proposed model.

(4) In Chapter 4, the basic properties of the dual-porosity soils used in the laboratory experiments are presented. The pore geometry of structural soils has been studied using scanning electron microscopy and mercury intrusion porosimetry. Two methods were used to measure the soil water characteristic curve data of the materials: the Tempe cell method and the centrifuge method.

(5) In Chapter 5, derivation of a bimodal lognormal soil water characteristic curve function for dual-porosity soils based on pore size distribution; and tests of the proposed model using available datasets. Also the measured soil water characteristic curves (presented in Chapter 4) are used to verify the proposed model.

(6) In Chapter 6, a new model was proposed for predicting unsaturated hydraulic conductivity of dual-porosity structural soils based on the bimodal soil water characteristic curve model which has been proposed in Chapter 5. Experimental data verification and parametric analyses were undertaken to demonstrate the fit and predicting capability of the proposed equations.

(7) Conclusions and future work are presented bimodal soil water characteristic curves and corresponding conductivity curves in Chapter 7.

The relationship between chapters is illustrated in Figure 1.1.

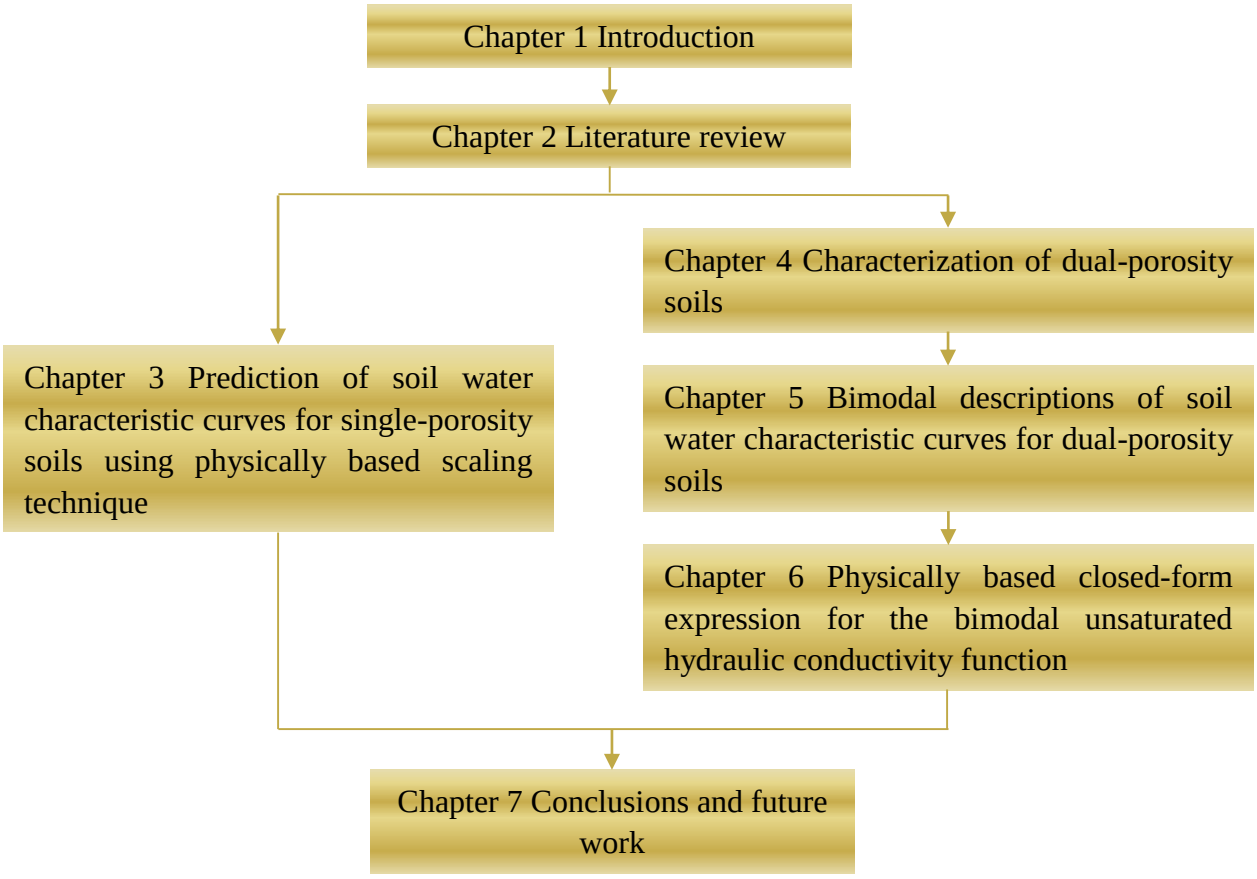

Figure 1.1 Flowchart of the structure of the dissertation

REFERENCES

Coppola, A. 2000 Unimodal and bimodal descriptions of hydraulic properties for aggregated soils. Soil Science Society of America Journal, 64(4), 1252-1262.

MEA, Millennium Ecosystem Assessment—Ecosystems and Human Well-Being: Desertification Synthesis (World Resources Institute, Washington, DC, 2005).

Millennium Ecosystem Assessment 2005 Ecosystems and Human Well-being: Desertification Synthesis. Millennium Ecosystem Assessment World Resources Institute, Island Press, Washington, DC.

Waltz F.C. Jr, Quisenberry V.L. and McCarty L.B. 2003 Physical and hydraulic properties of root zone mixes amended with inorganics for golf putting green. Agronomy Journal, 95(2), 395-404.

Reynolds, J.F. and Stafford Smith, M.D. eds. 2002 Global Desertification - Do Humans Cause Deserts? Dahlem Workshop Report 88. Dahlem University Press, Berlin.

CHAPTER 2

2. LITERATURE REVIEW

2.1 Soil water characteristic curve

2.1.1 Introduction

The water retention ability of soil is usually characterized by soil water characteristic curve (SWCC). SWCC is widely used in geotechnical, geoenvironmental and agricultural engineering. The SWCC is an important soil parameter function required when performing seepage analysis for unsaturated soil systems. The SWCC can be related to some other important soil properties such as the unsaturated permeability function (Fredlund et al., 1994) and the shear strength (Vanapali et al., 1996).

SWCC is defined as the relationship between gravimetric water content w (or volumetric water content θ, or the effective saturation S_e) and suction for the soil (Williams, 1982). There are also many numerous other terms, such as soil moisture content, for characterizing this relationship. The water content defines the amount of water contained within the pores of the soil. In soil science, the volumetric water content, θ, is most commonly used. In geotechnical engineering practice, however, the gravimetric water content w, which is the ratio of the mass of water to the mass of solids, is most commonly used. The effective saturation S_e is another term commonly used to indicate the percentage of the voids which are filled with water. Suction ψ may be either the matric suction (also known as capillary pressure) of the soil (i.e., u_a - u_w, where u_a is the pore-air pressure and u_w is the pore-water pressure) or total suction (i.e., matric plus osmotic suction). As a result of the different terminologies used, the soil-water characteristic curves have taken on numerous forms. Soil water characteristic curves over the entire suction range are often plotted on a logarithmic scale.

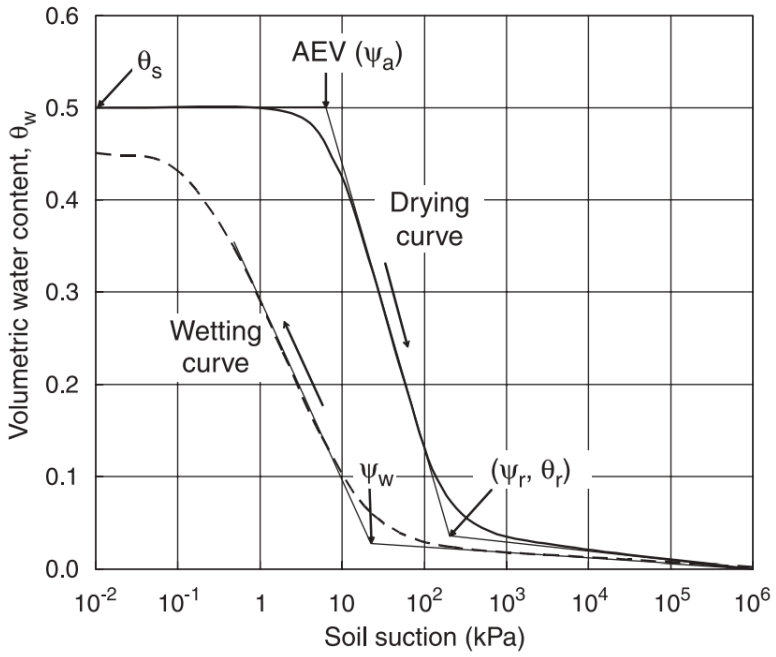

Figure 2.1 Idealized soil water characteristic curve (Yang et al., 2004)

A SWCC describing the desaturation process of soil is termed as a drying curve and a SWCC describing the saturation process of soil is termed as a wetting curve (Fetter, 1993). The resulting SWCCs for the drying path and wetting path exhibit hysteresis. A typical wetting SWCC and drying SWCC is illustrated in Figure. 2.1. The air-entry value (AEV, which is also called bubbling pressure), ψ_a, is defined as the matric suction at which air first enters the largest pores of the soil during a drying process (Brooks and Corey, 1964, 1966). As matric suction is increased from zero to the AEV of the soil, the volume water content, θ, of the soil is nearly constant. As the matric suction increases beyond the AEV, the water content steadily decreases to the residual water content, θ_r. The residual water content is the water content where a large suction change is required to remove additional water from the soil. Under the capillary forces in soil pores created by the surface tension and the adsorption forces on the surfaces of clay particles and in the clay interlayer, water can be retained in soils up to a maximum suction of 1000 MPa (Fredlund and Rahardjo, 1993). It has been experimentally supported for a variety of soils (Croney and Coleman, 1961) and is supported by thermodynamic considerations (Richards, 1965).

Values of ψ_a were generally determined using the tangent method (as shown in Figure.

2.1, as proposed by Brooks and Corey (1964). A consistent way to define the residual water content is also shown in Figure. 2.1. A tangent line is drawn from the inflection point. The curve in the high-suction range can be approximated by another line. The residual water content, θ_r, can be approximated as the ordinate of the point at which the two lines intersect. The soil suction corresponding to the residual water content is called the residual soil suction, ψ_r. The water-entry value, ψ_w, on the wetting SWCC, is defined as the matric suction at which the water content of the soil starts to increase significantly during the wetting process (Yang et al., 2004).

The saturated water content, θ_s, and the air-entry value ψ_a, generally increase with the plasticity or clay content of the soil. Other factors such as stress history, wetting and drying cycle, confining pressure and so on also affect the shape of the soil-water characteristic curves (Fredlund and Xing, 1994).

2.1.2 Hydraulic hysteresis

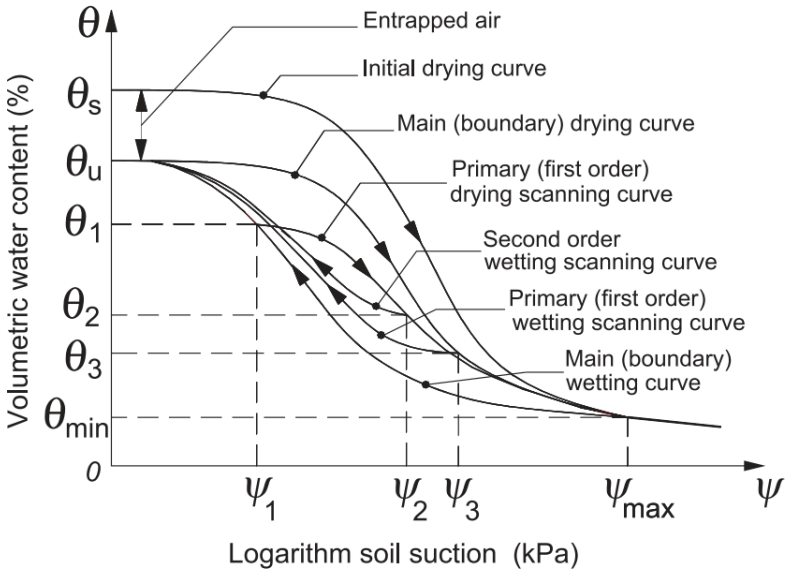

Figure 2.2 Hydraulic hysteresis (Pham et al., 2005)

The drying SWCC and the wetting SWCC are generally different. At a same soil suction, the water content on the drying SWCC is normally greater than on the wetting SWCC. This phenomenon is called hydraulic hysteresis. The main (boundary) wetting and drying curves (as shown in Figure. 2.2) correspond to wetting from a dry condition and drying from a fully saturated condition, respectively. If wetting or

drying commences from any point and follows a previous drying or wetting stage respectively, the new wetting or drying curve lies within the region enclosed by the main (boundary) wetting and drying curves. These new wetting and drying curves are termed as scanning curves. In cycles performed over a given suction range, the form of the final stable hysteresis loop should be independent of whether the first cycle starts on a wetting curve or a drying curve.

Hysteresis has introduced great difficulties in the application of SWCC in unsaturated soil mechanics. Because the occurrence of hydraulic hysteresis means that two samples of the same soil subjected to the same value of suction can be at significantly different values of effective saturation, S_e, if one is on a drying path and another is on a wetting path (or on the scanning curves). Hillel (1998) stated that hydraulic hysteresis may be attributed to several causes:

(1) The geometric non-uniformity of the individual pores (which are generally irregularly shaped voids interconnected by smaller passages), resulting in the 'ink bottle' effect (Haines, 1930).

(2) The contact-angle effect, by which the contact angle and the radius of curvature are greater in the case of an advancing meniscus than in the case of a receding one. Therefore, a given water content will tend to exhibit a larger suction in desorption than in adsorption.

(3) The encapsulation of air in 'blind' or 'dead-end' pores, which further reduces the water content of newly wetted soil. Failure to attain true equilibrium (strictly speaking, not true hysteresis) can accentuate the hysteresis effect.

(4) Swelling, shrinkage or aging phenomena, which result in differential changes of soil structure, depending on the wetting and drying history of the sample.

Pham et al. (2005) reviewed 28 hysteresis models and classified them into two categories: physically based models (domain models) and empirical models. In the domain models, if the behavior of the domain is not a function of the adjacent domains, the domain is said to be "independent". Then the behavior of the particular pore depends only on a range of soil suctions. Therefore, the model is called an

independent domain model. For example, Mualem (1973) developed a fairly successful independent domain model, in which only the primary drying and wetting curves were required, to predict the hysteresis within the primary wetting and drying SWCC curves. Mualem (1974) subsequently modified the model and adopted a new physical interpretation of the independent domain theory. Dependent models, such as Poulovassilis and Childs (1971) and Mualem (1984), can be developed from an independent model and return to independent model by simplification. Pham et al. (2005) pointed out that the Feng and Fredlund (2003) model, which is an empirical model, is the most accurate model for predicting the main (boundary) SWCC and the Mualem (1974) model is the most accurate model for predicting the scanning SWCCs.

Also, the hydraulic hysteresis is related with the soil stress-strain behavior. Wheeler et al. (2003) constructed a model to deal with the coupled hydraulic hysteresis and stress-strain behavior and indicated that the plastic volumetric strains will influence the water retention behavior and may induce the hydraulic hysteresis.

2.1.3 SWCC models

Numerous empirical equations have been proposed to describe the soil water characteristic curve (Table 2.1).

The Burdine (1953) model is a three-parameter model with the relationship fixed between two of the parameters. The parameter, a, is related to the inverse of the air entry value; parameter n is related to the pore size distribution of the soil. Parameter m is assumed to be a function of n, eliminating m as a fitting parameter. The effect of one parameter can be distinguished from the effect of the other parameter, and the model contains only two parameters. Burdine (1953) provides a reasonably accurate representation of data for a variety of soils.

Van Genuchten (1980) improved the Burdine (1953) model further. The van Genuchten (1980) model is more flexible and has been widely used in the engineering practice.

Table 2.1 Soil water characteristic curve models

Model name	Expression	Parameters
Gardner (1922)	$S_e = \frac{\theta - \theta_r}{\theta_s - \theta_r} = \frac{B}{\psi} - D$	B, D = Empirical coefficient
Burdine (1953)	$S_e = 1 \Big/ \left(1 + (a\psi)^n\right)^{1-2/n}$	a, n = Empirical coefficient
Gardner (1956)	$S_e = 1 \Big/ \left(1 + a\psi^n\right)$	a, n = Empirical coefficient
Brooks and Corey (1964)	$S_e = (\psi_a / \psi)^{\lambda}$	λ = pore-size distribution index
Brutsaert (1966)	$S_e = 1 \Big/ \left(1 + (\psi / a)^n\right)$	a, n = Empirical coefficient
Campbell (1974)	$\psi / \psi_a = (\theta / \theta_s)^{-b}$	b = Empirical coefficient
Mualem (1976)	$S_e = \left(1 + (a\psi)^n\right)^{-1+1/n}$	a, n = Empirical coefficient
Van Genuchten (1980)	$S_e = \left(1 + (a\psi)^n\right)^{-m}$	a, n, m = Empirical coefficient
Williams et al. (1983)	$\ln\psi = a + b\ln\theta$	a, b = Empirical coefficient
Mckee and Bumb (1987)	$S_e = \exp(-\psi / b)$	b = Empirical coefficient
Ross and Smettem (1993)	$S_e = (1+\alpha\psi)\exp(-\alpha\psi)$	α= Empirical coefficient
Fredlund and Xing (1994)	$S_e = \left(\ln\left(e + (a\psi)^n\right)\right)^{-m}$	a, n, m = Empirical coefficient
Kosugi (1994)	$S_e = F_n\left[\ln(h / h_m) / \sigma\right]$ $F_n(x) = \frac{1}{\sqrt{2\pi}} \int_x^{\infty} \exp(-t^2 / 2) dt$	$F_n(x)$, the complementary normal distribution function and t is a dummy variable; h_m and σ are the mean and standard deviation of $\ln(h)$.

S_e is the effective saturation; θ is the volumetric water content; ψ (or h) is the matric suction; ψ_a is the air entry value; θ_r is the residual water content; θ_s is the saturated water content.

The van Genuchten (1980) model fits the degree of saturation versus soil suction data over the entire range of soil suction. The equation uses three fitting parameters; namely, a, n and m. Parameter a is related to the inverse of the air entry value; parameter n is related to the pore size distribution of the soil and parameter m is related to the asymmetry of the model. The advantages of the van Genuchten (1980)

model are as follows: it provides a wide range of flexibility, allowing it to better fit data from a variety of soil types; the model parameters have physical meaning; the effect of one soil parameter can be distinguished from the effect of the others. However, the magnitude of the best-fit values of *n* and *m* may vary somewhat depending on the convergence procedure. The van Genuchten (1980) model contains three fitting parameters and this limits the type of correction factors that may be added to the model.

Fredlund and Xing (1994) proposed another widely used SWCC model. The advantages of the Fredlund and Xing (1994) model are as follows: it is continuous over the entire soil suction range; there is great flexibility for the model to fit a wide variety of datasets; the soil parameters are meaningful; the effect of one parameter can be distinguished from the effect of the other two parameters. It has been observed that the Fredlund and Xing (1994) model requires less iteration to converge to the best-fit parameters than the van Genuchten (1980) three-parameter model. Fredlund and Xing (1994) also presented a correction factor for use with their model to ensure that the SWCC goes through 1,000,000 kPa at zero water content.

Brutsaert (1966) studied four models of pore-size distribution, among them the lognormal distribution in relation to SWCCs. A more detailed analysis was presented by Kosugi (1994), who assumed the lognormal pore probability density function for pore radii. The advantages of the Kosugi's equations are defined by parameters that have physical significances which can be related to the properties of the materials.

2.1.4 SWCC measurement techniques

The SWCC measurement techniques can be grouped into at least two categories of methods:

(1) One method is to measure both the water content of a soil specimen and the suction (total suction or matric suction) in the soil specimen, or the humidity around the soil specimen. This method includes the techniques using filter papers (Marinho and Oliveira, 2006), psychrometers (Leong et al., 2003), traditional tensiometers (Fredlund and Rahardjo, 1993), suction probes (i.e., tensiometers for measuring high

soil suctions) (Ridley and Burland, 1996; Take and Bolton, 2003; Cui et al., 2008), and thermal conductivity sensors (Feng and Fredlund, 2003; Nichol et al., 2003).

(2) Another method is to control the suction and measure the water content in the soil specimen. This method includes the axis translation technique (Fredlund and Rahardjo, 1993), the osmotic technique (Delage and Cui, 2008; Monroy et al., 2007), and the humidity control technique (Likos and Lu, 2003). The axis translation technique is the most popular SWCC measurement method because of its accuracy and validity in the most concerned suction range. The traditional axis translation devices always use the air pressure to control the soil suction and show low accuracy in the low suction range. Water head control can help solve this problem in the axis translation technique.

2.1.5 SWCC prediction based on basic soil properties

The measurement of SWCC is time consuming. It would be convenient to estimate the SWCC from basic soil properties, such as the grain-size distribution and void ratio, in engineering practice.

A pedo-transfer function (PTF) (Bouma, 1989) is a function that yields a soil property function based on basic soils properties such as the grain-size distribution or porosity.

For the SWCC, indirect methods are classified into semiphysical and empirical methods (Schaap, 2005). Following an empirical approach, the SWCC is estimated from routinely available taxonomic data (e.g., sand, silt, or clay percentages, organic matter content, and porosity) using empirical pedo-transfer functions (PTFs) (Vereecken, 1988; Weynants et al., 2009).

Semiphysical or conceptual approaches for estimating the SWCC consider the close similarity between the shape of the grain-size distribution function and the SWCC. They do offer valuable conceptual insights into the physical relations between the grain-size distribution and the pore size distribution.

The first attempt to directly translate the grain-size distribution into a SWCC was made in the classical study by Arya and Paris (1981). In their AP model, the pore size is associated with a pore volume and is determined by scaling the pore length. Pore

lengths based on spherical particles are scaled to natural pore lengths using an empirical scaling parameter, α , which should be $\geqslant$1. Arya and Paris (1981) initially determined that α ranged between 1.31 and 1.43 for dif erent soils, with an average value of 1.38, but later it was found that α varied between 1.02 and 2.97 (Arya et al., 1982; Schuh et al., 1988; Mishra et al., 1989). Many investigators have suggested that predictions of the SWCC would improve if α were formulated such that it would vary across the range of particle sizes (Basile and D'Urso, 1997; Arya et al., 1999; Vaz et al., 2005). Fractal concepts have also been used to derive α (Tyler and Wheatcraft, 1989). However, the calculation procedures of these approaches are quite complicated or without paying much attention to the physical significance of the soil properties.

2.2 Unsaturated permeability function

2.2.1 Introduction

The unsaturated soil coefficient of permeability function (commonly referred to as permeability function) is the primary soil parameter required when performing seepage analysis for unsaturated soil systems. Examples of engineering applications where a permeability function is involving include the triggering of landslides due to rainfall infiltration, and the modeling of flow and volume change in collapsing soils, compacted soils and expansive clays. The permeability functions are also required when modeling contaminant migration in vadose zones and in the design of capillary barriers and cover systems.

Usually, the coefficient of permeability of a saturated soil is looked as a function of void ratio. The coefficient of permeability of an unsaturated soil (i.e. K) is a function of both void ratio e and the effective saturation, S_e (or the volumetric water content, θ). The unsaturated permeability can be expressed as a function of any two of the three parameters which are interrelated,

$$K = f(S_e, e);\ K = f(e, \theta);\ K = f(S_e, \theta) \tag{2-1}$$

If the soil structure is assumed to be incompressible, the saturated permeability, k_s, will quantify the effect of void ratio, and another function will account for the effect of volumetric water content (or the effective saturation) in the soil. The unsaturated

permeability function can be expressed as,

$$K = K_s f(\theta) \quad \text{or} \quad K = K_s f(S_e) \tag{2-2}$$

The suction and volumetric water content are related to the SWCC, so the permeability function can also be expressed as a function of suction (ψ), which is more frequently used in practices:

$$K = K_s f(\psi) \tag{2-3}$$

Estimation of unsaturated soil hydraulic conductivity becomes very important (Mualem, 1986). On one hand, researchers have conducted experiments using steady state method (Fleureau and Taibi, 1995) as well as transient methods. These studies reveal that most field and laboratory methods of determining the unsaturated soil hydraulic conductivity are either time consuming, tedious, or have other logistical difficulties. It is desirable to develop a direct method for the measurement of the permeability function that is time-saving and applicable to a wide range of coefficients of permeability and soil suctions. On the other hand, estimation procedures are generally resorted to where the soil unsaturated permeability can be estimated from the moisture retention curves or the soil-water characteristic curves (Fredlund and Xing, 1994; Fredlund et al., 1994). There are numerous permeability functions available for unsaturated soils.

2.2.2 Measurements of unsaturated coefficient of permeability

There are three main methods in the literature for the measurement of unsaturated permeability function in the laboratory or in situ; namely, the steady-state method, the instantaneous profile method, and the parameter estimation method.

1) Steady-state method

A number of researchers have measured the water and air coefficients of permeability of unsaturated soils by the steady-state method using permeameter devices (Klute, 1965; Fleureau and Taibi, 1995; Samingan et al., 2003). The steady-state method is performed by applying constant boundary conditions to a soil specimen. The coefficient of permeability, *K*, corresponding to the applied matric suction is

computed after the steady-state conditions are achieved (i.e., the hydraulic gradient, the flow rate, and the soil suction reach constant values).

The steady state method is the most accurate for the determination of the coefficient of permeability following Darcy's law (Benson and Gribb, 1997). But the steady state method has some limitations. Normally a high air-entry ceramic disk is used in the steady-state method for controlling soil suction. The use of a high air-entry ceramic disk induces two limitations. First, the soil suction will be limited by the air entry value of the ceramic disk. Second, the measured permeability of the soil must be much smaller than the saturated permeability of the ceramic disk.

In addition to the limitations induced by a ceramic disk, several other difficulties are also associated with this method (Klute, 1965; Olson and Daniel, 1981):

(1) The low coefficient of permeability of unsaturated soils, particularly at high matric suctions. It induces an extremely low flow rate and a long equilibrium time. The low flow rates necessitate extremely accurate water volume measurements, which demand the careful consideration of air diffusion through the water and water loss from the apparatus.

(2) Osmotic effect. The osmotic suction gradient may develop between the pore-water within the soil and pure water in some cases. This will induce flow across the specimen, in addition to the bulk flow related to the hydraulic head gradient, which may increase significantly as the water content of the soil decreases.

(3) Contact between the soil specimen and the permeameter. If the soil specimen shrinks during the measurement process and separates from the high air entry ceramic plates, the air gap between the soil and the high air entry ceramic plates will stop the seepage of water since air is nonconductive to the flow of water. It is important to maintain good contact between the soil and the porous plates by a loading method.

2) Parameter estimation method

The parameter estimation method is an indirect approach for estimating the parameters describing a specific permeability function based on the results from transient or steady-state flow data (Kool and Parker, 1987). To obtain the permeability

function via the indirect parameter estimation method, a flow event is modeled using the appropriate governing equation (e.g., Brooks and Corey equation, 1964) and sometimes also a prescribed analytical expression for the soil-water characteristic curve. In this technique, soil mechanics formulations using pore-water pressure rather than soil suction are preferred as explained by Fredlund and Rahardjo (1993). The unknown parameters for the permeability function are then obtained by minimizing an objective function that describes the differences between measured flow variables and the variables simulated with the numerical flow code. Limited experiment data are needed to calculate the permeability function parameters when using this technique. Once the parameters are decided, the permeability function is extended to a wider suction range.

Advantages of this method include time saving and greater flexibility in the design of experiments since no specific boundary and initial conditions are required. The main disadvantage of the method appears to be associated with its dependency on the selected model for the permeability function. In addition, there is limited understanding of the reliability of the computed permeability function when it is extended to a wider suction range.

The parameter estimation method has been applied to the laboratory one-step procedure (Wildenschild et al., 1997) and the multi-step outflow procedure (Eching et al., 1994; van Dam et al., 1994; Caron and Elrick, 2005). The parameter estimation method has also been used with data obtained using an evaporation method (Brandyk et al., 2003) as well as an internal drainage method (Hillel et al., 1972). The method has also been applied to the field determination of permeability function using a pond-infiltration procedure (Bohne et al., 1993), the tension disk infiltrometer flow procedure, and a cone penetrometer-based procedure (Gribb et al., 1998).

3) Instantaneous profile method

The instantaneous profile method is an unsteady-state method that can be used either in laboratory or in situ for unsaturated permeability measurement. The instantaneous profile method seems to be first described by Richards and Weeks (1953) and has

been refined by many investigators (e.g. Hamilton et al., 1981; Daniel, 1983).

This method uses a cylindrical specimen of soil that is subjected to a continuous water flow from one end of the specimen. The water content and suction distributions along the column can be monitored over time. Sometimes both of them are monitored, sometimes only one of them is monitored and another one is inferred from the SWCC. In the instantaneous profile test, the flow rate is controlled for obtaining the gradual suction profiles versus water content profiles at various times. The water content and suction distributions along the specimen can be monitored over time. The total water flow volume passing one section can be calculated by the water storage change inside the soil specimen. The hydraulic gradient can be calculated using the measured soil suctions at different sections. The average coefficient of permeability is calculated based on the total flow volume passing through a section in a unit time under the measured hydraulic gradient. The instantaneous profile method is an unsteady-state method that can be used either in the laboratory or in situ. It is perhaps the only available experimental method for directly measuring unsaturated permeability function over a wide range of soil suctions. This method, however, has several disadvantages; namely,

(1) The method is time consuming and commonly takes several months to conduct an instantaneous profile test.

(2) A proper flow rate for soil wetting is difficult to choose. If the flow rate is too high the gradually changing suction versus water content change profiles cannot be discerned.

(3) The accuracy of the test is related to the space between water content versus suction monitoring points. Theoretically, the closer the water content and suction sensors are the more accurate is the calculated unsaturated permeability function. However, the use of too many sensors may cause soil disturbance and affects the water infiltration process.

2.2.3 Unsaturated hydraulic conductivity models

In general, the various permeability functions can be categorized into two groups:

empirical models and statistical models.

1) Empirical equations

Examples from the literature of various empirical forms for the permeability function are given in Table 2.2. The constants describing these permeability functions can be obtained by fitting the experimental data.

Table 2.2 Different models for characterizing permeability functions

Form of equation	Reference
Coefficient of permeability as a function of volumetric water content	
$K = a\theta^b$	Gardner (1956)
$K = K_s\left(\frac{\theta}{\theta_s}\right)^{2b+3}$ and $b = \frac{\Delta \log \psi}{\Delta \log \theta}$	Hillel (1998)
$K = K_s \exp(b(\theta - \theta_r))$	Dane and Klute (1977)
Coefficient of permeability as a function of matric suction	
$K = a + b\psi$	Richards (1931)
$K = a\psi^{-b}$	Weeks and Richards (1967)
$K = K_s \Big/ \left[1 + a\left(\frac{\psi}{\rho_w g}\right)^b\right]$	Arbhabhirama and Kridakorn (1968)

a, *b* are constants; *K* is the unsaturated permeability; K_s is the saturated permeability; ψ is the matric suction; θ is the volumetric water content; θ_r is the residual volumetric water content.

Because the permeability function has a similar shape with the SWCC, let us suggest a general relationship between the permeability function as,

$$K = K_s S_e^{\ p} \tag{2-4}$$

where *K* is unsaturated permeability; K_s is the saturated permeability; S_e is the effective saturation, equal to $(\theta-\theta_r)/(\theta_s-\theta_r)$; *p* is a constant, which depends on the soil type. Leong and Rahardjo (1997) made a critical evaluation of the relationships between S_e and ψ and showed that the following equation suggested by Fredlund and Xing (1994) is robust:

$$S_e = \frac{C(\psi)}{\left\{\ln\left[e + \left(\frac{\psi}{a}\right)^b\right]\right\}^c} \tag{2-5}$$

where a is a constant, which has the same unit as suction; b, c are constants; $C(\psi)$ is a correction factor, recommended as 1.

2) Statistic models

In statistic models the coefficient of permeability function is derived from the SWCC. These models are based on three assumptions (Mualem, 1986):

(1) The porous medium consists of a set of randomly distributed interconnected pores characterized by a pore radius r and its statistical distribution, $f(r)$.

(2) The Hagen-Poiseuille equation is valid, which is expressed as,

$$v = -\left(\frac{r^2 g}{C\eta}\right) i \tag{2-7}$$

where v is the average flow velocity; i is the hydraulic gradient; r is the pore radius; η is the kinematic coefficient of viscosity; C is the shape constant of the flow system; g is the gravitational acceleration.

(3) The SWCC is considered analogous to the pore-size distribution function using Kelvin's capillary law.

Childs and Collis-Gorge (1950) investigated the influence of the random connection of pores on the coefficient of permeability. The pores on two imaginary faces are assumed to be randomly connected by a series of capillaries. The probability of larger pores of radius r connected to smaller pores of radius ρ is given by,

$$prob(r, \rho) = f(r) f(\rho) \tag{2-8}$$

where $f(r)$ is the probability of pores with a radius r; $f(\rho)$ is the probability of pores with a radius ρ. Two other assumptions were made: first, the effective resistance to flow in the pore sequence is confined by the smaller pores; second, the only contribution to permeability is by a direct pore sequence so the possibilities of by-passing sequences of pores are ignored. Then the discharge flow dq through the tunnel by a pair of r and ρ is

$$dq = Mf(r)f(\rho)\rho^2 i \tag{2-9}$$

where M is a constant accounting for geometry and fluid properties. By integrating the equation over all the filled pores and applying Darcy's law, the permeability is expressed as,

$$K(\theta) = M\left[\int_{\rho=R_{\min}}^{\rho=R(\theta)}\int_{r=\rho}^{r=R(\theta)}\rho^2 f(\rho)f(r)drd\rho\right] + M\left[\int_{\rho=R_{\min}}^{\rho=R(\theta)}\int_{r=R_{\min}}^{r=\rho} r^2 f(\rho)f(r)drd\rho\right] \tag{2-10}$$

The closed form solution of eq. 2-10 is not readily obtained in reality.

Burdine (1953) and Mualem (1974, 1976) proposed approaches for unsaturated hydraulic conductivity. A generalized form of the model for predicting the relative hydraulic conductivity K_r from SWCC is written as (Hoffmann-Riem *et al*., 1999):

$$K_r = K / K_s = S_e^{\lambda}\left(\int_0^{S_e}\frac{dS_e}{h^{\beta}} \Big/ \int_0^1 \frac{dS_e}{h^{\beta}}\right)^{\gamma} \tag{2-11}$$

where K_s and K are the saturated and unsaturated hydraulic conductivities (cms^{-1}), respectively. The parameters λ, β as tortuosities and pores connectivity for γ (subject to $\lambda \geqslant 0$, $\beta > 0$, and $\gamma > 1$). The computed coefficient of permeability from this statistical model showed good agreement with the measured coefficient of permeability (van Genuchten, 1980; Fredlund et al., 1994). It is also a common practice to carry out the summation from the lower limit, which is the lowest volumetric water content of the SWCC, to the upper limit.

2.2.4 Pedo-transfer functions of unsaturated permeability

Parametric PTFs that predict the parameters of closed form analytical expressions of SWCC and permeability function, such as the equations proposed by Brooks and Corey (1964) or van Genuchten (1980) (referring to Table 2.1) have the greatest ability to be used in mechanistic water flow models.

Pore size is also used to predict the hydraulic conductivity of soils recently. Kosugi (1999) developed combined soil water retention-hydraulic conductivity model for

soils with a lognormal pore-size distribution based on the Mualem-Dagan pore-size model. Xu and Sun (2002) derived an unsaturated permeability function from a fractal model of pore-size distribution, in which the fractal dimension is obtained from porosimetric measurements.

Recently, investigators have tried to incorporate new descriptors into PTFs, such as soil structural information (Lin et al., 1999) or terrain attributes (Romano and Palladino, 2002). For example, Lin et al. (1999) developed a point scale system for quantifying soil morphology; the approach permitted the determination of interrelationships among different morphological features. Practical applications confirmed that soil structure is crucial in characterizing hydraulic behavior in macro-pore flow region, whereas texture has a major impact on the hydraulic properties controlled by micro-pores. Romano and Palladino (2002) proposed an approach for including terrain attributes by accounting for certain landscape variables, such as slope (i.e. $\tan\beta$, where β is the slope angle) and aspect (i.e. $\cos\varphi$, where φ is the angle clockwise from north) etc.

More empirical models have been obtained by solving various mathematical methods. Until recently, most PTFs were derived through multiple regression methods (Wosten et al., 1990, 2001; Rawls and Brakensiek, 1985), but the artificial neural networks approach (e.g., Pachepsky et al., 1996; Minasny et al., 1999, 2004; Minasny and McBratney, 2002) is becoming more and more popular; performances equivalent or superior to PTFs derived by regression-type methods have been also reported (Minasny et al., 1999; Nemes et al., 2003).

2.3 Pore geometry

2.3.1 Introduction to pore geometry

Soil fabric is of great importance in geotechnical, geo-environmental and agricultural engineering as this property influences many soil characteristics, such as compressibility, hydraulic conductivity, soil water characteristics, frost and heave problem, and stress state variables of soils, especially for unsaturated soils. Soil micro-porosity structure is difficult to measure and is highly variable for a single soil

type. Micro-porosity structure changes with stress state, water actions, temperature fluctuations, long-term gravimetric actions, and weathering.

2.3.2 Experimental techniques for studying pore geometry

Normally, scanning electron microscopy (SEM) (Collins and McGrown, 1974) and optical microscope (Cousin et al., 2005) are used to study the soil fabric qualitatively. Based on the photographs from the optical microscope test and the backscattered electron scanning images from the SEM, the soil surface macro-micro fabric can be recognized.

The nitrogen adsorption (Prost et al., 1998) and mercury intrusion porosimetry (MIP) (Cuisinier and Laloui, 2004) can characterize the soil fabric quantitatively by measuring a pore size distribution curve. The pore-size distribution (PSD) has often been advanced as a parameter function to help interpret geotechnical behaviors. It has been correlated with saturated hydraulic conductivity and frost heave, and prediction of soil deformation and SWCCs prediction (Prapaharan et al., 1985).

1) Dehydration method

The sample should be dehydrated before being taken for testing for pore geometry. Normally, the soil sample can be dehydrated by air-drying, oven-drying, freeze-drying and critical-point-drying techniques (Fratesi et al., 2004). Oven drying and air-drying should be avoided because of the shrinkage phenomena which will alter the original microstructure, especially for clay (Delage and Lefebvre, 1984). As recommend by many researchers, the freeze-drying method is the least disturbing dehydration technique (Gillott, 1973). But the results by freeze-drying technique are less reproducible than that by the oven-drying method (Penumadu and Dean, 2000).

In the freeze-drying technique, the soil sample was quickly frozen with liquid nitrogen and then placed in a commercially available freeze-drier for approximately one day for the sublimation of water. The freeze-drying technique is based on the assumption that during rapid freezing of a soil using liquid nitrogen, the water in the soil does not have enough time to recrystallize. Therefore, the water passes directly to the solid state. The transition from liquid to a solid is not accompanied by a linear

expansion of the phase being formed and consequently does not cause deformation to the specimen (Penumadu and Dean 2000). After freezing, the specimen is placed in a freezing unit with a vacuum chamber and dried by sublimation of the frozen water at a low temperature (e.g., lower than -20 ℃). The freeze-drying technique appears to be the most appropriate method for dehydrating soil samples for use in microscopy and mercury intrusion testing (Penumadu and Dean, 2000).

2) Measurements of PSD by MIP

MIP tests are routinely and effectively used to evaluate the PSDs of powder and bulk materials with open and interconnected pore structures. MIP tests allow the measurement of pore radii ranging from a few nanometers up to several tens of micrometers. This wide range allows the identification of different soil pore classes along the PSD curve. MIP is based on the principle that a non-wetting fluid such as mercury does not enter a porous medium unless a sufficient pressure is applied. During the MIP test, a dehydrated sample is initially surrounded with mercury at a specific low pressure. Then the mercury pressure is increased step by step until it reaches the capacity of the system. The volume of mercury that intrudes into the pores is measured for each pressure increment.

An assumption is made that cylindrical flow channels exist in the soil with a radius, r, and the pores which are intruded by mercury under an applied pressure, P, can be calculated using Jurin's equation:

$$r = \frac{2T_s \cos\alpha}{P} \tag{2-12}$$

where r is the entrance pore radius; T_s is the surface tension force of the liquid; The surface tension of mercury, T_s , is 472 μN/m^2 at 20 ℃; α is the contact angle of fluid (the wetting phase)-air interface to solid (non-wetting phase).

Then, the intrusion mercury volume when the pressure increases from P_1 to P_2 reflects the volume of pores with diameters from ($2T_s cos\alpha/P_1$) to ($2T_s cos\alpha/P_2$).

The cumulative injected mercury volume indicates the cumulative pore volume. The mercury intrusion pressure indicates the pore radius according to eq. 2-12. The pore

size distribution can be derived from:

$$f(r) = \frac{dv(r)}{dr} \tag{2-13}$$

where $v(r)$ is the volume of pores with radii larger than r in 1 gram of dry soil; $f(r)$ is the pore size distribution. When the pore radius approaches zero, $v(r)$ will be,

$$\lim_{r \to 0} = \frac{dv(r)}{dr} = e / G_s \tag{2-14}$$

where e is the void ratio and G_s is the specific gravity. However, there are some difficulties in the adequacy of the PSD as measured by MIP and the interpretation of the test results.

3) Difficulties associated with MIP

The interfacial contact angle is used to describe the three-phase interface between solid particles, pore liquid, and pore air in soils. This angle is defined as the angle measured inside the liquid phase from the solid surface to a point tangent to the liquid-air interface. Contact angles less than $90°$ indicate an attractive solid-liquid interaction. Contact angles greater than $90°$ indicate a repulsive solid-liquid interaction. A variation in contact angle from $100°$ to $170°$ is found with the increase of pore diameter (Neumann and Good, 1979), as shown in Fig. 2-12. From Fig. 2-12, the influence of surface tension on contact angle can be negligible. Thus it is important to use an appreciate contact angle value in the interpretation of MIP test data. From the research of Penumadu and Dean (2000), The hysteresis of mercury-air contact angle can be negligible (average advancing contact angle of $162°$ and average receding angle of $158°$ for kaolinite clay).

Penumadu and Dean (2000) considered the problem of elastic compression of the pore spaces prior to actual intrusion into the bulk of the specimen. They found that, for soft, initially slurried clays, up to 20% of the intruded volume could be attributed to such compression. However, for compacted soils, mercury percolates through the sample at relatively low pressures (Simms and Yanful, 2002), the initial elastic deformation may be reduced to a lower level.

Every MIP device has its own range of injected mercury pressure. Referring to eq. 2-12, the measurable range of pore radius is varied with different MIP device. There may be a considerable volume of pores with radii out of the measurement range.

2.3.3 SWCC prediction from PSD

When the matric suction is low (for example, less than 3000 kPa), the variation in the interlayer and the adsorbed water are minimal in the compacted soils (Cases et al., 1992; Saiyouri et al., 2000). So, liquid transport is significant in the range of low suctions, where capillary forces dominate. Hence, pore geometry controls the SWCC in that suction range. At higher suctions the relative humidity of the soil pores begins to decrease, and vapor flow becomes significant. At these suctions the slope of the SWCC, with suction plotted on a log scale, is proportional to both the liquid limit and the plasticity index (Reddi and Poduri, 1997; Marhino and Stuermer, 1998). Thus, in the high range of suctions, water content is controlled by the specific surface and charge of the clay minerals, and changes in interlayer and adsorbed water are important. The PSD measured in the MIP test can be effectively used for SWCC prediction. In a SWCC test, the relationship between the radius of the pores which are filled by water and the soil suction follows the following relation (Batchelor, 1967)

$$r = \frac{2T_{s,w}\cos\alpha}{P} \tag{2-15}$$

where the surface tension of water $T_{s,w}$ is 72.8 mN/m^2 at 20 ℃; α is the contact angle between the air-water interface at the surface of soil particle, and is taken as 0 °in this study. Therefore, SWCC is also a macro performance indicator for PSD. If the SWCC is integrated over the differential pore volume, the water content is equal to the volume of pores up to a radius r,

$$w(r) = \int_0^r f(r)dr \tag{2-16}$$

where $f(r)$ is the pore size distribution, which can be measured in the MIP (referring to eq. 2-13).

The water-air-solid contact angle is closely related to soil hydrophobicity. Soil

hydrophobicity is defined as the tendency for a soil particle or soil mass to resist hydration. Wettability is the ability of a liquid to spread over and wet a material such as soil. Wetting or non-wetting (drying) behaviour can be quantified by measuring the contact angle, which is defined as the angle measured inside the liquid phase from the solid surface to a point tangent to the liquid-air interface. The contact angle varies from $0°$ (hydrophilic material) to $180°$ (completely non wettable, hydrophobic material).

Figure 2.3 shows the concept of the drying contact angle and the wetting contact angle as a liquid drop on a tilted solid surface. After the drop reaches steady-state flow under the influence of gravity, the wetting (advancing) contact angle α_w is defined as the contact angle that develops at the advancing front of the drop. Similarly, a drying (receding) contact angle α_d is defined as the contact angle that develops at the receding front of the drop. Normally, the wetting contact angle is larger than the drying contact angle.

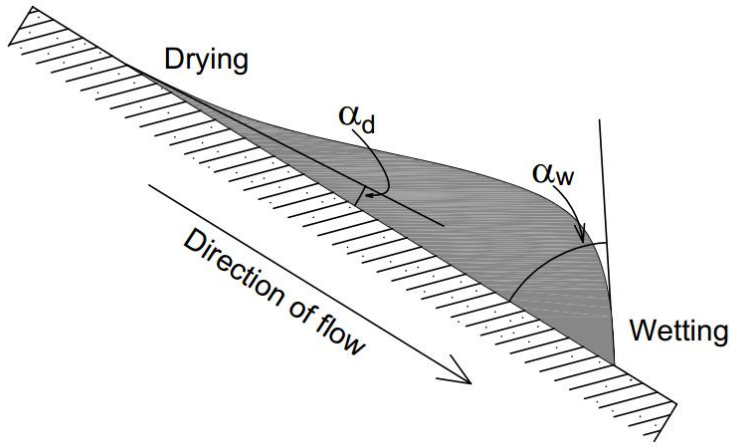

Figure 2.3 Hysteresis between wetting and drying (advancing and receding) contact angle of water (Kumar and Malik, 1990)

Wetting contact angles in sands can be as high as 60 to $80°$ (Letey et al., 1962; Kumar and Malik, 1990). Drying contact angles, on the other hand, have been estimated from $0°$ to as much as 20 to $30°$ smaller than the wetting angles (Laroussi and DeBacker, 1979).

2.4 Unsaturated hydraulic properties of structural soils

2.4.1 Soil water characteristic curve of dual-porosity structure soils

Numerous unimodal functions (e.g. Brooks and Corey, 1964; van Genuchten, 1980; Fredlund and Xing, 1994; Kosugi, 1994) have been developed to describe SWCCs. These functions were generally derived from idealized pore space models that assume a unimodal pore-size distribution. Nevertheless, evidences have been shown that the pore-size distributions of some soils are often bimodal or multimodal (Othmer et al., 1991; Durner, 1994; Spohrer et al. 2006; Zhang and Li, 2010). For example, the structural soils consist of interconnected networks of matrix (inter-aggregate) and structural (intra-aggregate) pores forming two (or more) distinct pore spaces (Kutílek, 2004). Typically, spaces of sizes in the order of 10^{-4} to 10^{-2} m are associated with structural pores, while the porous matrix contains smaller pore sizes in the range of 10^{-7} to 10^{-5} m (Tuller and Or, 2002). The existences of two vastly different pore domains resulting in pore-size distributions of structural soils are often bimodal. In such soils the independent draining of the structural and matrix pores frequently results in two distinct air-entry values, which any single unimodal function does not reproduce adequately (Othmer et al., 1991; Durner, 1994). To encounter these problems, in the last decades several approaches have been developed to describe bimodal or multimodal SWCCs (Table 2.3). Durner (1994) extended the unimodal van Genuchten functions (van Genuchten 1980) to fit bimodal and multimodal SWCCs by introducing weighting factors for combining individual functions. In these approaches the SWCC function of the whole porous medium has been described by linearly overlapping functions of the same form or of different forms (Coppola, 2000). Burger and Shackelford (2001a, b) proposed piecewise-continuous forms of the Brooks-Corey (1964), van Genuchten (1980), and Fredlund-Xing (1994) SWCC functions to fit the bimodal experimental SWCCs for diatomaceous earth (DE) and sand-DE mixtures. Although above approaches were successfully applied to structural soils, they are lack of a physical basis for their parameters due to the fact that the unimodal SWCC functions they extended were known as empirical equations.

Table 2.3 Reviews of bimodal SWCC functions

Model name	Expression	Parameters
Durner (1994)	$S_e = \sum \phi_i \left[\frac{1}{1+(\alpha_i h)^{n_i}} \right]^{m_i}$ $0 < \phi_i < 1$ and $\sum \phi_i = 1; \quad i = 1, 2$	α_i, m_i, n_i = Empirical coefficient
Coppola (2000)	$S_e = \phi_1 (1+\alpha_1 h)\exp(-\alpha_1 h) + \phi_2 \left[\frac{1}{1+(\alpha_2 h)^{n_2}} \right]^{m_2}$ $0 < \phi_i < 1$ and $\sum \phi_i = 1; \quad i = 1, 2$	α_1, α_2, m_2, n_2 = Empirical coefficient. ϕ_i, the volumetric percentage of the soil components with the *i*th pore series.
Burger and Shackelford (2001)	$\theta = \begin{cases} \theta_r + (\theta_j - \theta_r)\left[\frac{1}{1+(\alpha' \psi)^{\beta'}} \right]^{(1-1/\beta')} & ; \ \psi_j < \psi \\ \theta_j + (\theta_s - \theta_j)\left[\frac{1}{1+(\alpha \psi)^{\beta}} \right]^{(1-1/\beta)} & ; \ \psi \le \psi_j \end{cases}$	α, β, α', β'= Empirical coefficient. Artificial selection of the junction point (ψ_j, θ_j) somewhat arbitrarily.

2.4.2 Unsaturated hydraulic conductivity of structural soils

The equation proposed by van Genuchten (1980) for the SWCC is widely adopted and generally coupled with Mualem's (1976) expression for predicting hydraulic conductivity. The van Genuchten-Mualem model has produced satisfactory results in soils with a unimodal pore-size distribution. Nevertheless, the pore-size distributions of some soils is often bimodal or multimodal (Durner, 1994; Zhang and Chen, 2005; Spohrer et al. 2006; Zhang and Li, 2010). For example, structural soils consist of interconnected networks of matrix (inter-aggregate) and structural (intra-aggregate) pores forming two (or more) distinct pore spaces (Kutílek, 2004). The existence of two vastly different pore domains results in pore-size distributions of structural soils that are often bimodal. In such soils the independent draining of the structural and matrix pores frequently results in two distinct air-entry values, which any single unimodal function does not reproduce adequately (Othmer et al., 1991; Durner, 1994). To counter these problems, several approaches have been developed to describe bimodal or multimodal SWCCs in the past decades. Peters and Klavetter (1988) first proposed the superposition of two unimodal pore systems to represent bimodal

pore-size distributions. This approach was generalized by Othmer et al. (1991), Durner (1994) and Zhang and Chen (2005) to consider multimodal pore-size distributions, each of which is characterized by its own SWCC function. Recently, Liu et al. (2013) proposed a more physically based SWCC model by superposing the unimodal lognormal model of Kosugi (1994). Superposition of the unimodal SWCC model has also been used for modelling the hydraulic conductivity of structured soils. Priesack and Durner (2006) derived a closed-form expression for the multimodal unsaturated conductivity function by combining the multimodal representation of van Genuchten's SWCC function (van Genuchten, 1980) with the conductivity representation model of Mualem (Mualem, 1976). Spohrer et al. (2006) investigated the applicability of unimodal and bimodal representations of van Genuchten's SWCC functions for modelling water flow in a tropical acrisol. A physically based approach to represent the hydraulic properties of structured porous media was proposed by Tuller and Or (2002), which considered equilibrium liquid configurations in bimodal pore space. However, the derived functions of this approach are rather complex (Priesack and Durner, 2006). Kutílek (2004) also proposed a physically based hydraulic model for structural soils using the lognormal hydraulic model of Kosugi (1994) and partitioned the structural and matrix pore domains by the air-entry value of the matrix pore.

2.5 Summary

In this chapter, the previous researched that had close relationship with the hydraulic properties of the single- and dual-porosity structural soils were reviewed. Existing problems were concluded as follow: (1) There are many methods to predict unimodal soil water characteristic curve for single-porosity soils. However, the calculation procedures of these approaches are quite complicated or without paying much attention to the physical significance of the soil properties. (2) In the last decades, several approaches have been developed to describe bimodal or multimodal soil water characteristic curves. Although these approaches were successfully applied to structural soils, they are lack of a physical basis for their parameters due to the fact

that the unimodal soil water characteristic curve functions they extended were known as empirical equations. (3) Equations to predict unsaturated hydraulic porosities of structural soils also have been developed by researches. However, the derived functions of this approach are rather complex or lack of physical significance of the parameters. The objectives of the dissertation will be focus on these problems.

REFERENCES

Arbhabhirama, A. and Kridakorn, C. 1968. Steady downward flow to a water table. Water Resources Research, 4(6), 1249-1257.

Arya, L.M., Leij F.J., Van Genuchten, M. Th. and Shouse, P. 1999 Scaling parameter to predict the soil water characteristic from particle-size distribution data. Soil Science Society of America Journal, 63(3) 510-519.

Arya, L.M., and Paris, J.F. 1981. A physico-empirical model to predict the soil moisture characteristic from particle-size distributi on and bulk density data. Soil Science Society of America Journal, 45(6), 1023-1030.

Arya, L.M., Richter, J.C. and Davidson, S.A. 1982. A comparison of soil moisture characteristic predicted by the Arya-Paris model with laboratory-measured data. AgRISTARS Tech. Rep. SM-L1-04247, JSC-17820. NASA, Johnson Space Ctr., Houston, TX.

Basile, A. and D'urso, G. 1997 Experimental corrections of simplified methods for predicting water retention curves in clay-loamy soils from particle-size determination. Soil Technology, 10(3) 261-272.

Batchelor, G.K. 1967. An introduction to fluid dynamics. Cambridge University Press.

Benson, C.H., Abichou, T.H., and Olson, M.A. 1995. Winter effects on hydraulic conductivity of compacted clay. Journal of Geotechnical Engineering, 121(1), 69-79.

Brandyk, T., Szatylowicz, J., Oleszczuk, R., and Gnatowski, T. 2003. Water-related physical attributes of organic soils. In Organic soils and peat materials for sustainable agriculture, Parent, L.E., and Ilnicki, P., CRC Press, Boca Raton, FL, 33-67.

Bohne, K., Roth, C., Leij, F.J., and van Genuchten, Th.M. 1993. Rapid method for estimating the unsaturated hydraulic conductivity from in filtration measurements. Soil Science, 155, 237-244.

Bouma J., and Bregt A.K. 1989. Assessment of re presentative soil data for phosphate

leaching land qualities in space and time. In Proc. ISSS symposium, Wageningen, 201-204.

Brooks, R., and Corey, A. 1964 Hydraulic properties of porous medium. Hydrology Paper No. 3, Colorado State Univ., Fort Collins,Colo.

Brooks, R.H., and Corey, A.T. 1966. Properties of porous media affecting fluid flow. Journal of Irrigation and Drain Divsion, 92(2), 61-89.

Brutsaert, W. 1966. Probability laws for pore size distributions. Soil Science, 101, 85-92.

Burdine, H.T. 1953. Relative permeability calculations form pore-size distribution data. Transaction, Society of Petroleum Engineers, 198, 71-77.

Burger, C. A., and Shackelford, C. D. 2001a Evaluating dual porosity of pelletized diatomaceous earth using bimodal soil-water characteristic curve functions. Canadian Geotechnical Journal, 38(1), 53-66.

Burger, C. A., and Shackelford, C. D. 2001b Soil-water characteristic curves and dual porosity of sand-diatomaceous earth mixtures. Journal of Geotechnical and Geoenvironment Engineering, 127(9), 790-800.

Campbell, G.S. 1985. Soil physics with basic. Elsevier, New York.

Caron, J., and Elrick, D. 2005. Measuring the unsaturated hydraulic conductivity of growing media with a tension disc. Soil Science Society of America Journal, 69(3), 783-793.

Cases, J.M., Beraend, I., Besson, G., Francois, M., Uriot, J., Thomas, F., and Poirer, J.E. 1992. Mechanism of adsorption and desorption of water vapor by homoionic montmorillonite I. The sodium exchanged form. Langmuir 8, 2730-2739.

Child, E.C., and Collis-Georges, N. 1950. The permeability of porous materials. In Proceedings of the Royal Society of London, Series A, 201, 392-405.

Collins, K., and McGrown, A. 1974. The form and function of microfabric features in a variety of natural soils. Geotechnique, 24, 447-466.

Coppola, A. 2000 Unimodal and bimodal descriptions of hydraulic properties for aggregated soils. Soil Science Society of America Journal, 64(4), 1252-1262.

Cousin, I., Issa, O.M., and Vissonnais, Y.L. 2005. Microgeometrical characterization and percolation threshold evolution of a soil crust under rainfall. Cateba, 62, 173-188.

Croney, D., and Coleman, J.D. 1961. Pore pressure and suction in soils. In Proceedings of Conference on Ore Pressure and Suction in Soils. Butterworths, London, 31-37.

Cuisinier, O., and Laloui, L. 2004. Fabric evolution during hydromechanical loading of a compacted silt. International Journal for Numerical and Analytical Methods in Geomechanics, 28(6), 483-499.

Cui, Y. J., Tang, A. M., Mantho, A. T., and Laure, E.D. 2008. Monitoring field soil suction using a miniature tensiometer. Geotechnical Testing Journal, 31(1), 95-100.

Dane, J. H. and Klute A. 1977 Salt Effects on the Hydraulic Properties of a Swelling Soil. Soil Science Society of America Journal, 41(6), 1043-1049.

Daniel, D. 1983. Permeability test for unsaturated soil. Geotechnical Testing Journal, 6(2), 81-86.

Delage, P., and Cui, Y. J. 2008. A novel filtration system for polyethylene glycol solutions used in the osmotic method of controlling suction. Canadian Geotechnical Journal, 45(3), 421-424.

Delage, and Lefebvre, G. 1984. Study of the structure of a sensitive Champlain clay and its evolution during consolidation of the total volume of water in the low-porosity. Canadian Geotechnical Journal, 21, 21-35.

Durner, W. 1994 Hydraulic conductivity estimation for soils with heterogeneous pore structure. Water Resource Research, 30(2), 211-223.

Eching, S.O., J.W. Hopmans, and O. Wendroth. 1994. Unsaturated hydraulic conductivity from transient multistep outflow and soil water pressure data. Soil Science Society of America Journal, 58, 687-695.

Feng, M., and Fredlund D.G. 2003. Calibration of thermal conductivity sensors with consideration of hysteresis. Canadian Geotechnical Journal, 40(5), 1048-1055.

Fetter, C.W. 1993 Contaminant hydrogeology. New York, Macmillan.

Fleureau, J.M., and Taibi, S. 1995. Water air perm abilities of unsaturated soils. In proceedings of the 1st International Conference on Unsaturated soils. Edited by E.E. Alonso and P. Delage. A.A. Balkema, Rotterdam, The Netherlands, Vol. 2, pp. 479-484.

Fratesi, S.E., Lynch, F.L., Kirkland, B.L., and Brown, L.R. 2004. Effects of SEM preparation techniques on the appearance of bacteria and biofilms in the Carter Sandstone. Journal of Sedimentary Research, 74(6), 858-867.

Fredlund D.G. and Rahardjo, H. 1993. Soil mechanics for unsaturated soils. John Wiley and Sons, Inc., New York.

Fredlund, D. G., and Xing, A. 1994 Equations for the soil-water characteristic curve. Canadian Geotechnical Journal, 31(4), 521-532.

Fredlund, D.G., Xing, A.Q., and Huang, S.Y. 1994. Predicting the permeability function for unsaturated soils using the soil-water characteristic curve. Canadian Geotechnical Journal, 31(4), 533-546.

Gardner, W.R. 1956. Mathematics of isothermal water conduction in unsaturated soils. In Highway Research Board Special Report 40 International Symposium on Physico-chemical Phenomenon in Soils, Washington D.C., 78-87

Gillott, J.E. 1973. Methods of sample preparation for microstructural analysis of soil. In Soil Microscopy 4th International Working Meeting on Soil Micromorphology, Kingston, Jamaica, 143-164.

Gribb, M.M., Simunek, J., and Leonard, M.F. 1998. Development of cone penetrometer method to determine soil hydraulic properties. Journal of Geotechnical and Geoenvironmental Engineering, 124(9), 820-829.

Haines, W.B. 1930. Studies in the physical properties of soil–V: The hysteresis effect in capillary properties and the modes of water distribution associated therewith. Journal of Agricultural Science, 20, 97-116.

Hamilton, D.C., Gloeckler, G., Krimigis, S.M., and Lanzerotti, L.J. 1981. Composition of nonthermal ions in the Jovian magnetosphere. Journal of

Geophysical Research, 86, 8301.

Hillel, D. 1998. Environmental soil physics. Academic Press, San Diego, CA, USA.

Hillel, D., Krentos, U.D., and Stylianou, Y. 1972. Procedure and test of an internal drainage method for measuring soil hydraulic characteristics in situ. Soil Science, 114, 395-400.

Hoffmann-Riem, H., van Genuchten, M.Th. and Fluhler, H. 1999 A general model of the hydraulic conductivity of unsaturated soils. pp. 31–42. In: van Genuchten, M.Th. et al. (ed.) Proc. Int. Workshop, Characterization And Measurements Of The Hydraulic Properties Of Unsaturated Porous Media, 22–24 October 1997. University of California, Riverside.

Klute, A. 1965. Laboratory measurement of hydraulic conductivity of saturated soil. In C.A. Black et al. (eds.), Methods of soil analysis, Part 1. Agronomy 9, 210-220.

Kool, J.B., and Parker, J.C. 1987. Development and evaluation of closed-form expressions for hysteretic soil hydraulic-properties. Water Resources Research, 23, 105-114.

Kosugi, K. 1994. Three-parameter lognormal distribution model for soil water retention. Water Resource Research, 30(4), 891-901.

Kosugi, K. 1999. General model for unsaturated hydraulic conductivity for soils with lognormal pore-size distribution. Soil Science Society of America Journal, 63(2), 270-277.

Kumar, S., and Malik, R.S. 1990. Verification of quick capillary rise approach for determining pore geometrical characteristics in soils of varying texture. Soil Science, 150(6), 883-888.

Kutílek, M. 2004 Soil hydraulic properties as related to soil structure. Soil Tillage Research, 79(2), 175-184.

Laroussi, C.H., and DeBacker, L.W. 1979. Relations between geometrical properties of glass bead media and their main hysteresis loops. Soil Science Society of America Journal, 43, 646-650.

Leong, E. C., Tripathy, S., and Rahardjo, H. 2003. Total suction measurement of

unsaturated soils with a device using the chilled-mirror dew-point technique. Geothchnique, 53(2), 173-182.

Letey, J., Osborn, J., and Pelishek, R.E. 1962. Measurement of liquid-soli d contact angles in soil and sand. Soil Science, 93, 149-153.

Likos, W. J., and Lu, N. 2003. Automated humidity system for measuring total suction characteristics of clay. Geotechnical Testing Journal, 26(2), 179-190.

Lin, H.S., Mclnnes, K.J., Wilding, L., and Hallmark, C.T. 1999. Effects of soil morphology on hydraulic properties. II. Hydraulic pedotransfer functions. Soil Science Society of America Journal, 63, 955-961.

Liu, S. Y., Yasufuku N., Liu, Q., Omine, K. & Hemanta, H. 2013 Bimodal and multimodal descriptions of soil-water characteristic curves for structural soils. Water Science and Technology, 67(8), 1740-1747.

Marinho, F. A. M., and Oliveira, O. M. 2006. The filter paper method revisited. Geotechnical Testing Journal, 29(3), 250-258.

Marhino, F.A.M. and Stuermer, M.M. 1998. Aspects of the storage capacity of a compacted residual soil. In Proc. 2nd Int. Conf. Unsaturated Soil, Beijing 1, 581-585.

McKee, C. and Bumb, A. 1984. The importance of unsaturated flow parameters in designing a hazardous waste site. Hazardous Wasters and Envirionmental Emergencies (Hazardous Materials Control Research Institute National Conference. Houston, TX, March, 50-58.

Minasny, B., Hopmans, J.W., Harter, T., Eching, S.O., Tuli, A., and Denton, M.A. 2004. Neural networks prediction of soil hydraulic functions for alluvial soils using multistep outflow data. Soil Science Society of America Journal, 68, 417-429.

Minasny, B., McBratney, A.B., and Bristow, K. I. 1999. Comparison of different approaches to the development of pedotransfer functions for water retention curves. Geoderma, 93, 225-253.

Minasny, B., and McBratney, A.B. 2002. The neuro-method for fitting neural network

parametric pedotransfer functions. Soil Science Society of America Journal, 66, 352-361.

Mishra, S., Parker, J.C. and Singhal, N. 1989. Estimation of soil hydraulic properties and their uncertainty from particle size distribution data. Journal of Hydrology, 108, 1-18.

Monroy, R., Ridley, A., Dineen, K., and Zdravkovic, L. 2007. The suitability of the osmotic technique for the long-term testing of partly saturated soils. Geotechnical Testing Journal, 30(3), 220-226.

Mualem, Y. 1973. Modified approach to capillary hysteresis based on a similarity hypothesis. Water Resources Research, 9(5), 1321-1331.

Mualem, Y. 1974. A conceptual model of hysteresis. Water Resources Research, 10(3), 514-520.

Mualem, Y. 1976 A new model for predicting the hydraulic conductivity of unsaturated porous media. Water Resource Research, 12(3), 513-522.

Mualem, Y. 1984. A modified dependent domain theory of hysteresis. Journal of Soil Science, 137, 379-390.

Mualem, Y. 1986. Hydraulic conductivity of unsaturated soils: prediction and formulas. Methods of soil analysis. Part I. physical and mineralogical methods. 2nd Ed., Agronomy, A. Klute. Ed., Am. Soc. of Agronomy, Inc., and Soil Sci. Soc. of Am., Inc., Madison, Wis., 799-823.

Nemes, A., Schapp, M.G., and Wosten, J.H.M. 2003. Functional evaluation of pedotransfer functions derived from different scales of data collection. Soil Science Society of America Journal, 67, 1093-1102.

Neumann, A.W. and Good. R.J. 1979. Techniques of measuring contact angles. Surface and Colloid Science, 11, 31-61.

Nichol, C., Smith, L., and Beckie, R. 2003. Long-term measurement of matric suction using thermal conductivity sensors. Candian Geothchnical Journal, 40(3), 587-597.

Olson, R.E., and Daniel, D.E. 1981. Measurement of the hydraulic conductivity of

fine-grained soils. In Zimmie, T.F. and Riggs, C.O. Editors (ed.), Permeability and Groundwater Contaminant Transport, American Society for Testing and Materials, 18-64.

Othmer, H.B., Diekkrüger, B., and Kutílek, M. 1991 Bimodal porosity and unsaturated hydraulic conductivity. Soil Science, 152(3), 139-150.

Pachepsky, Y.A., Timlin, D., and Varallyay, G. 1996. Artificial neural networks to estimate soil water retention from easily measurable data. Soil Science Society of America Journal, 60, 727-733.

Penumadu, D., and Dean, J. 2000. Compressibility effect in evaluating the pore-size distribution of kaolin clay using mercury intrusion porosimetry. Canadian Geotechnical Journal, 37(2), 393-405.

Peters, R.R., and Klavetter, E.A. 1988 A continuum model for water movement in an unsaturated fractured rock mass. Water Resource Research, 24(3), 416-430.

Pham, H.Q., Fredlund, D.G. and Barbour, S.L. 2005. A study of hysteresis models for soil-water characteristic curves. Canadian Geotechnical Journal, 42(6), 1548-1568.

Poulovassilis, A. and Childs, E.C. 1971. The hysteresis of pore water: the non-independence of domains. Journal of Soil Science, 112, 301-312.

Prapaharan, S., Altschaeffl, A. G. and Dempsey, B. J. 1985. Moisture curve of compacted clay: mercury intrusion method. Journal of Geotechnical and Geoenvironment Engineering, 111, 1139-1143.

Priesack, E. & Durner, W. 2006 Closed-form expression for the multi-modal unsaturated conductivity function. Vadose Zone Journal, 5(1), 121-124.

Prost, R., Koutit, T., Benchara, A., and Huard, E. 1998. State and location of water adsorbed on clay minerals: consequences of the hydration and swelling-shrinkage phenomena. Clays and Clay Minerals, 46(2), 117-131.

Rawls, W.J., and Brakensiek, D.L. 1985. Prediction of soil water properties for hydrologic modeling. In Jones, E., Ward, T.J. (Eds.), Watershed Manage. Eighties. Proceedings of the Symposium of ASAE, Denver, 293-299.

Reddi, L.N. and Poduri, R. 1997. Use of liquid limit state to genera lize water retention properties of fine-grained soils. Geotechnique, 47(5), 1043-1047.

Richards, B.G. 1965. Measurement of the free energy of soil moisture by the psychrometric technique using thermistors. In Moisture equilibria and moisture changes in soils beneath covered areas. Edited by G.D. Aitchison. Butterworth and Co. Ltd., Sydney, Australia, 39-46.

Richards L. A. 1931. Capillary conduction of liquids through porous mediums. Physics, 1(5), 318-333.

Richards, S.J. and Weeks, L.V. 1953. Capillary conductivity values from moisture yield and tension measurements on soil columns. Soil Sci. Soc. Am. Proc. 17, 206-209.

Ridley, A. M., and Burland, J. B. 1996. A pore pressure probe for the in situ measurement of a wide range of soil suctions. Advances in Site Investigation Practice, London, Thomas Telford, pp. 510-520.

Romano, N., and Palladino, M. 2002. Prediction of soil water retention using soil physical data and terrain attributes. Journal of Hydrology, 265, 56-75.

Saiyouri, N., Hicher, Y. and Tessier, D. 2000. Microstructural approach and transfer water modeling in compacted unsaturated swelling clays. Mech. Cohesive-Frictional Mater, 5, 41-60.

Samingan, A.S., Leong, E., and Rahardjo, H. 2003. A flexible wall permeameter for measurement of water and air coefficients of permeability of residual soils. Canadian Geotechnical Journal, 40(3), 559-574.

Schuh, W.M., Cline, R.L.and Sweeney, M.D. 1988. Comparison of a laboratory procedure and a textural model for predicting in situ soil water retention. Soil Science Society of America Journal, 52(3), 1218-1227.

Simms, H., and Yanful, E.K. 2002. Predicting soil-water characteristic curves of compacted plastic soils from measured pore-size distributions. Geotechnique, 52(4), 269-278.

Spohrer, K., Herrmann, L., Ingwersen, J. & Stahr, K. 2006 Applicability of uni- and

bimodal retention functions for water flow modeling in a tropical acrisol. Vadose Zone Journal, 5(1), 48-58.

Take W.A., and Bolton, M.D. 2003. Tensiometer saturation and the reliable measurement of soil suction. Geotechnique, 53(2), 159-172.

Tuller, M., and Or, D. 2002. Unsaturated hydraulic conductivity of structured porous media: A review of liquid configuration-based models. Vadose Zone Journal, 1(1), 14-37.

Tyler, S.W., and Wheatcraft, S.W. 1989 Application of fractal mathematics to soil water characteristic estimation. Soil Science Society of America Journal, 53(4) 987-996.

Van Dam, J.C., Stricker, J.N.M., and Droogers, P. 1994. Inverse method to determine soil hydraulic functions from multistep outflow experiments. Soil Science Society of America Journal, 58, 647-652.

Van Genuchten, M.Th. 1980 A closed-form equation for predicting the hydraulic conductivity of unsaturated soils. Soil Science Society of America Journal, 44(5), 892-898.

Vanapalli, S.K., Fredlund, D.G., and Pufahl, D.E. 1996. Model for the prediction of shear strength with respect to so il suction. Canadian Geotechnical Journal, 33 (3): 379-392.

Vaz, C.M.P., Iossi, M.D.F., Naime J.D.M., Macero, A., Reichert, J.M., Reinert, D.J. and Cooper, M. 2005 Validation of the Arya and Paris water retention model for Brazilian soils. Soil Science Society of America Journal, 69(3) 577-583.

Vereecken, H. 1988. Pedotransfer func i ons for the genera i on of hydraulic properties of Belgian soils. Katholieke Univ. Leuven, Leuven, Belgium.

Weeks, L. V. and Richards, S. J. 1967. Soil-water properties computed from transient flow data. Soil Science Society of America Journal, 31(6), 721-725.

Weynants, M., Vereecken, H. and Javaux, M. 2009. Revisiting Vereecken pedotransfer funcitons: Introducing a closed-form hydraulic model. Vadose Zone J, 8(1), 86-95.

Wheeler, S.J., Sharma, R.S., and Buisson, M.S.R. 2003. Coupling of hydraulic

hysteresis and stress-strain behaviour in unsaturated soils. Geotechnique, 53(1), 41-54.

Wildenschild, D., K.H. Jensen, K.J. Hollenbeck, T.H. Illangasekare, D. Znidarcic, T. Sonnenborg, and M.B. Butts. 1997. A two-stage procedure for determining unsaturated hydraulic characteristics using a syringe pump and outflow observations. Soil Science Society of America Journal, 61, 347-359.

Williams, J. 1982. The surface of the Earth, an introduction to geotechnical science. Ongman Inc., New York.

Wosten, J.H.M., Schuren, C.H.J.E., Bouma, J., and Stein, A. 1990. Functional sensitivity analysis of four methods to generate soil hydraulic functions. Soil Science Society of America Journal, 54, 832-836.

Wosten, J.H.M., Pachepsky, Y.A., and Rawls, W.J. 2001. Pedotransfer functions: bridging the gap between available basic soil data and missing soil hydraulic characteristics. Journal of Hydrology, 251, 123-150.

Xu, Y.F., and Sun, D.A. 2002. A fractal model for soil pores and its application to determination of water permeability. Physica a statistical mechanics and its applications, 316(4), 56-64.

Yang, H., Rahardjo, H., Leong, E. C. and Fredlund, D.G. 2004a. Factors affecting drying and wetting soil-water characteristic curves of sandy soils. Canadian Geotechnical Journal, 41(5), 908-920.

Zhang, L. M. & Chen, Q. 2005 Predicting bimodal soil-water characteristic curves. Journal of Geotechnical and Geoenvironmental Engineering, 131(5), 666-670.

Zhang, L.M., and Li. X. 2010 Microporosity structure of coarse granular soils. Journal of Geotechnical and Geoenvironment Engineering, 136(10), 1425-1436.

CHAPTER 3

3. PREDICTION OF SOIL WATER CHARACTERISTIC CURVE FOR SINGLE-POROSITY SOILS USING PHYSICALLY BESED SCALING TECHNIQUE

3.1 INTRODUCTION

The knowledge of hydraulic behavior of single-porosity soils is the foundation of seepage analysis in the desert (unsaturated zone). The soil water characteristic curve (SWCC) reflects the storage capacity of soil (Schulze et al. 1985), is an important hydraulic property of unsaturated zone. The SWCC is often required as input in soil water flow and contaminant migration models supporting hydrologic, environmental engineering (Henry and Smith, 2006; Ireson et al., 2009). However, direct measurement of the SWCC is time consuming, expensive, labor intensive, and subject to numerous errors. As a result, indirect approaches that estimate the SWCC from routinely available taxonomic data (e.g., texture, bulk density, particle density, and organic matter content) using pedotransfer functions have become interested (Arya et al., 2008).

Arya and Paris (1981) proposed a physico-empirical model (AP model) that used to estimate the SWCC from particle-size distribution (PSD). The basis for this approach is mainly on the shape similarity of the two curves. The AP procedure introduced an empirical parameter, α, used to scale pore attributes from hypothetical formations to natural structures. Arya and Paris (1981) initially determined α as constant, whereas several researchers have suggested that variable α would improve the predictions of the SWCC (Basile and D'Urso, 1997; Arya et al., 1999; Vaz et al., 2005). Fractal concepts have also been used to derive α (Tyler and Wheatcraft, 1989). However, the calculation procedures of these approaches are quite complicated or without paying

much attention to the physical significance of the soil properties.

In the past decades, the scaling technique has been used to characterize hydraulic properties of field-scale vadose zones, using measurement scales that are typically much smaller (Miller and Miller, 1956; Peck et al., 1977; Tuli et al., 2001). With growing water quality issues, this scale-transfer question is being asked more frequently than ever (Hopmans et al., 2002). Kosugi and Hopmans (1998) presented an elegant physically based scaling technique (PBS) which provides convenient way to coalesce multiple SWCCs into a single reference SWCC (Tuli et al., 2001; Bhabani et al., 2005).

The objective of this study was to extend the PBS approach to the AP model, yielding α to estimate SWCC from PSD. A total of 50 experimental soil data that representing a range of textures that include sand, sandy loam, loam, silt loam, and clay, were selected from the UNSODA hydraulic property database (Nemes et al., 2001) for this purpose. In addition, 19 soil samples with different textures were used to test this method. The results predicted from the PBS approach were compared with other methods to verify its effectiveness.

3.2 MATERIALS AND METHODS

3.2.1 Experimental data

Experimental SWCCs, PSD, bulk density, and particle density data were obtained from the Unsaturated SOil hydraulic DAtabase (UNSODA) (Nemes et al., 2001). The UNSODA contains of SWCC, hydraulic conductivity and water diffusivity data as well as pedological information of some 790 soil samples from around the word (e.g. United States, Netherlands, United Kingdom, Germany, Belgium, Denmark, Russia, Italy, and Australia). Sixty-nine soil samples, representing a range of textures that include sand (S), sandy loam (SL), loam (L), silt loam (SiL), and clay (C), were selected for this study. Among them, 50 soil samples were used to calculate α using PBS approach, 19 soil samples used to verify the calculated α value. All soils are identified in Table 3.1

Table 3.1 Textural classes and UNSODA codes for samples

Textural class	UNSODA codes	Use
Sand	1462, 1463, 1464, 1465, 1466, 1467, 3330, 3331, 3332, 3340, 4523, 4660, 4661	Calculating α
	1460, 2100, 4650, 4651	Testing α
Sandy loam	1161, 1380, 1381, 2532, 3290, 3310, 3320, 3321, 3323	Calculating α
	3291, 3300, 3301, 3311	Testing α
Loam	1370, 2530, 2531, 4591, 4600, 4610, 4620	Calculating α
	3293, 3302, 3303, 4592	Testing α
Silt loam	1280, 1281, 1282, 1341, 1342, 1350, 1352, 1490, 2000, 2002, 2010, 2011, 4510, 4671, 4672, 4673	Calculating α
	1340, 1351, 2001, 2012	Testing α
Clay	1162, 1163, 2360, 2362, 4680	Calculating α
	1400, 2361, 4681	Testing α

3.2.2 Arya and Paris Model

The AP model translates the percentage of particles smaller than the diameter axis of the PSD curve to volumetric water content and the particle diameter axis to suction head (Arya and Paris, 1981; Arya et al., 1999; Arya et al., 2008). First, the PSD is divided into *n* size fractions that was originally suggested by Arya and Paris (1981) as 20 diameter classes (1, 2, 3, 5, 10, 20, 30, 40, 50, 70, 100, 150, 200, 300, 400, 600, 800, 1000, 1500, and 2000 μm). In each fraction, the solid mass was assembled to form a hypothetical, cubic close-packed structure consisting of uniform-sized spherical particles. Starting with the first fraction (smallest particles), calculated pore volumes are progressively summed and considered filled with water. Each summations of filled pore volumes is divided by the bulk volume of the whole sample to obtain volumetric water content at the upper bound of successive mass fractions.

An equivalent pore radius is calculated for each fraction and converted to soil suction head using the capillary equation. Calculated suction heads are sequentially paired with calculated volumetric water contents to obtain a predicted SWCC. The capillary equation that relates soil suction head (h_i) and pore radius (r_i) as follows:

$$h_i = \frac{2\gamma \cos\Theta}{\rho_w g r_i} \tag{3-1}$$

where γ is the surface tension at the air-water interfacial (N m^{-1}), Θ is the contact angle, ρ_w is the density of water (kg m^{-3}), and g is the acceleration due to gravity (m s^{-2}).

The calculation of the volumetric water contents from the PSD as the contribution of each fraction to soil wetting:

$$\theta_i = \phi S_w \sum_{i=1}^{I} W_i \tag{3-2}$$

where ϕ is the total soil porosity (cm^3 cm^{-3}), S_w is the ratio of measured saturated water content to theoretical porosity and W_i is the soil mass of the ith fraction (i =1, ... , I). Soil porosity can be calculated from soil bulk density ρ_b (kg cm^{-3}) and particle density ρ_s (kg cm^{-3}): ϕ =1-(ρ_b/ρ_s).

Porous radius of ith fraction (r_i) is determined from soil particle diameter (D_i) considering packing of uniform-sized spherical particles and an empirical parameter α that corrects for natural structure soil

$$r_i = \frac{D_i}{2}\left[\frac{2en_i^{1-\alpha_i}}{3}\right]^{0.5} \tag{3-3}$$

where n_i is the number of particles of ith fraction, and e is the void ratio, given as follows:

$$n_i = \frac{6W_i}{\pi D_i^3 \rho_s} \tag{3-4}$$

$$e = \frac{\rho_s - \rho_b}{\rho_b} \tag{3-5}$$

The soil suction head is then calculated with the combination of Eq.(3-1), (3-3), (3-4)

and (3-5) as follows:

$$h_i = \frac{\gamma}{\rho_w g D_i \sqrt{\frac{2(\rho_s - \rho_b)}{3\rho_b}\left(\frac{W_i}{6\pi D_i^3 \rho_s}\right)^{1-\alpha_i}}} \tag{3-6}$$

Once the empirical parameter α_i is known, the calculated volumetric water contents are paired with the predicted soil suction heads (Eq. (3-6)) to construct SWCC.

3.2.3 Physically based scaling technique

The single objective of scaling is to coalesce a set of functional relationships into a single curve using scaling factors that describes the set as a whole (Tuli et al., 2001). Miller and Miller (1956) introduced the similar-media concept to conveniently describe soil variability in a unified manner. They assumed that the microscopic structures of two "geometrically similar" soils differ only by a characteristic length λ (Warrick et al., 1977). The scaling factor δ_j is defined as the ratio of a characteristic length λ_j of soil sample j and the characteristic length λ_{ref} of a reference soil (Peck et al., 1977) as follows:

$$\delta_j = \frac{\lambda_j}{\lambda_{ref}} \tag{3-7}$$

Kosugi and Hopmans (1998) presented an elegant physically based scaling (PBS) technique which introduced the median pore radius r_m, as the characteristic length to scale SWCC for soils that are characterized by a lognormal pore size distribution, f:

$$f(\ln r) = \frac{1}{\sigma\sqrt{2\pi}} \exp\left[-\frac{(\ln r - \ln r_m)^2}{2\sigma^2}\right] \tag{3-8}$$

where r is the pore radius (cm), and σ is the standard deviation of the frequency distribution. Based on this assumption, the lognormal SWCC function as a cumulative curve of Eq. (3.8) was given by Kosugi and Hopmans (1998):

$$S_e(\ln h) = \frac{\theta - \theta_r}{\theta_s - \theta_r} = F_n\left[\frac{(\ln h_m - \ln h)}{\sigma}\right] \tag{3-9}$$

where θ_s and θ_r denote the saturated and residual water contents (cm^3cm^{-3}), $\ln(h_m)$ and σ are the mean and standard deviation of $\ln(h)$, respectively. The median suction head

h_m (cm) is related to the median pore radius (r_m) by Eq. (3-1). $F_n(x)$ is the normal distribution function defined as

$$F_n = \frac{1}{\sqrt{2\pi}} \int_x^{\infty} \exp(-x^2 / 2) dx \tag{3-10}$$

Then, the reference SWCC function $S_{e,R}$, is given by the following parametric relation (Kosugi and Hopmans, 1998):

$$S_{e,R}(\ln h) = F_n \left[\frac{(\ln h_{m,R} - \ln h)}{\sigma_R} \right] \tag{3-11}$$

where $\ln(h_{m,R})$ and σ_R represent the mean and standard deviation of $\ln(h)$ for the reference soil, and are computed from

$$\ln(h_{m,R}) = \frac{1}{J} \sum_{j=1}^{J} \ln h_{m,j} \tag{3-12}$$

$$\sigma_R^2 = \frac{1}{J} \sum_{j=1}^{J} \ln \sigma_j^2 \tag{3-13}$$

where J denotes the number of soil samples in the set and the individual $\ln(h_{m,j})$ and σ_j^2 values are determined from the fitting of Eq. (3-9) to individual SWCC data. Accordingly, scaling factors for each soil sample, j, can be computed directly from (Kosugi and Hopmans, 1998; Tuli et al., 2001):

$$\delta_j = \frac{r_{m,j}}{r_R} = \frac{h_{m,R}}{h_{m,j}} \tag{3-14}$$

3.2.4 Derive α using physically based scaling technique

Initially, the PBS technique was used to compute α value for all 50 calculating soils in Table 3.1. Later calculating soils were divided into five subpopulations based on the soil texture: sand, sandy loam, loam, silt loam and clay soils. Each textural class subpopulation was then computed to its respective α value. In present study the parameter α assumed as a single value for each soil texture and all soils combined together, respectively. The detailed procedure to derive α values as follows:

1) Scaling of measured soil water characteristic curves

The experimental SWCC data points were fitted to lognormal model (Eq. (3-9)), yielding parameters $h_{m,measured}$ and $\sigma_{measured}$ for each soil sample j. Subsequently, the measured reference SWCC function $S_{e,R_{measured}}$ was calculated using Eqs. (3-11)-(3-13) for each soil texture and all soils combined together. In this study, we assume that the porosity is equivalent to θ_s. For soils that did not provide porosity or θ_s value, the first point of the experimental SWCC data that corresponds to the lowest suction head was used as θ_s (Chan and Govindaraju, 2004), and θ_r was assumed to be zero when the suction being infinity (Fredlund and Xing, 1994).

2) Scaling of predicted soil water characteristic curves

The AP model is based mainly on the similarity between the shapes of the cumulative PSD curve and the SWCC. Therefore, PSD data were also fitted to lognormal function to determine the cumulative PSD curve. The function proposed by Buchan (1989) as follows:

$$f\left(\ln D\right)=F_n\left[\frac{\left(\ln D-\mu\right)}{\sigma}\right] \tag{3-15}$$

where $f(\ln D)$ is the cumulated frequency distribution function associated with the natural logarithm of particle-size diameter, D, for particle-size classes i =1, ... , I, and μ and σ denote the mean and standard deviation of the ln-transformed particle diameter, respectively. Subsequently, selected 20 diameter classes that was originally suggested by Arya and Paris (1981).

A series of potential α values ($\alpha_{potential}$) were selected for each soil texture and all soils combined together, respectively. By use of Eqs. (3-2)-(3-6) SWCC can be estimated from PSD for each soil samples. Then, the predicted SWCC data points were fitted to lognormal model (Eq. (3-9)) to determine the parameters $h_{m,predicted}$ and $\sigma_{predicted}$ for each soil core j. After that, using Eq. (3-11) to calculate the predicted reference SWCC function $S_{e,R_{predicted}}$ according potential α value for each soil group.

3) Calculate optimal α values

An iterative procedure was used that minimized the root mean square error (RMSE) between $S_{e,R_{measured}}$ and $S_{e,R_{predicted}}$ to determine optimal α values for each soil texture and all soils combined together. The RMSE given by

$$RMSE(\alpha_{potential}) = \left\{ \frac{\sum_{l=1}^{L} \left[S_{e,R_{measured}}(\ln h_l) - S_{e,R_{predicted}}(\ln h_l, \alpha_{potential}) \right]^2}{L-1} \right\}^{0.5} \quad (3\text{-}16)$$

where L, denotes the total number of suction head (h) values, that were fixed ranging between 0.1 cm and 10^{10} cm in present study. Microsoft Excel 2010 (Microsoft Corporation) was used for all of the nonlinear optimization runs.

3.2.5 Verification

After obtained the optimal α values for each texture and all the soils, testing soils in Table 3.1 were used to verify effectiveness of PBS approach. To compare the results with previous similar studies, the SWCCs were also predicted with the methods in Table 3.2. Statistical comparison of the results was carried out in terms of the coefficient of determination (R^2), and root mean square error (RMSE) to determine the accuracy of these methods and the correlation between the measured and predicted SWCC.

The Table 3.2 lists the represented methods to predict SWCCs according AP model, including constant α and variable α methods. Except methods in the Table 3.2, there are some approaches to estimate SWCC base on AP model. For example, in Basile and D'Urso (1997), α was assumed as a function of soil suction head (h). However, the use of the $\alpha = f(h)$ relationship is quite complicated due to the interdependence of α and h in the application of the AP model (Vaz et al., 2005). Fractal concepts have also been used to determine α value (Tyler and Wheatcraft, 1989). However, fractal approaches account only for the effects of the tortuosity of pore lengths but not for other factors that influence the SWCC, such as bulk density. These methods were ignored in present study due to their defects.

Table 3.2 Represented methods to predict SWCCs according AP model

Method	α value and equation
Constant α	α=1.38 (Arya and Paris, 1981), and 0.938 (Arya and Dierolf, 1992) for all the soil classes. And α = 1.285, 1.459, 1.375, 1.150, and 1.160 for the sand, sandy loam, loam, silt loam, and clay soils (Arya et al., 1999).
Logistic equation (Arya et al., 1999)	$(Y+\Delta Y)=\frac{Y_f Y_i}{Y_i+(Y_f-Y_i)\exp[-\mu(x+\Delta x)]}$ where Y is the dependent variable log N_i, Y_f is the final value of log N_i, Y_i is the initial value of log N_i, μ is the rate coefficient, x is the independent variable log n_i, ΔY = Δlog N_i, Δx = Δlog n_i, and α_i= log N_i/log n_i. n_i and N_i is the number of spherical particles in the ideal and natural structure soil, respectively. These parameters values were shown in Table 2 of Arya et al. (1999).
Linear equation (Arya et al., 1999)	$\alpha_i=\left[\frac{a+b\log(8W_i/D_i^3)}{\log n_i}\right]$ Parameters for equation were represented in Table 3 of Arya et al. (1999).
$\alpha = f(\theta)$ (Vaz et al., 2005)	α_i=0.947+0.427exp$(-\theta_i/0.129)$ where θ_i is the water content of each fraction (cm^3 cm^{-3}).

3.3 RESULES AND DISCUSSION

3.3.1 Scaling of measured soil water characteristic curves

The measured SWCCs of 50 soils for calculating the optimal α are shown in Figure 3.1-3.6. And all the SWCCs were successfully described by the lognormal model (Eq. (3-9)) with more than 91.04 % of SWCCs having R^2> 0.95 and all SWCCs with R^2 > 0.91. Such high values of R^2 indicate the effectiveness of the lognormal model in describing measured SWCC data.

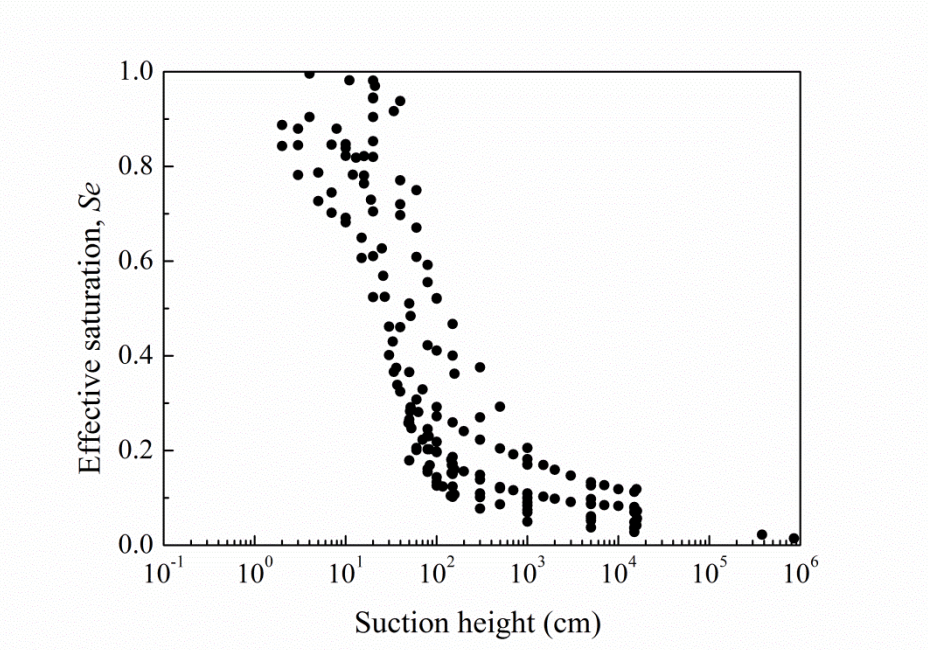

Figure 3.1 Unscaled measured SWCCs for sand

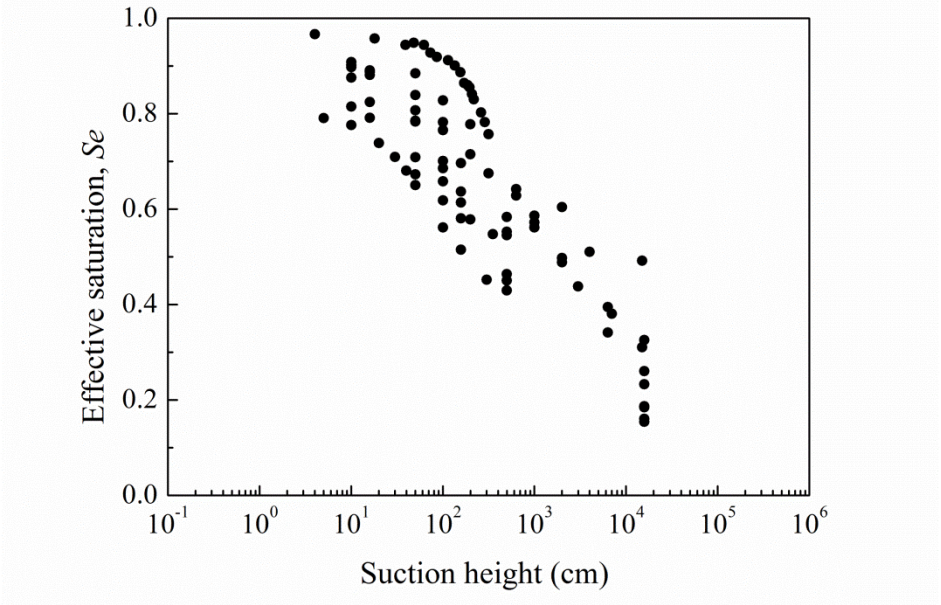

Figure 3.2 Unscaled measured SWCCs for sandy loam

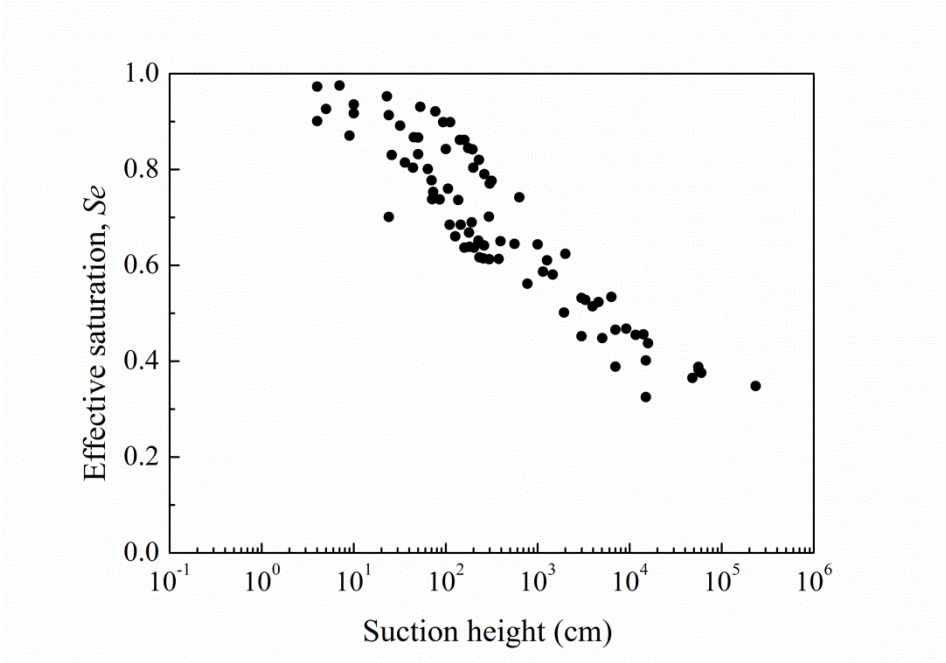

Figure 3.3 Unscaled measured SWCCs for loam

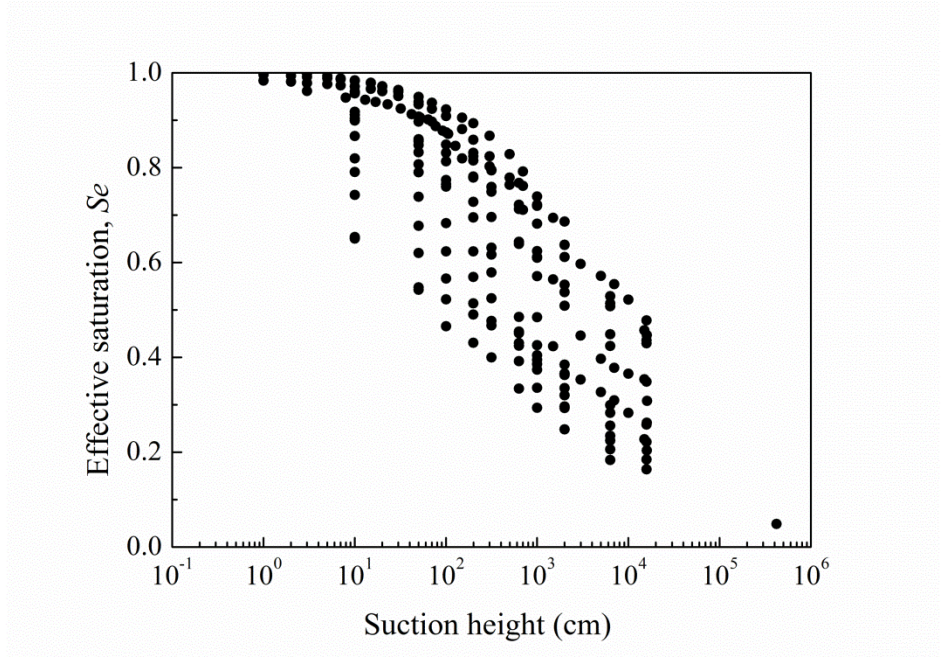

Figure 3.4 Unscaled measured SWCCs for silt loam

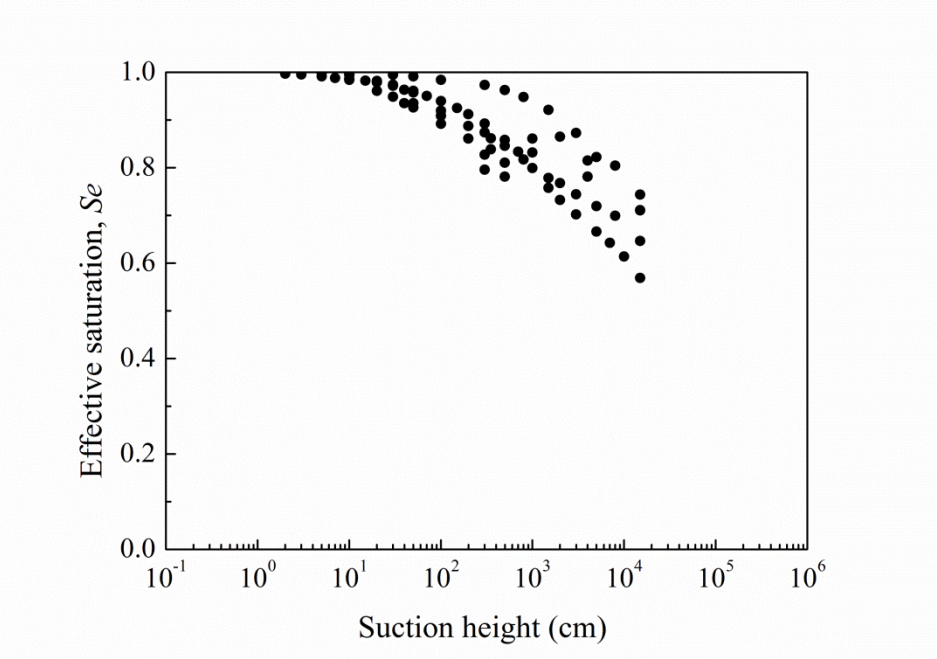

Figure 3.5 Unscaled measured SWCCs for clay

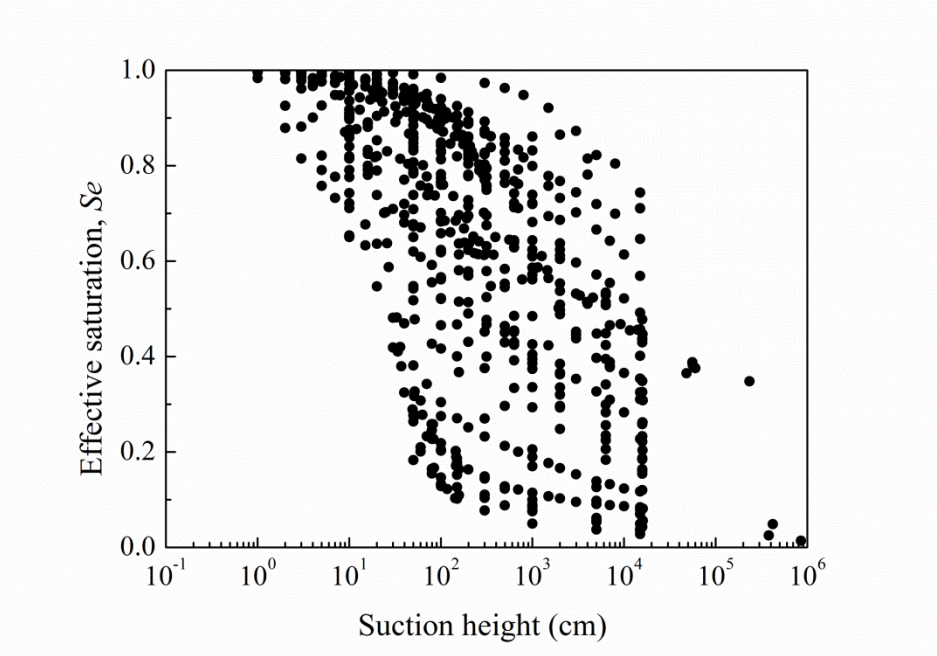

Figure 3.6 Unscaled measured SWCCs for all soils combined together

We applied the PBS technique to soils with similar texture. Figures 3.7-3.12 show scaled SWCCs (open circles) and reference SWCC (solid lines) for each textural class. Scaled SWCCs and reference SWCC for all data of 50 calculating soils are also shown in this figure. Resulting reference SWCC parameters are shown in Table 3.2. The effectiveness of scaling within respective textural class is evaluated by estimating the RMSE between scaled (open circles) and the reference (solid lines) SWCCs are shown in Table 3.3. Table 3.3 indicates the RMSE value is highest when all the 50

SWCCs are scaled together and it is reduced when soils are scaled after grouping them by soil textures. Thus, as expected, soils that are separated by textural group more similar than when all soils are combined together. Consequently, soil texture may serve as a guide for distinguishing similar media.

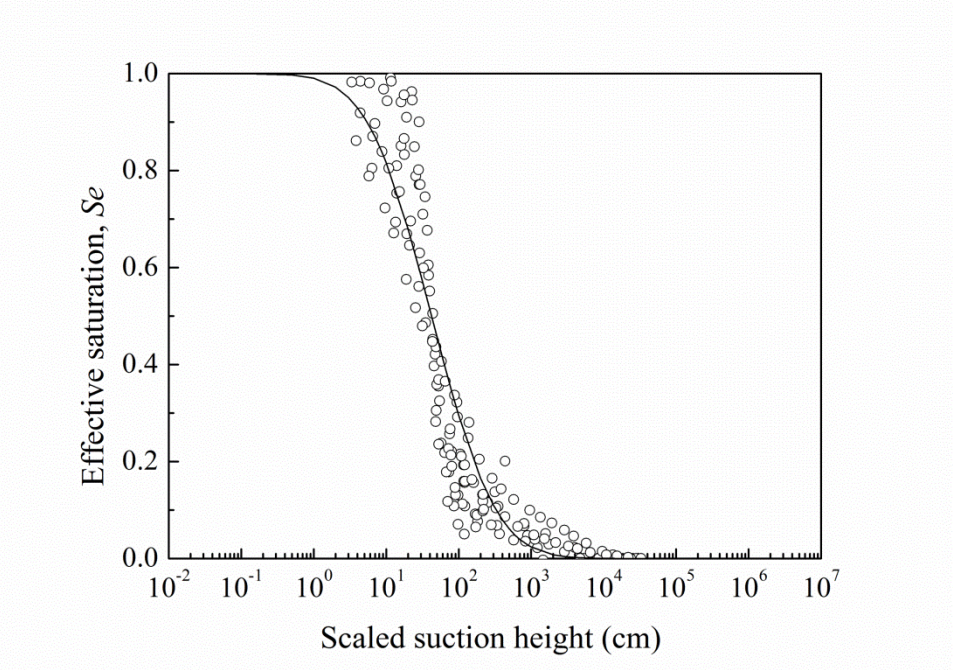

Figure 3.7 Scaled measured SWCCs for sand

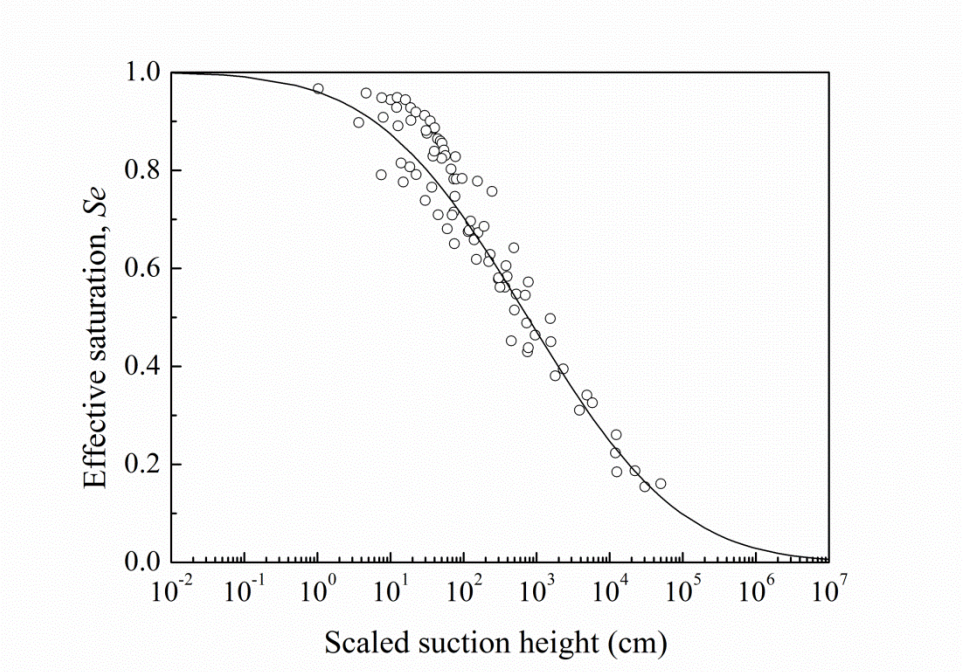

Figure 3.8 Scaled measured SWCCs for sandy loam

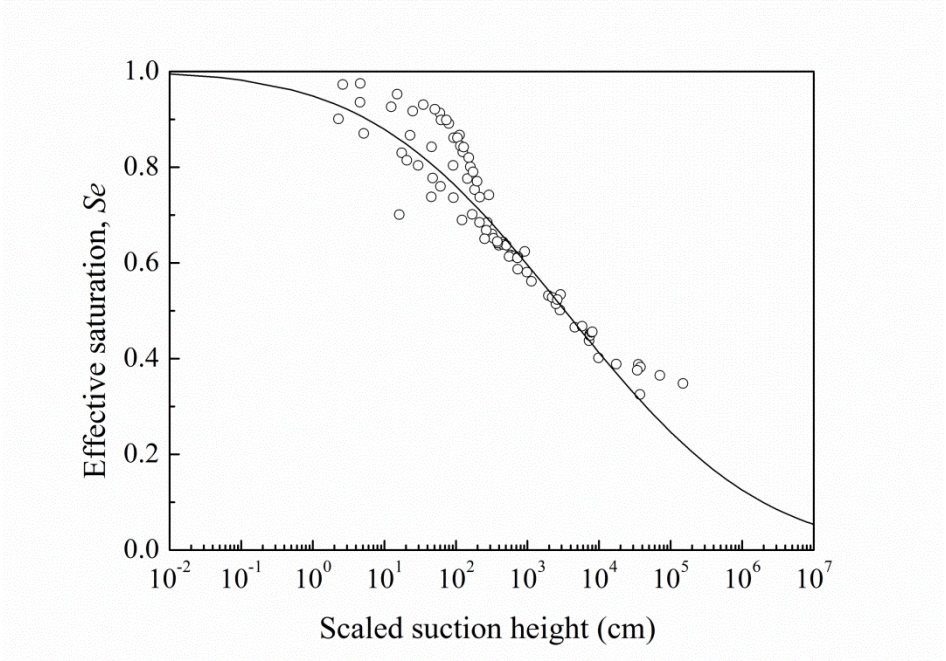

Figure 3.9 Scaled measured SWCCs for loam

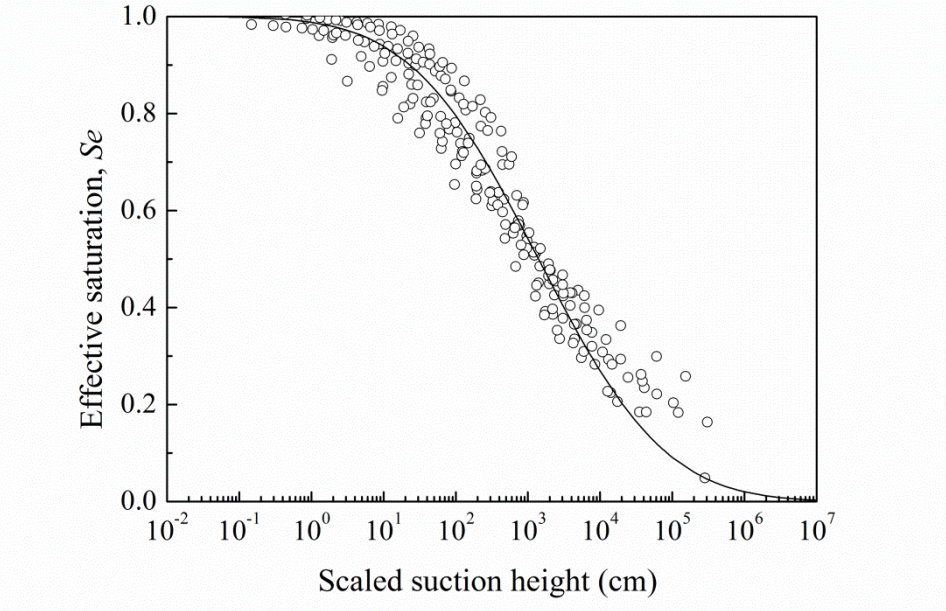

Figure 3.10 Scaled measured SWCCs for silt loam

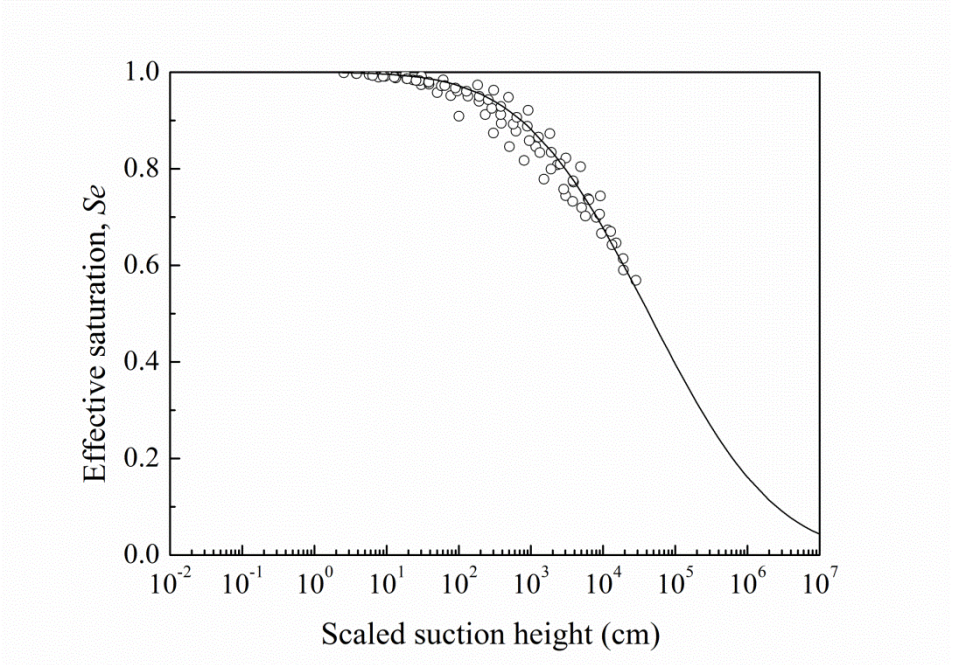

Figure 3.11 Scaled measured SWCCs for clay

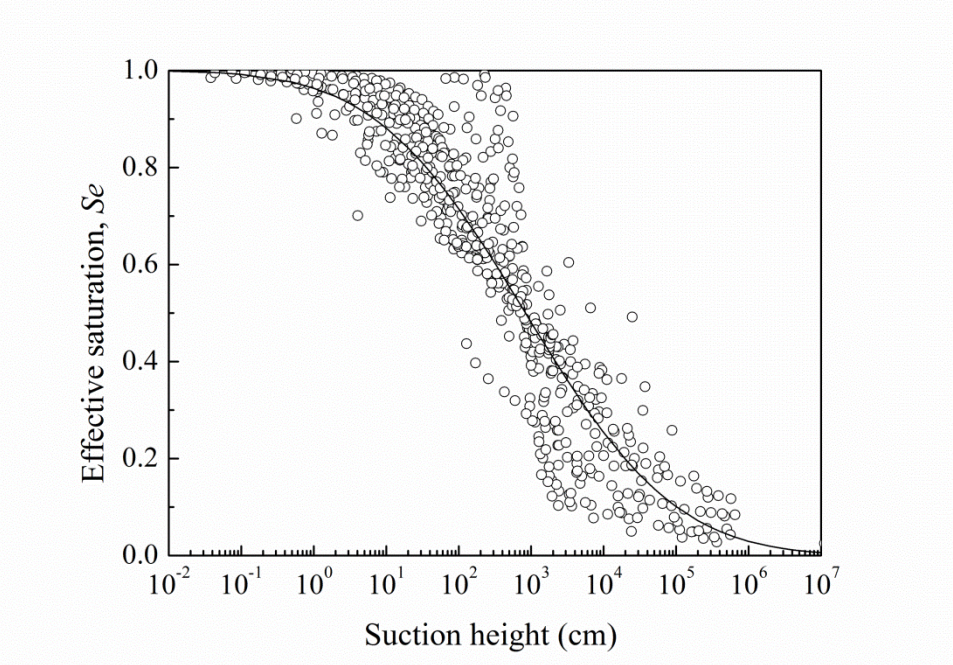

Figure 3.12 Scaled measured SWCCs for all soils combined together

Table 3.3 Scaling results for each texture and all soils combined together

Soil texture	$h_{m,ref}$ (cm)	σ_{ref}	RMSE
Sand	42.08	1.25	0.119
Sandy loam	756.09	3.78	0.105
Loam	3333.71	4.97	0.063
Silt loam	1452.21	4.33	0.122
Clay	43047.72	3.18	0.042
All soils	835.11	3.75	0.226

3.3.2 Optimal α values (α_{opt})

The optimal α with RMSE between $S_{e,R_{measured}}$ and $S_{e,R_{predicted}}$ for each texture and all soils combined together are shown in the Table 3.4. The better performance of sandy loam and loam soil textures are expressed by the lower RMSE values, which is likely caused by the smaller variations in soils compare with other textural classes.

Table 3.4 Optimal α value (α_{opt}) for each soil each texture and all soils combined together

Soil texture	Sand	Sandy loam	Loam	Silt loam	Clay	All data
α_{opt}	1.43	1.76	1.58	1.39	1.30	1.48
RMSE	0.034	0.012	0.017	0.085	0.033	0.038

Figures 3.13-3.18 show the measured reference soil water characteristic curve (reference $SWCC_m$) and the optimal predicted reference soil water characteristic curve (optimal reference $SWCC_p$) correspond to α_{opt} for each texture and all soils. Figures 3.13-3.18 also include the predicted reference soil water characteristic curve for the possible α values (possible reference $SWCC_p$), allowing a qualitative evaluation of the sensitivity of the parameter α on the predicted SWCC. From figures 3.13-3.18, the prediction approach seems to fit the measured SWCC data better for sandy loam and loam soil textures, as reflected by the better agreement between the

experimental with calculated reference curves (Figures 3.14 and 3.15).

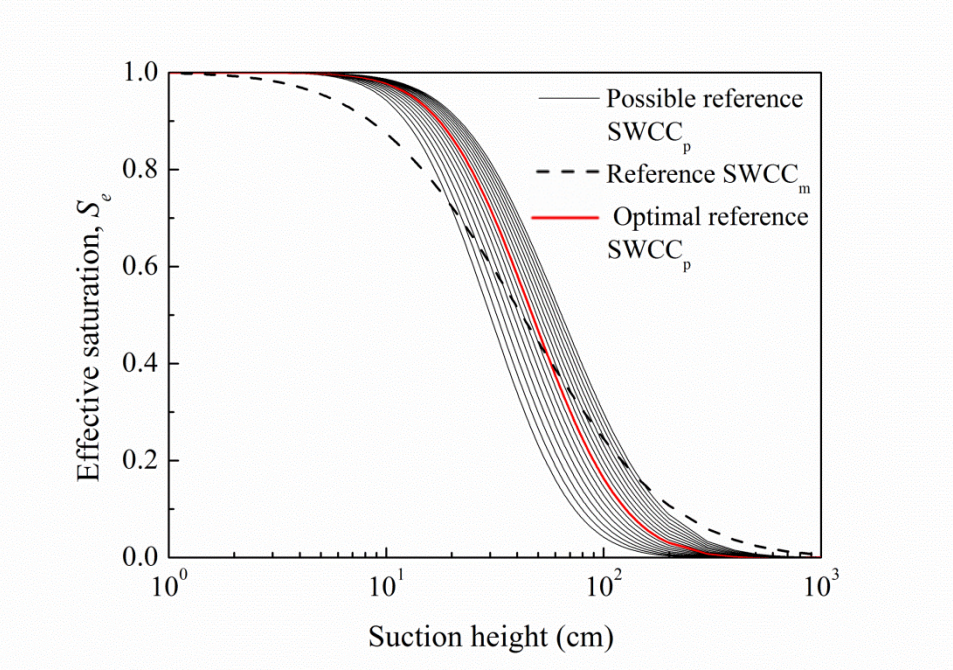

Figure 3.13 Reference $SWCC_m$ (red solid line), possible reference $SWCC_p$ (gray solid lines) and optimal reference $SWCC_p$ (black dash line) correspond to α_{opt} for sand

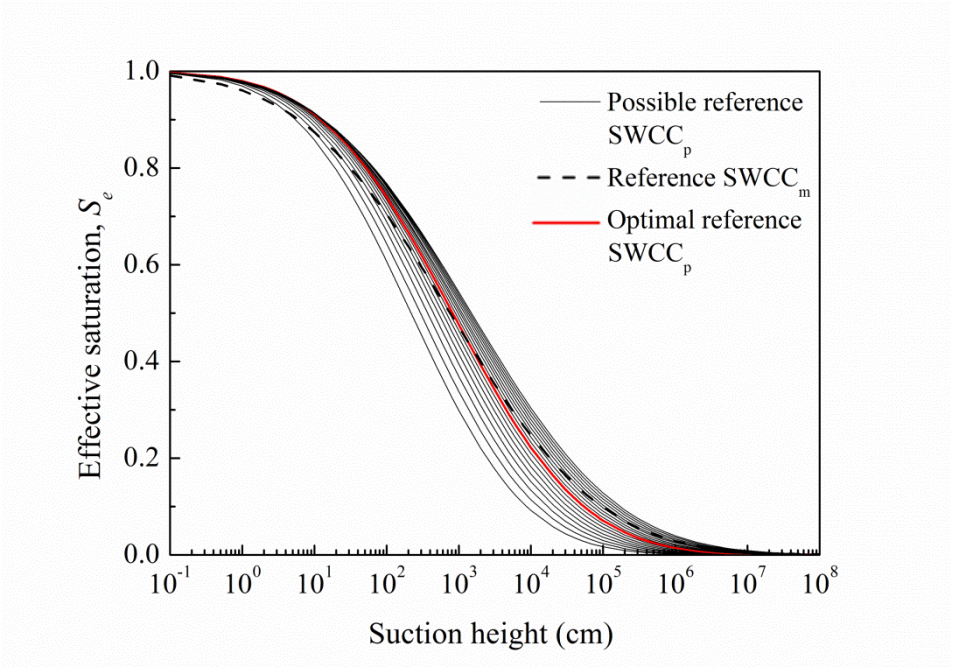

Figure 3.14 Reference $SWCC_m$ (red solid line), possible reference $SWCC_p$ (gray solid lines) and optimal reference $SWCC_p$ (black dash line) correspond to α_{opt} for sandy loam

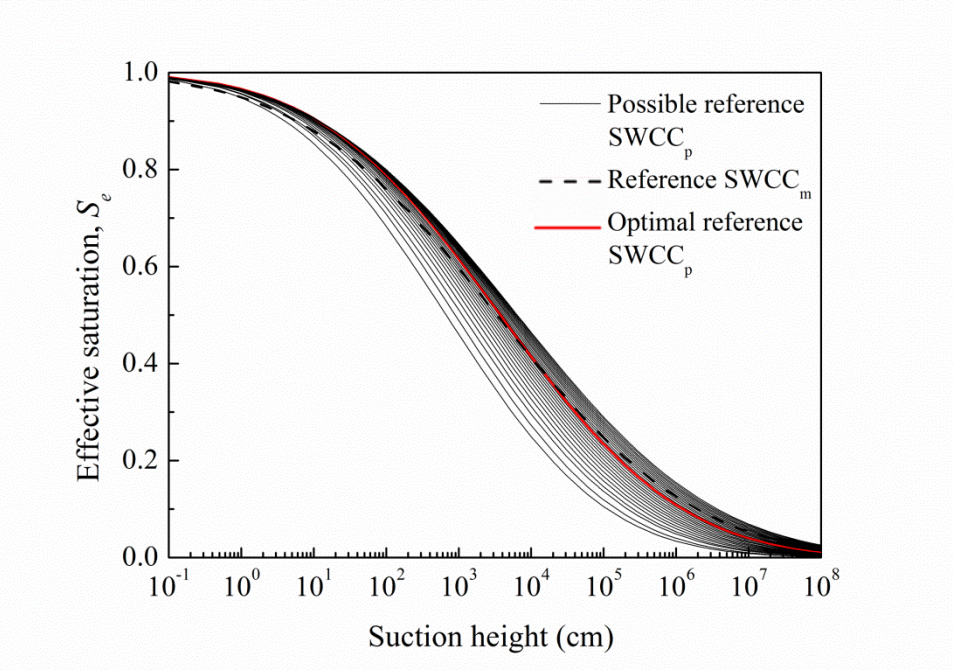

Figure 3.15 Reference $SWCC_m$ (red solid line), possible reference $SWCC_p$ (gray solid lines) and optimal reference $SWCC_p$ (black dash line) correspond to α_{opt} for loam

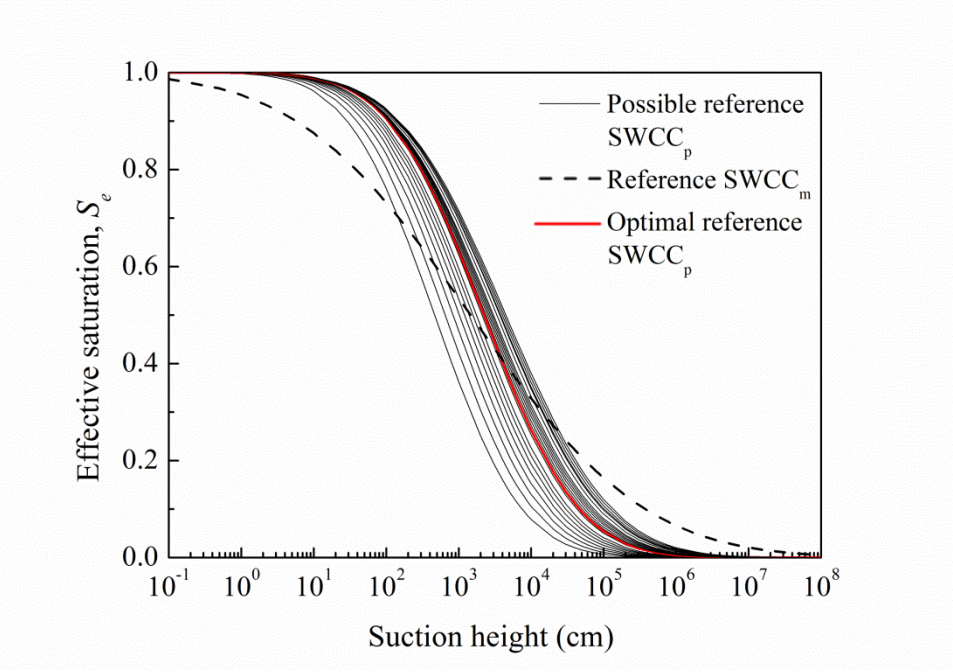

Figure 3.16 Reference SWCCm (red solid line), possible reference SWCCp (gray solid lines) and optimal reference SWCCp (black dash line) correspond to α_{opt} for silt loam

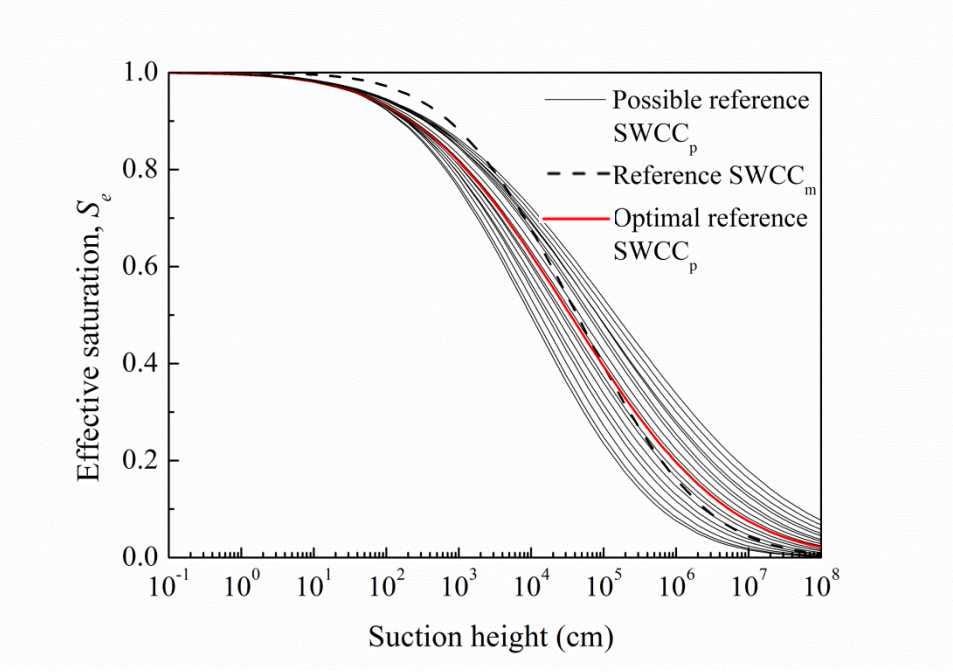

Figure 3.17 Reference $SWCC_m$ (red solid line), possible reference $SWCC_p$ (gray solid lines) and optimal reference $SWCC_p$ (black dash line) correspond to α_{opt} for clay

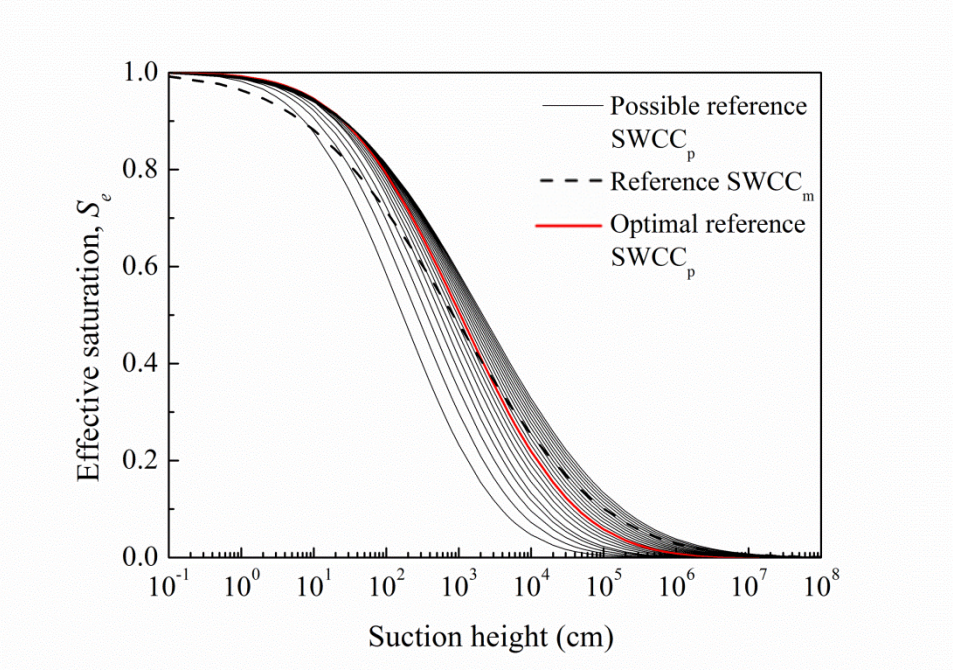

Figure 3.18 Reference SWCCm (red solid line), possible reference SWCCp (gray solid lines) and optimal reference SWCCp (black dash line) correspond to α_{opt} for all the soils

3.3.3 Verification results

The SWCCs of all testing soils were predicted using optimal α values in Table 3.4 for each texture and all the soils. The results were compared with the predictions of the methods in Table 3.2. Figures 3.19-3.23 show the ability of eight α equations to predict the data for five textural soils. Typical examples of predicted and measured SWCCs for sand (code: 4650), sandy loam (code: 3311), loam (code: 3302), silt loam (code: 2012), and clay (code: 2361) soils are presented in figures 3.19-3.23. Figures 3.19-3.23 show that compare with other approaches, the use of proposed α_{opt} values for each texture ($\alpha_{opt,\,T}$, blue dash lines) and all the soils ($\alpha_{opt,\,A}$, blue solid lines) improve the AP estimation. It is worth to note that when applied the $\alpha_{opt,\,T}$ values for corresponding textural class obtain the best agreement between the experimental with calculated SWCCs in all case. For other approaches, using linear equation causes a great overestimation of water content, θ, in all case. In contrary, using α=0.938, logistic equation and $\alpha=f(\theta)$ cause underestimation of water content, θ, in higher suction range.

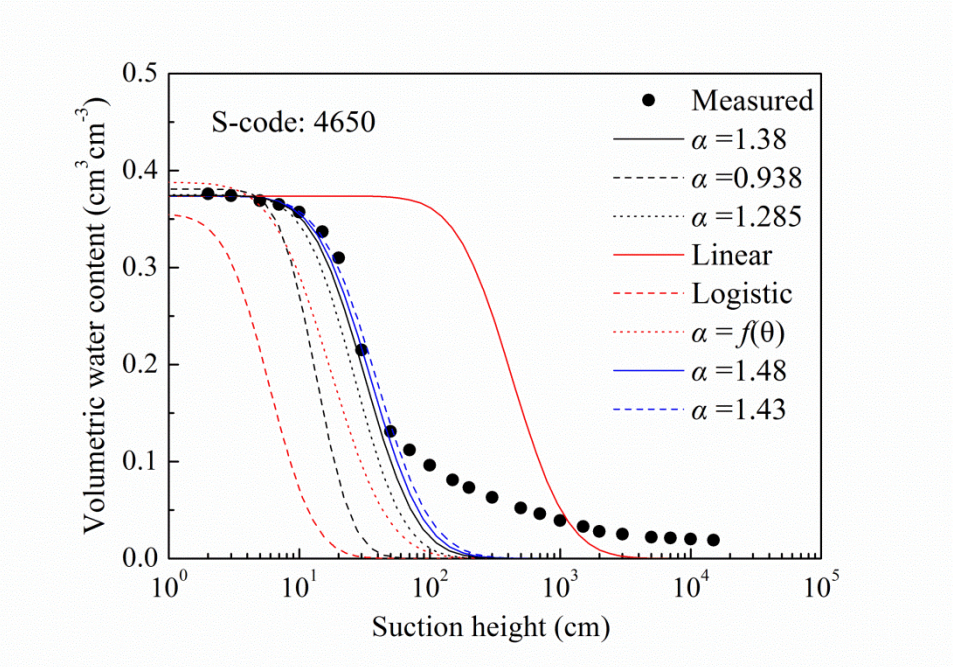

Figure 3.19 Comparison of SWCC prediction methods with experimental data for sand

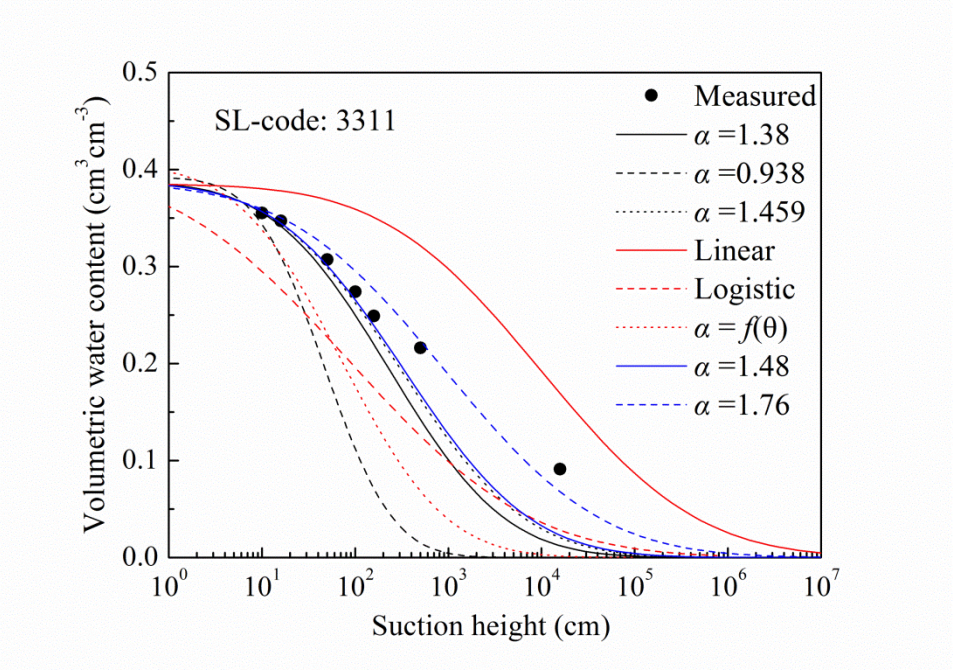

Figure 3.20 Comparison of SWCC prediction methods with experimental data for sandy loam

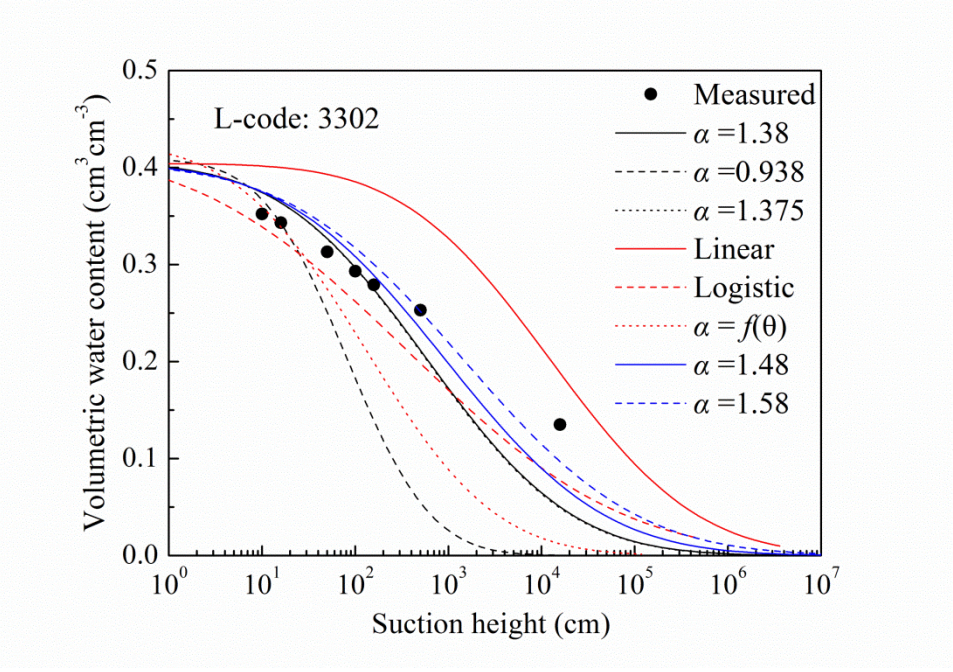

Figure 3.21 Comparison of SWCC prediction methods with experimental data for loam

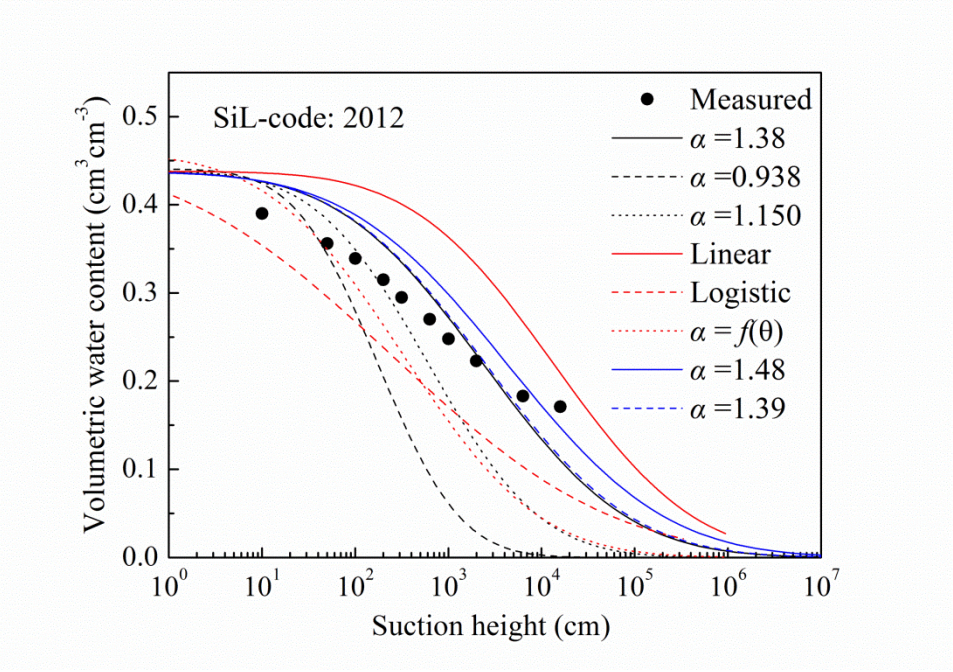

Figure 3.22 Comparison of SWCC prediction methods with experimental data for silt loam

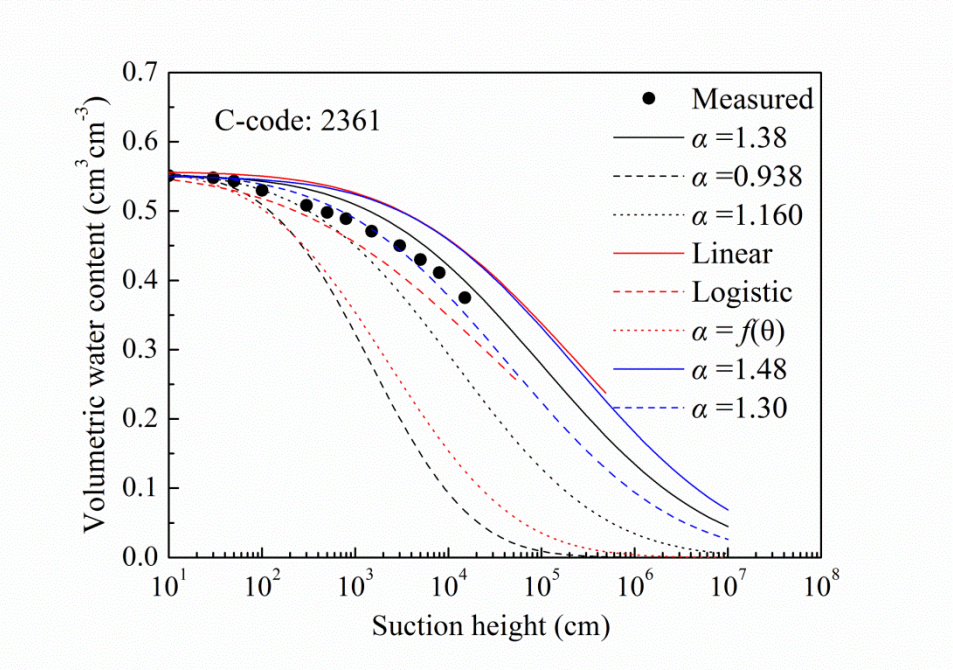

Figure 3.23 Comparison of SWCC prediction methods with experimental data for clay

The overall predictive ability of the eight α equations are presented in Figures 3.24-3.31, which is evaluated by comparing measured and predicted water content, θ, at the applied suction heads for all testing soils in Table 3.1. And Table 3.5 shows the root mean square error (RMSE) between measured and estimated θ. Table 3.5 indicates that the best AP model estimation is obtained with the optimal α values for corresponding textural class (i.e. $\alpha_{opt,\,T}$) that provides RMSE of 0.032, followed the optimal α values for all the soils (i.e. $\alpha_{opt,\,A}$) provides RMSE of 0.038. The results indicate that more accurate predicted results will be got when calculating α for each textural class respectively. This is probably due to soils are separated by textural class are more similar than when all soils are considered together. The worst estimation is obtained with logistic equation that provides RMSE of 0.235, although it works relatively well for clay soils (see Figure 3.23).

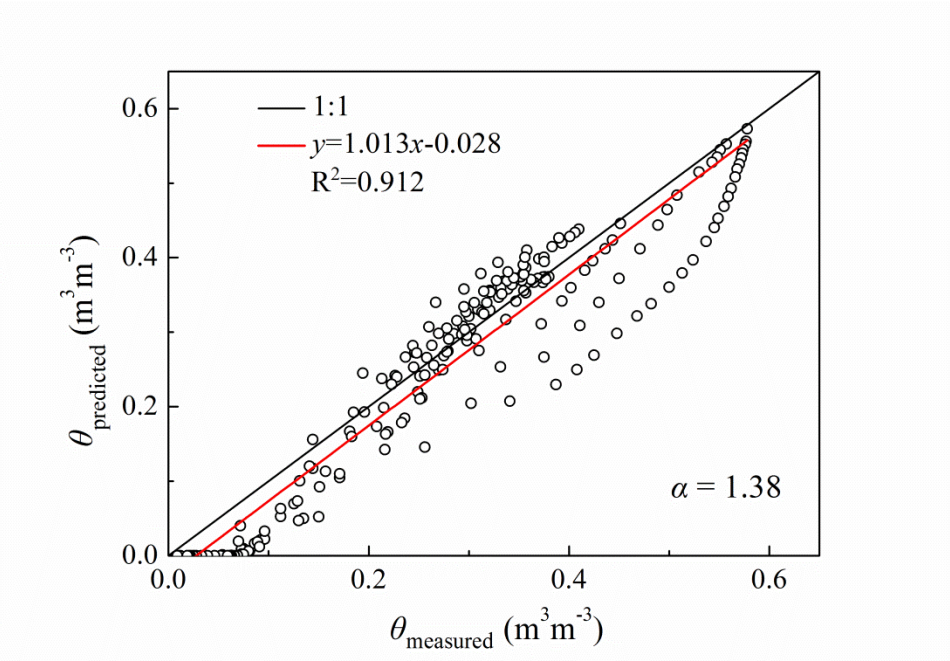

Figure 3.24 Comparison measured and predicted volumetric water content, θ, using α=1.38 for all testing soils. The 1:1 line is a black solid line and the best-fit line is a red solid line, R^2 denotes coefficient of determination

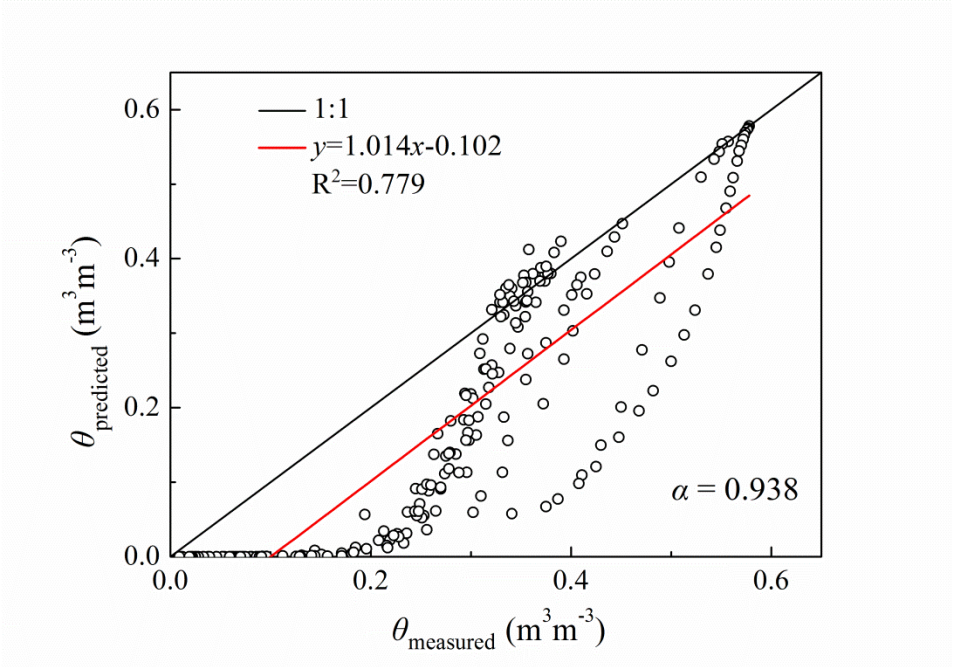

Figure 3.25 Comparison measured and predicted volumetric water content, θ, using α=0.938 for all testing soils. The 1:1 line is a black solid line and the best-fit line is a red solid line, R^2 denotes coefficient of determination

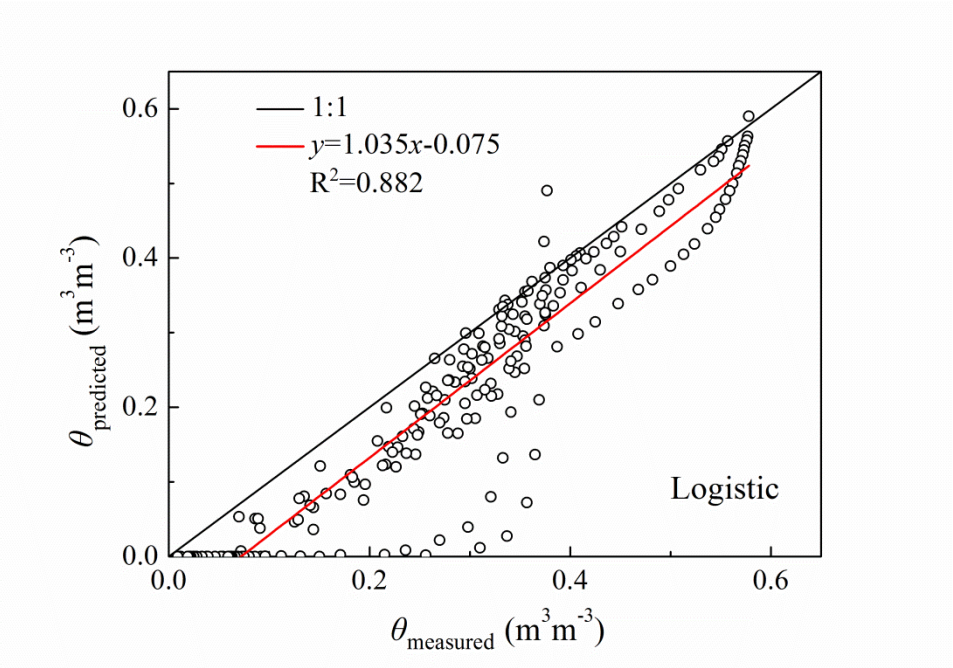

Figure 3.26 Comparison measured and predicted volumetric water content, θ, using logistic equation for all testing soils. The 1:1 line is a black solid line and the best-fit line is a red solid line, R^2 denotes coefficient of determination

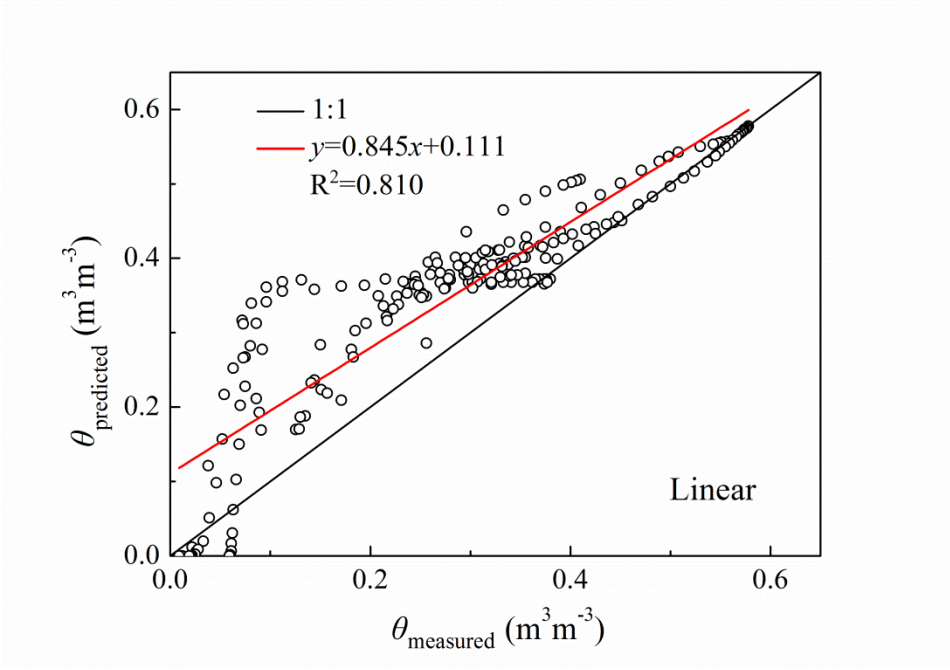

Figure 3.27 Comparison measured and predicted volumetric water content, θ, using linear equation for all testing soils. The 1:1 line is a black solid line and the best-fit line is a red solid line, R^2 denotes coefficient of determination

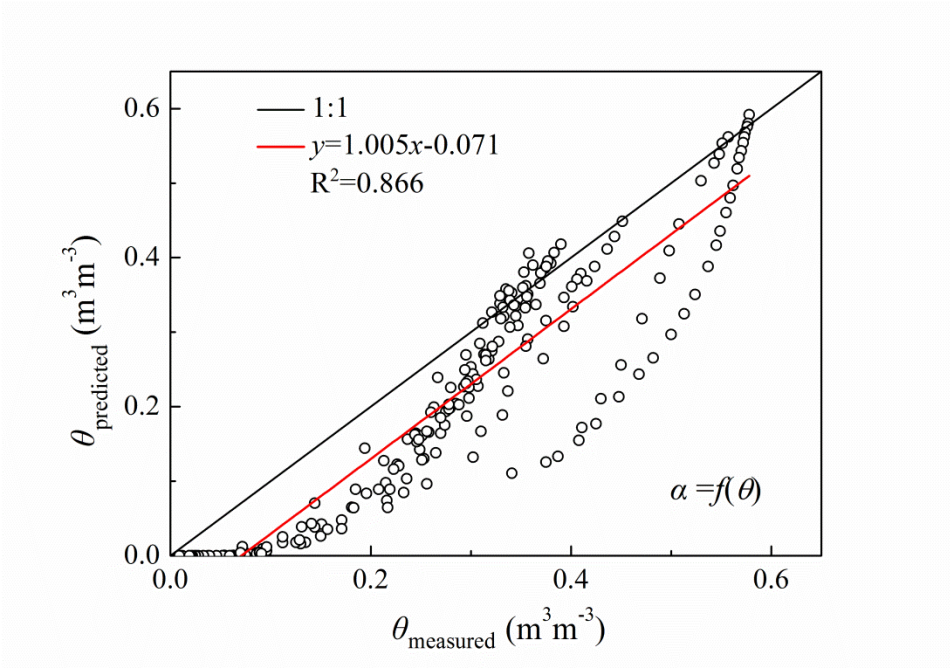

Figure 3.28 Comparison measured and predicted volumetric water content, θ, using Vaz's equation for all testing soils. The 1:1 line is a black solid line and the best-fit line is a red solid line, R^2 denotes coefficient of determination

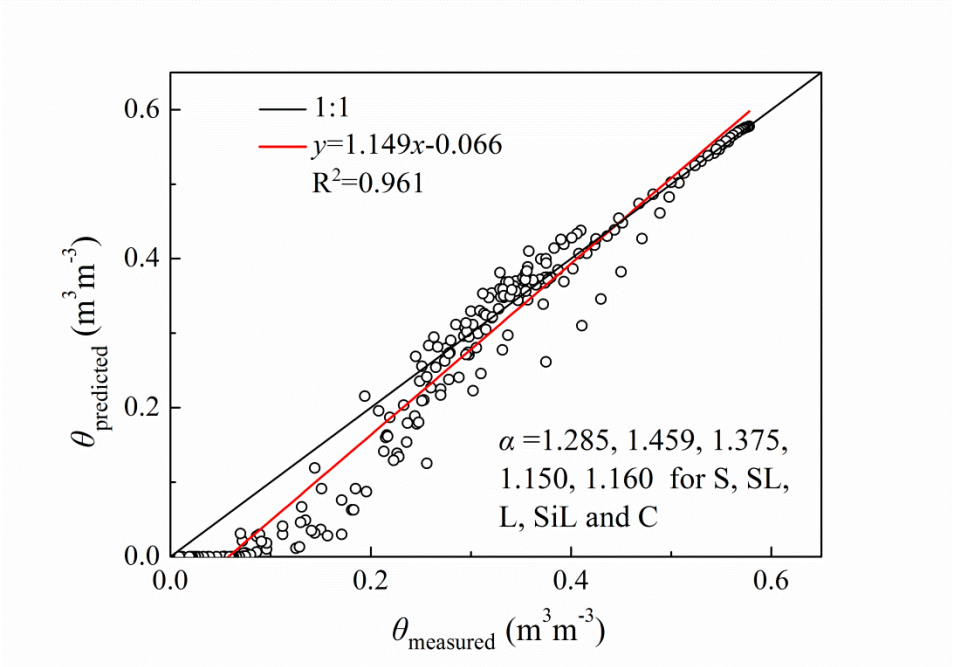

Figure 3.29 Comparison measured and predicted volumetric water content, θ, using α value proposed by Arya et al., (1999) (i.e. α=1.285, 1.459, 1.375, 1.150, and 1.160 for the S, SL, L, SiL, and C soils) for all testing soils. The 1:1 line is a black solid line and the best-fit line is a red solid line, R^2 denotes coefficient of determination

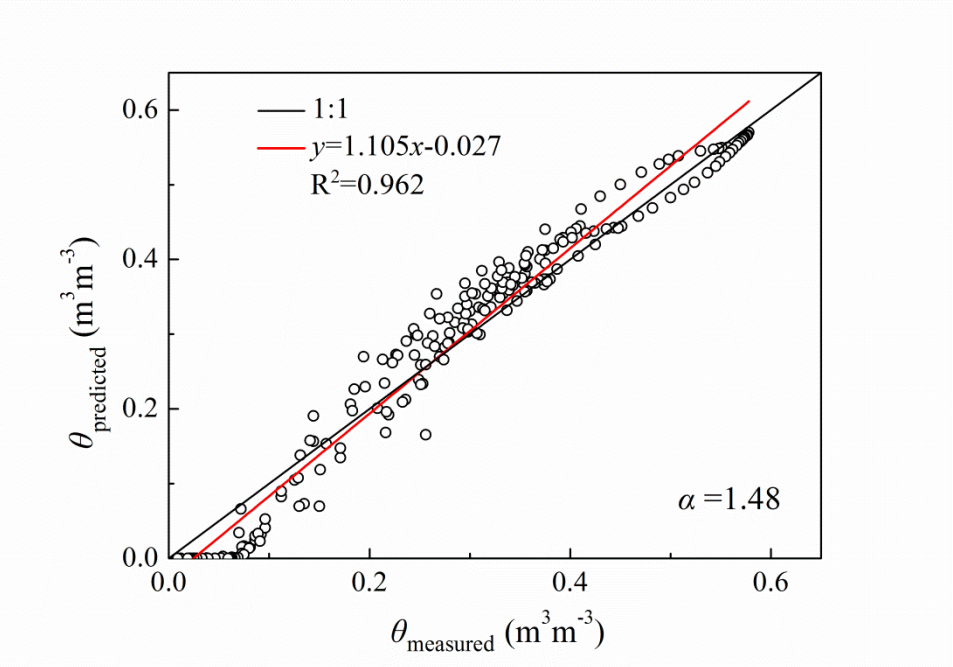

Figure 3.30 Comparison measured and predicted volumetric water content, θ, using α=1.48 for all testing soils. The 1:1 line is a black solid line and the best-fit line is a red solid line, R^2 denotes coefficient of determination

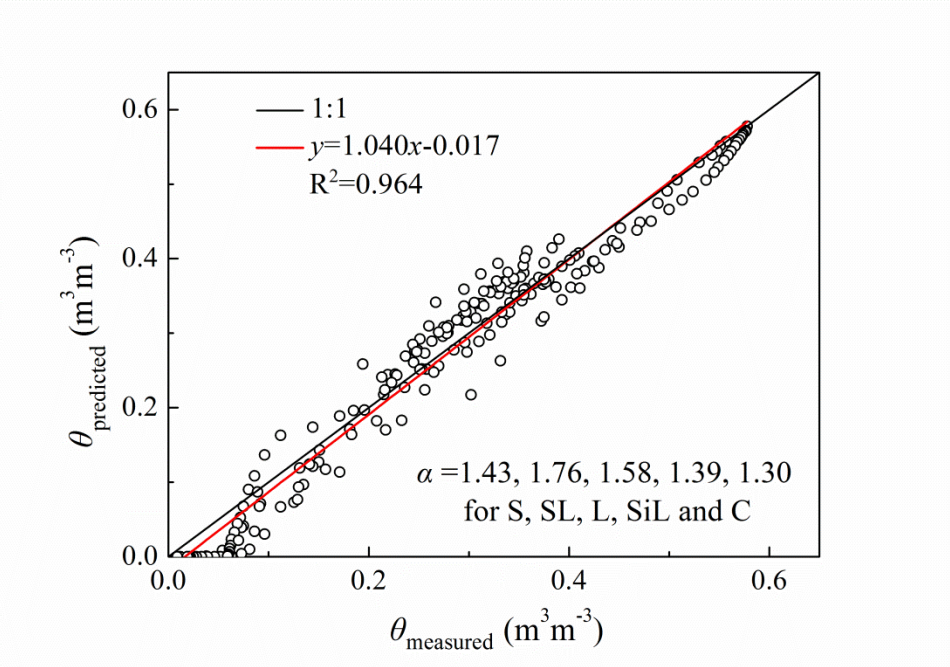

Figure 3.31 Comparison measured and predicted volumetric water content, θ, using α value (i.e. α=1.43, 1.76, 1.58, 1.39, and 1.30 for the S, SL, L, SiL, and C soils) for all testing soils. The 1:1 line is a black solid line and the best-fit line is a red solid line, R^2 denotes coefficient of determination

Table 3.5 Comparison of RMSE values for different SWCCs prediction results

Method	α=1.38	α=0.938	Linear	Logistic	$\alpha=f(\theta)$	$\alpha=\alpha_{c,T}$[a]	$\alpha=\alpha_{opt,A}$[b]	$\alpha=\alpha_{opt,T}$[c]
RMSE	0.054	0.128	0.095	0.235	0.093	0.049	0.038	0.032

[a]$\alpha_{c,T}$ is constant α value for each soil texture (i.e. α=1.285, 1.459, 1.375, 1.150, and 1.160 for the S, SL, L, SiL, and C soils) proposed by Arya et al., (1999); [b]$\alpha_{opt,A}$ is optimal α value for all soils combined together (i.e. α=1.48); [c]$\alpha_{opt,T}$ is optimal α value for each soil texture (i.e. α=1.43, 1.76, 1.58, 1.39, and 1.30 for the S, SL, L, SiL, and C soils).

Figures 3.24-3.31 show that the proposed $\alpha_{opt,T}$ values for corresponding textural class (Figure 3.31) appear an overall good agreement between measured and predicted water content, θ. The linear regression has the highest coefficients of determination (R^2) of 0.964 and the regression line differed only slightly from the 1:1 line. Although the regression appears to be good with an R^2 of 0.962, the $\alpha_{opt,A}$ values for all the soils

(Figure 3.30) led to underestimation in the dry range and overestimation in the wet range (Figure 3.31 also has this phenomenon but appear slightly). This can partially be explained that at low suction heads, AP model assumes complete desorption of all pores, however, it is impossible in the practical case. And at high suction heads, a significant percentage of water may be held as film and in poorly connected pores. As a result, the model will tend to underestimate the water content in the high suction regions and overestimate the water content in the low suction regions.

Regarding other methods, some approaches appear to produce great bias. Figures 3.24-3.31 show that use of α=0.938 (Figure 3.25), logistic equation (Figure 3.26), and $\alpha=f(\theta)$ (Figure 3.28) underestimate soil water content both in the dry range and wet range. In contrast, linear equation (Figure 3.27) overestimates soil water content in all ranges.

In summary, compared with other predicted approaches the PBS approach exhibited better agreement between the measured and estimated SWCC, especially when applied the PBS approach to soils with similar texture. We conclude that the PBS technique combine with the AP model is a more effective and feasible approach to predict SWCC from PSD.

3.4 SUMMARY

In this chapter, the physically based scaling technique (Kosugi and Hopmans, 1998) was extended to the Arya and Paris model, calculating α to predict soil water characteristic curve from particle-size distribution. A total of 50 experimental soil data that representing a range of textures that include sand, sandy loam, loam, silt loam, and clay, were selected from the Unsaturated Soil hydraulic Database (Nemes et al., 2001) for this purpose. In addition, 19 soil samples with different textures were used to test this method. Results showed that the physically based scaling technique improved the Arya and Paris estimation and outperformed other approaches. Especially, when applied the physically based scaling technique approach to soils with similar texture. It should be noted that this study has examined only Unsaturated Soil hydraulic Database. Notwithstanding its limitation, this study can clearly demonstrate

the potential capability to apply the physically based scaling technique for estimating the soil water characteristic curve is a robust method in soil hydrologic studies.

REFERENCES

Arya, L.M. and Paris, J.F. 1981 A physico-empirical model to predict the soil moisture characteristic from particle-size distribution and bulk density data. Soil Science Society of America Journal, 45(6) 1023-1030.

Arya, L.M., Leij F.J., Van Genuchten, M. Th. and Shouse, P. 1999 Scaling parameter to predict the soil water characteristic from particle-size distribution data. Soil Science Society of America Journal, 63(3) 510-519.

Arya, L.M., Bowman, D.C., Thapa, B.B. and Kassel, D.K. 2008 Scaling soil water characteristics of golf course and athletic field sands from particle-size distribution. Soil Science Society of America Journal, 72(1) 25-32.

Basile, A. and D'urso, G. 1997 Experimental corrections of simplified methods for predicting water retention curves in clay-loamy soils from particle-size determination. Soil Technology, 10(3) 261-272.

Bhabani, S.D., Nathan, W.H., and P. Suresh, C.R. 2005 Defining Geometric Similarity in Soils. Vadose Zone Journal, 4(2) 264-270.

Buchan G.D. 1989 Applicability of the simple lognormal model to particle-size distribution in soils. Soil Science, 147(3) 155-161.

Chan, T.P. and Govindaraju, R.S. 2004 Soil water retention curves from particle-size distribution data based on polydisperse sphere systems. Vadose Zone Journal, 3(4) 1443-1454.

Fredlund, D.G. and Xing, A. 1994 Equations for the soil water characteristic curve. Canadian Geotechnical Journal, 31(4) 521-532.

Henry, E.J. and Smith, J.E. 2006 Numerical demonstration of surfactant concentration-dependent capillarity and viscosity effects on infiltration from a constant flux line source. Journal of Hydrology, 329(1) 63-74.

Hopmans, J.W., Nielsen, D.R. and Bristow, K.L. 2002 How useful are small-scale soil hydraulic property measurements for large-scale vadose zone modeling? (In Pa Raats et al. (Eds.) Environmental mechanics: Water, mass, and energy transfer in the biosphere. Geophys. Monogr. (129 pp.247-258). AGU, Washington, DC.)

Ireson, A.M., Mathias, S.A., Wheater, H.S., Butler, A.P. and Finch, J. 2009 A model for flow in the chalk vadose zone incorporating progressive weathering. Journal of Hydrology, 365(3) 244-260

Kosugi, K. and Hopmans, J.W. 1998 Scaling water retention curves for soils with lognormal pore size distribution. Soil Science Society of America Journal, 62(6) 1496-1505.

Miller, E.E. and Miller, R.D. 1956 Physical theory of capillary flow phenomena. Journal of Applied Physics, 27(4) 324-332.

Nemes, A., Schaap, M.G. and Leij, F.J. 2001 Description of the unsaturated soil hydraulic database UNSODA version 2.0. Journal of Hydrology, 251(3) 151-162.

Peck, A.J., Luxmoore, R.J. and Stolazy, J.C. 1977 Effects of spatial variability of soil hydraulic properties in water budgetmodelling. Water Resource Research, 13(2) 348-354.

Schulze, B.E., Hutson, J.L. and Cass A. 1985 Hydrological characteristics and properties of soils in Southern Africa 2: Soil water retention models. Water SA 11(3) 129-136.

Tuli, A., Kosugi, K. and Hopmans, J.W. 2001 Simultaneous scaling of soil water characteristic and unsaturated hydraulic conductivity functions assuming lognormal pore size distribution. Water Resource Research, 24(6) 677-688.

Tyler, S. and Wheatcraft, S. 1989 Application of fractal mathematics to soil water characteristic estimation. Soil Science Society of America Journal, 53(4) 987-996.

Vaz, C.M.P., Iossi, M.D.F., Naime J.D.M., Macero, A., Reichert, J.M., Reinert, D.J. and Cooper, M. 2005 Validation of the Arya and Paris water retention model for Brazilian soils. Soil Science Society of America Journal, 69(3) 577-583.

Warrick, A.W., Mullen, G.J. and Nielsen, D.R. 1977 Scaling field measured soil hydraulic properties using similar media concept. Water Resource Research, 13(2) 355-362.

CHAPTER 4

4. CHARACTERIZATION OF DUAL-POROSITY SOILS

4.1 INTRODUCTION

Dual-porosity soils such as diatomaceous earths and zeolites not only have pores between particles also have pores inner particles. These structural soils have been identified as soil amendment materials in high sand content root zones (Waltz et al. 2003).

Natural diatomaceous earth, also known as diatomite, is a sedimentary deposit formed from the inorganic skeletal remains of single-cell algae and plankton. Dead algae and plankton, called diatoms, settle on the bottom of seas and lakes and form layers of diatomaceous earth. The organic matter decays and the shells form a deposit with interconnected pores of sizes appropriate for microbiological growth and filtering of solids suspended in water. The structure and distribution of these interconnected pores result in a relatively high porosity (typically >70%) and high surface area (Breese 1994). This naturally occurring diatomaceous earth has been used as engineered fill in California (Khilnani and Capik 1989; Day 1995). The diatomaceous earth layers also are mined and processed to segregate the particles by size and remove impurities for commercial use.

In the process of mining diatomaceous earth for industrial applications, the diatomaceous earth deposits first are crushed into aggregate sizes before being subjected to a mill drying process that results in smaller particle sizes. The diatomaceous earth then is packed as a natural milled product for use as a filter aid and filler material to enhance and alter material properties. If the diatomaceous earth is to be used as a filter material, further processing, known as either calcination (thermal processing) or flux calcination (calcination with a fluxing agent), may be

necessary to increase the permeability. In the process of calcination, the particles of diatomaceous earth are bonded together to form larger particle sizes (Lange 1983; Breese 1994). A range of particle sizes from powder to pellets several millimetres in diameter can be produced in the calcination process. Other properties of diatomaceous earth pertaining to industrial applications are described by Breese (1994).

The majority of mined and processed diatomaceous earth is used in filter applications to separate suspended solids from fluids (Breese 1994). These applications include filtering of solvents, pharmaceuticals, beer, wine, whiskey, raw sugar, liquors, antibiotics, and industrial, municipal, and swimming pool waters. Diatomaceous earth also is used as a biological growth medium for microorganisms in biological filtration, a soil amendment to increase drainage and water-holding capacity, and a hydroponic medium for plant growth. For example, Lukasik et al. (1996) evaluated the use of diatomaceous earth coated with metal hydroxides to improve adsorption of microorganisms during biological filtration. In addition, diatomaceous earth recently has been used for bioremediation of contaminated soil and as the biological growth medium in constructed wetlands for runoff treatment (Stavnes et al. 1996; Sundine Enterprises, Inc. 1996).

Zeolites constitute a large class of secondary minerals consisting of aluminosilicate with loosely bonded alkali and/or alkali-earth cations and water molecules (Hey, 1930). They are commonly formed at low temperature and pressure in the presence of water (Armbruster and Gunter, 2001). More than 80 natural zeolite species have been identified (Coombs et al., 1998). Of these, chazabite, clinoptilolite, erionite, mordenite, and phillipsite are the most commonly used for agronomic, horticultural, and soil remediation applications. Zeolites have two properties that make them desirable for agronomic and horticultural use: (1) high cation exchange capacity (CEC) due to the substitution of Al^{3+} for Si^{4+} during formation and (2) large internal channels created by three dimensional (3D) framework of silica and alumina tetrahedron that gives zeolites low bulk densities and allow for retention of water and exchange of cations.

Zeolites seem to have the greatest potential as an amendment. Zeolites have physical characteristic similar to sand, thereby retaining rapid drainage and resistance to compaction it increases CEC and water retention capacity. zeolites have a preference for bonding K^+ ions over Ca^{2+} ions (Li et al ., 2000). This suggests that inorganic amendments have potential substitutes for peat. In addition to being widely used as molecular sieves in the petrochemical industries, zeolites have been used as materials for supplying plants with potassium and phosphate (Chen and Gabelman, 1990; Williams and Nelson, 1997) and as adsorbents for reducing nitrogen transformation.

For aggregated diatomaceous earth and zeolites, two distinct pore size distributions commonly exist, one for the macroscopic porosity region between the particles (interpellet porosity) and another distribution for the microscopic porosity region within the particles (intrapellet porosity). The existence of two distinct pore size distributions in other porous media has resulted in the measurement of bimodal soil water characteristic curves. In the majority of studies, bimodal soil water characteristic curves have been observed for structured soils, such as aggregated loams (Smettem and Kirby 1990; Wilson et al. 1992; Durner 1994; Mallants et al. 1997). Othmer et al. (1991) attributed the observation of bimodal soil water characteristic curves for a fluvial loess deposit to the existence of wormholes resulting in “vertical tubular macropores.” Bimodal soil water characteristic curves also have been observed for porous media that exhibit significant secondary structure, such as fractured tuff (Peters and Klavetter 1988; Pruess et al. 1990; Wang and Narasimhan 1985, 1990).

Based on the bimodal pore size distributions typically associated with naturally occurring, aggregated diatomaceous earth and zeolites, the soil water characteristic curves for commercially processed, pelletized diatomaceous earth and zeolites also are expected to be bimodal. Thus, the hypothesis for this study is that the soil water characteristic curves for pelletized diatomaceous earth are bimodal. This hypothesis will be evaluated by measuring the soil water characteristic curve data of four pelletized diatomaceous earth and zeolites using two different methods of

measurement to cover a broad range of suctions.

4.2 Materials and methods

4.2.1 Materials

The materials used in this study represent two sizes of processed diatomaceous earth pellets and two zeolites with different particle-size distributions. The diatomaceous earth was utilized as both raw and calcined forms which were collected from Oita Prefecture of Japan (Showa Chemical Industry Co., Ltd.) under the product names RC417 and #3000, respectively. The advantages of calcination are removal of organic matter, removal of carbonate compounds, higher filtration rate depending on opening up of the diatom frustules, and aggregation owing to sintering and shrinkage of the particles. The two raw zeolites with different size used in this study are referred to as 2460 and 1424 (Shin Tohoku Chemical Industry Co., Ltd.), respectively. Chemical compositions of materials are given in Table 4.1.

Table 4.1 Chemical compositions of materials

Constituents	#3000	RC417	2460	1424
SiO_2 (%)	85.17	86.48	72.10	72.10
Al_2O_3 (%)	5.46	8.62	12.90	12.90
Fe_2O_3 (%)	1.86	2.20	0.70	0.70
CaO (%)	0.93	0.91	2.60	2.60
MgO (%)	0.20	0.52	0.00	0.00
K_2O (%)	0.47	0.25	2.10	2.10
Na_2O (%)	5.52	0.73	1.80	1.80
H_2O (%)	0.00	0.00	7.00	7.00
others (%)	0.39	0.29	0.80	0.80

Figure 4.1 is a photograph of the #3000 and RC417 pellets and the two zeolites.

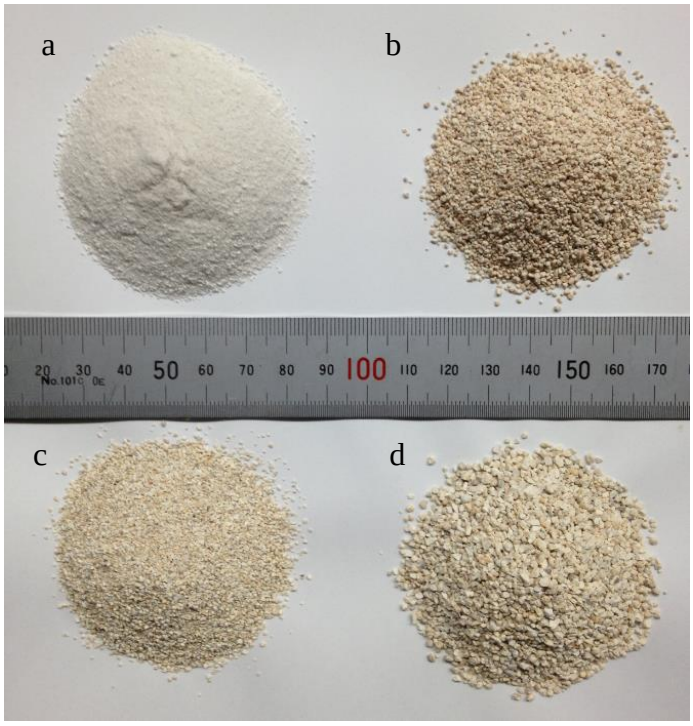

Figure 4.1 Photograph of materials (a, #3000; b, RC417; c, 2460; d, 1424)

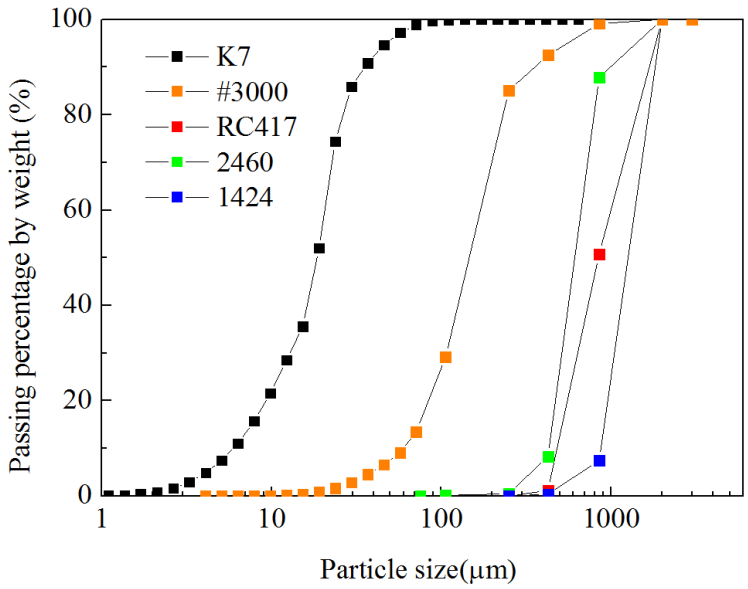

Figure 4.2 Particle size distribution for diatomaceous earth and zeolites

Figure 4.2 shows the particle-size distributions for the materials. The results are compared with a single-porosity sandy soil, K7 sand. As shown in Figure 4.2, the K7 sand is finer than both diatomaceous earth and zeolites. The RC417 is coarser than the 2460 pellets and finer than the 1424 pellets. Both of the zeolites as well as the #3000 and RC417 pellets classify as poorly graded materials.

The measured specific gravity and the maximum and minimum densities for each

material are shown in Table 4.2, along with the calculated total porosity at the maximum densities. The lower dry densities for the diatomaceous earth and zeolite pellets reflect the existence of internal pore space in the pellets. The primary characteristic of the diatomaceous earth and zeolites pellets is the existence of a microscopic porosity within the pellets. Thus, a packing of the pellets will consist of both a macroscopic porosity between the pellets (interpellet porosity) and a microscopic porosity within the pellets (intrapellet porosity).

Table 4.2 Physical properties of materials

Property	#3000	RC417	2460	1424	K7
Specific gravity, G_s	2.30	2.33	2.35	2.35	2.61
Maximum dry density, $\rho_{d,\max}$ (g/cm^3)	0.42	0.45	0.85	0.74	1.58
Minimum dry density, $\rho_{d,\max}$ (g/cm^3)	0.30	0.37	0.69	0.62	1.24
Total porosity, $n_{\max}$ (%)	81.74	80.44	63.83	68.51	39.46

$n_{\max}=1-\rho_{d,\max} / G_s\rho_w$, where ρ_w = density of water.

The total porosity of the #3000 and RC417 pellets also ranges from about 12 to 18 percentage points higher than the total porosity of the zeolites. The total porosity of the 2460 is approximately 5 percentage points lower than the total porosity of the 1424 due to the slightly larger particle sizes of the 1424. Compare k7, the lower specific gravity, lower dry densities and higher total porosity for the diatomite and zeolites reflect there are inner structures in the particles.

4.2.2 Measurement of micro-porosity structure

The micro-porosity structure of a soil provides important information on the hydraulic conductivity, and soil-water characteristics of the soil. To investigate the formation of a micro-porosity structure of the diatomaceous earth and zeolites pellets, scanning electron microscopy (SEM) was used to characterize the soil surface structure directly, and mercury intrusion porosimetry (MIP) was used to quantify the soil pore size distribution (PSD).

A scanning electron microscope (Shimadzu Corp., Superscan SS-550S), as shown in Figure 4.3, was used in this study. The macro-micro fabric at the soil surface can be recognized from the backscattered electron scanning images.

MIP is routinely and effectively used to measure the PSDs of powder and bulk materials with open and interconnected pore structures. An automated mercury porosimeter (Shimadzu Corp., Autopore III), as shown in Figure 4.4, was used in this study.

Figure 4.3 Photography of Scanning Electron Microscope

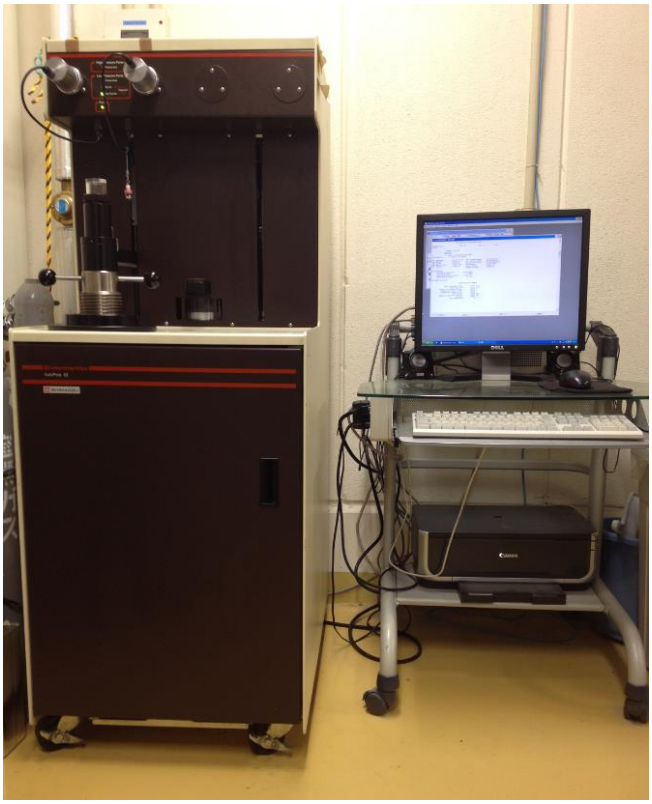

Figure 4.4 Photography of Automated Mercury Porosimeter

4.2.3 Measurement of soil water characteristic curves

Two methods were used to measure the soil water characteristic curve data of the materials reported in this study: the Tempe cell method and the centrifuge method. Soil suctions < 5 kPa were measured using Tempe cells (Figure 4.5); volumetric water contents corresponding to soil suctions ranging from 5 to 1680 kPa were measured using a centrifuge apparatus (Figure 4.6) (model No. 6500, KUBOTA Corporation).

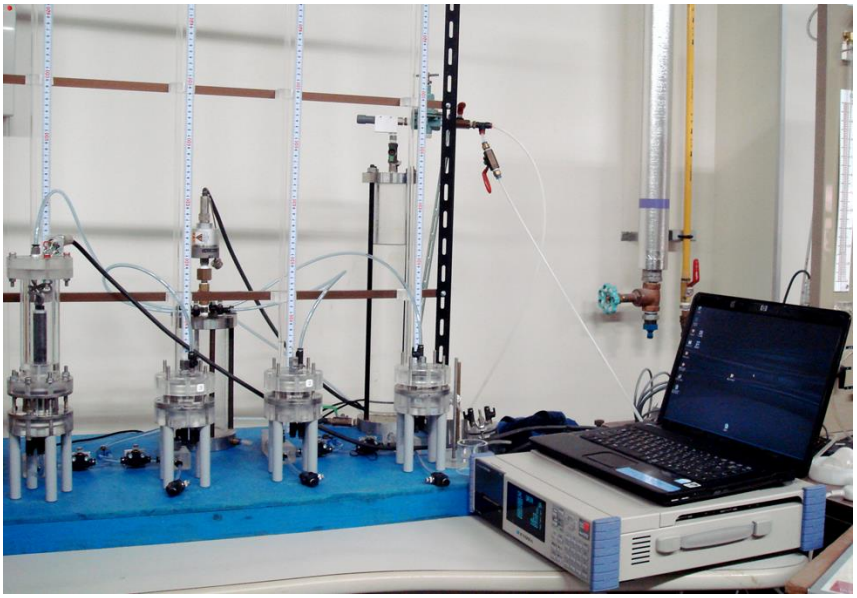

Figure 4.5 Photography of SWCC measurement using Tempe cells

Figure 4.6 Photography of High Speed Refrigerated Centrifuge

Soil suction measurements were performed for specimens prepared at the maximum dry density to reduce the effect of changes in density on the size of the macroscopic pores. The dimensions of the specimen container were measured using a micrometer, and the volumes of the specimen containers were calculated from these measurements. The mass of dry material based on the maximum dry density was calculated using the volumes of the specimen containers.

For the Tempe cell and centrifuge measurements, the dry mass of material corresponding to the maximum dry density was placed directly into the specimen rings and saturated through the porous plate.

4.3 RESULTS

4.3.1 Micro-porosity structure

1) MIP

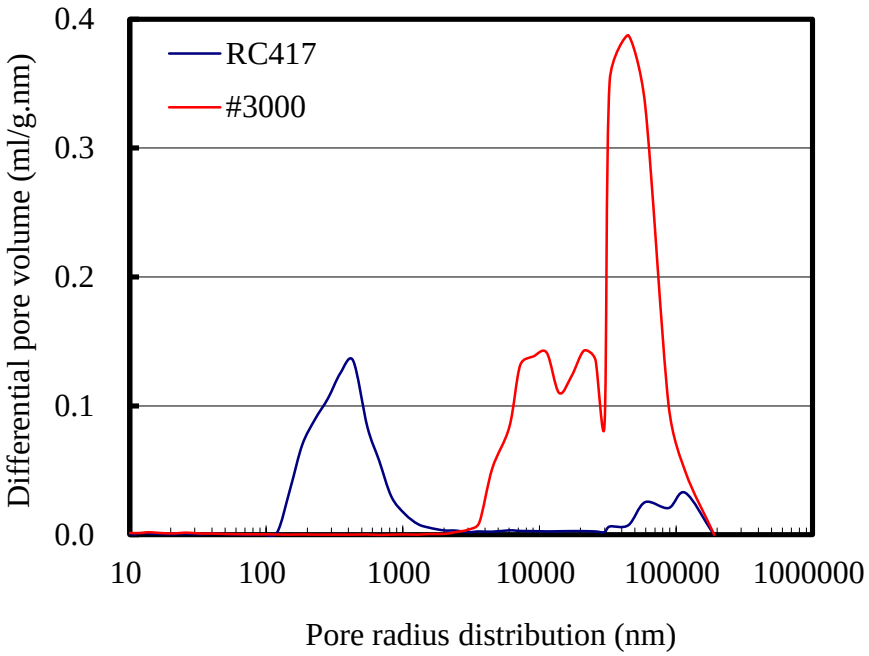

Figure 4.7 Pore radius distribution by mercury intrusion of diatomaceous earth

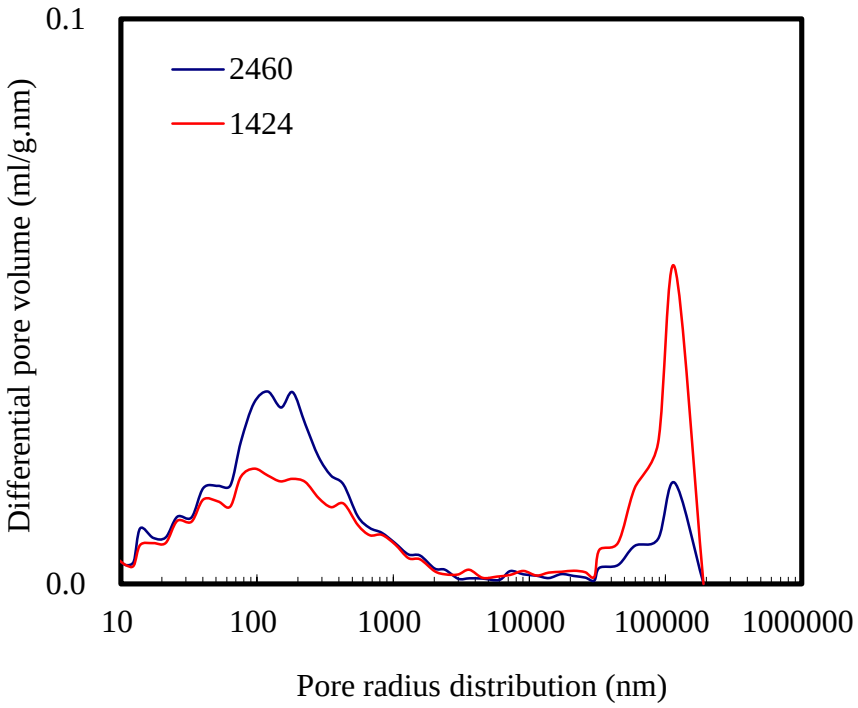

Figure 4.8 Pore radius distribution by mercury intrusion of zeolites

Mercury intrusion porosimetry was used to determine the pore radius distribution in the meso and macro range. Figure 4.7 and 4.8 show that the pore radius distribution of diatomaceous earth and zeolites which measured by Hg-intrusion porosimetry.

Figure 4.7 and 4.8 indicate that the porosity of the raw diatomaceous earth (RC417) and raw zeolites samples (2460 and 1424) essentially consists of the intra-aggregate pores with inter-aggregate pores. The peaks value of intra-aggregate and inter-aggregate pores of RC417 at pore radii, around 300-500 nm and 100000-200000 nm, respectively. However, the #3000 pore radius distribution is very different. This result is in good agreement with the coalescence behaviour of the diatoms. The #3000 loss of smaller pores was also verified by mercury intrusion (Figure 4.7) and scanning electron microscope analysis (Figure 4.9(d)). It is assumed by the authors that after calcined, the numerous small pores of diatoms will close due to the sintering and coalescence. Zhang et al. (2005) reported the existence of three different stages in diatomite sintering behaviour. In the first one, a drop of the open porosity from 71.6 to 68.1% is observed between 850 and 1000 ℃. In the second stage, a decrease of the porosity from 68.1 to 36.7% occurs between 1050 to 1250 ℃. Finally, a decrease to 5%

of the open porosity was reached at 1350 ℃. The peaks value of intra-aggregate and inter-aggregate pores almost same for 2460 and 1424, at pore radii around 100-200 nm and 100000-200000 nm, respectively. The inter-aggregate porosity of the 2460 is lower than the 1424 due to the slightly larger particle sizes of the 1424.

2) SEM

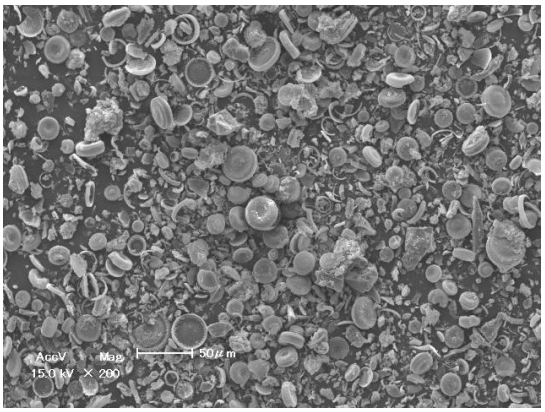

(a) RC417

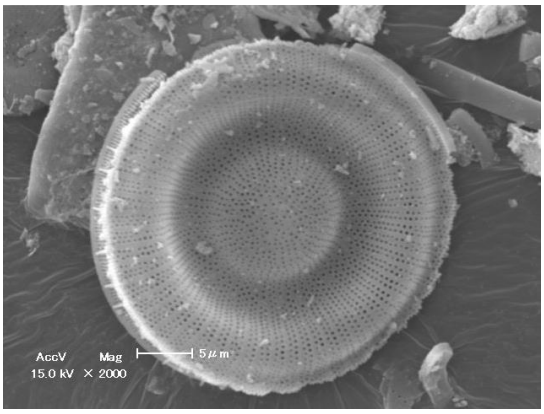

(b) RC417

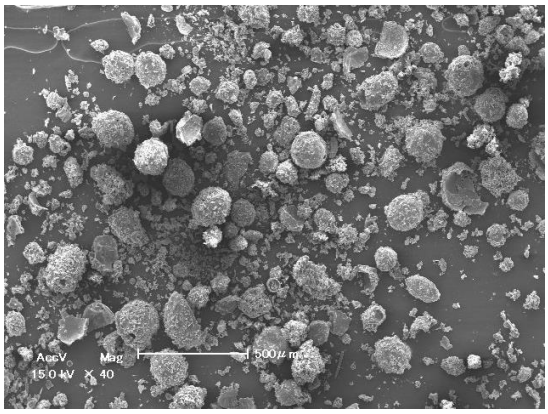

(c) #3000

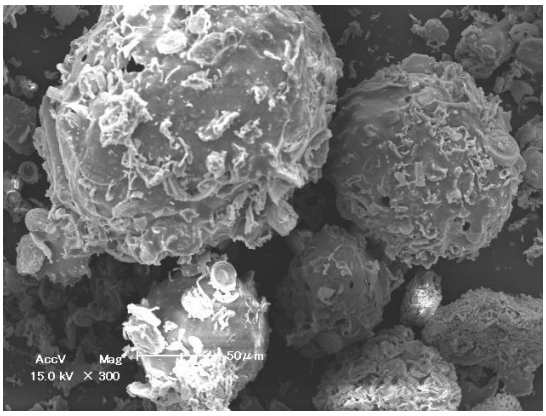

(d) #3000

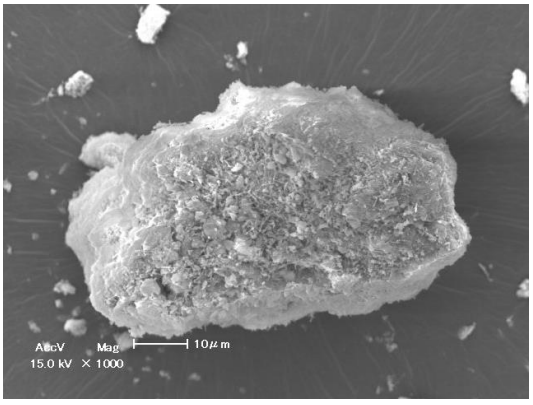

(e) 1424

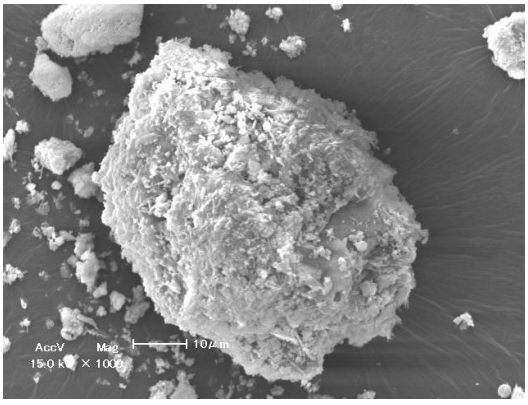

(f) 2460

Figure 4.9 Scanning electron photomicrographs of materials

Figure 4.9 presents the electron photomicrographs of the diatomaceous earth and zeolites. It can be seen that the diatomaceous earth mainly consists of the centric diatoms particles (Cyclotella) having two disks attached to each other by a circular girdle. Tateishi (1997) reported that the diatom fossils of Oita diatomite are mainly composed of Cyclotella, and contain a small amount of Melosira and Stephanodiscus. Figure 4.9(a) shows that numerous skeletal pores and chambers make up the microfossil skeleton of diatom particles. This formation justifies the existence of skeletal pores defined by Tanaka and Locat (1999). Since the diatomite is composed almost exclusively of diatom fossils, it has numerous skeletal pores in diatom particles and interparticle pores between diatom particles. From the SEM images of calcined diatomite (Figure 4.9(c)、(d)), it is seen that the particles became aggregated to coarser size. A clear coalescence of porous diatom frustule is seen in the calcined diatomite. Figure 4.9(d) shows that the porous structure of the diatomite material is completely closed due to melting. This confirms the pore size distribution analysis (see Figure 4.7). From the SEM images of zeolites (Figure4.9 (e)、(f)), it is seen that the particles are composed by aggregate which have inner structure. This confirms the pore size distribution analysis (see Figure 4.8).

4.3.2 Soil water characteristic curves

All of the measured soil water characteristic curve data for diatomaceous earth and zeolites are shown in Figures 4.10-4.13. The trend in the measured data in Figures indicates that the soil water characteristic curves for both the diatomaceous earth and zeolites materials are bimodal, as expected. The bimodal shapes of the soil water characteristic curves are indicated both by the data corresponding to low suctions ($\leqslant$1 kPa) measured using the Tempe cells and by the requirement that the soil water characteristic curve approach the saturated volumetric water content (i.e., total porosity) for the materials at low suctions.

The soil water characteristic curves of the two different sizes of diatomaceous earth pellets (i.e., RC417 and #3000) are different in terms of both the microscopic and the macroscopic portions. Due to the sintering and coalescence the permeability of the

calcined diatomite increased compared to that of the raw diatomite. This is explained by the agglomeration or enlargement of the particles upon calcination since larger particles result in higher flow rates (Kouteren, 1994). However, the soil water characteristic curves of the two different sizes of zeolites pellets are similar in terms of both the microscopic and the macroscopic portions, as expected on the basis of the similar particle sizes and inner structure in the particles. And the water holding capacity of raw diatomaceous earth and zeolites are higher than K7 sand, even though the particle size of these materials is coarser. The results suggest that raw diatomaceous earth and zeolite could be as sand amendments for revegetation in drylands.

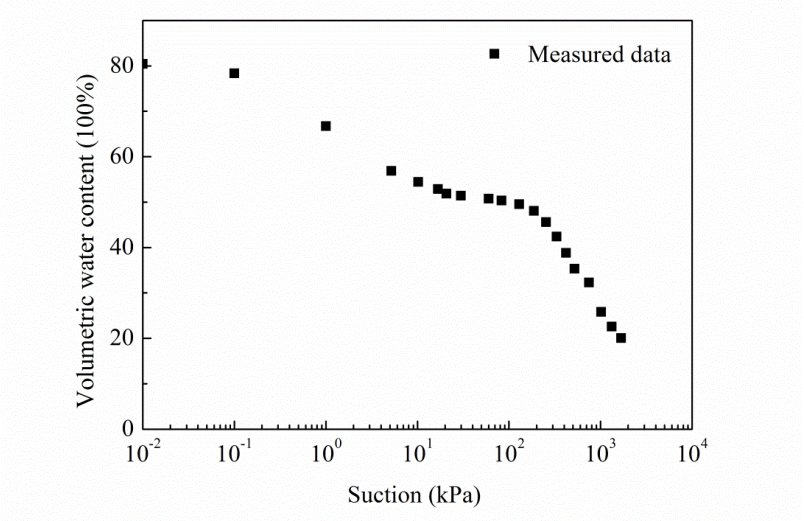

Figure 4.10 Measured soil water characteristic curve data for RC417

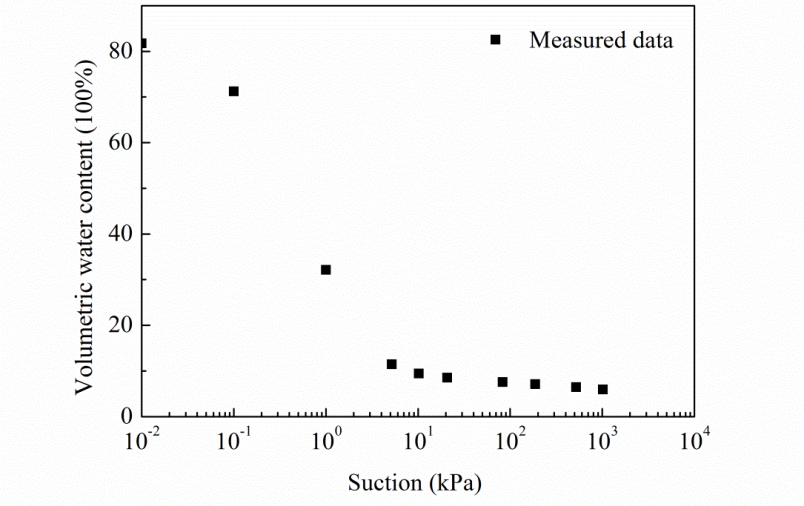

Figure 4.11 Measured soil water characteristic curve data for #3000

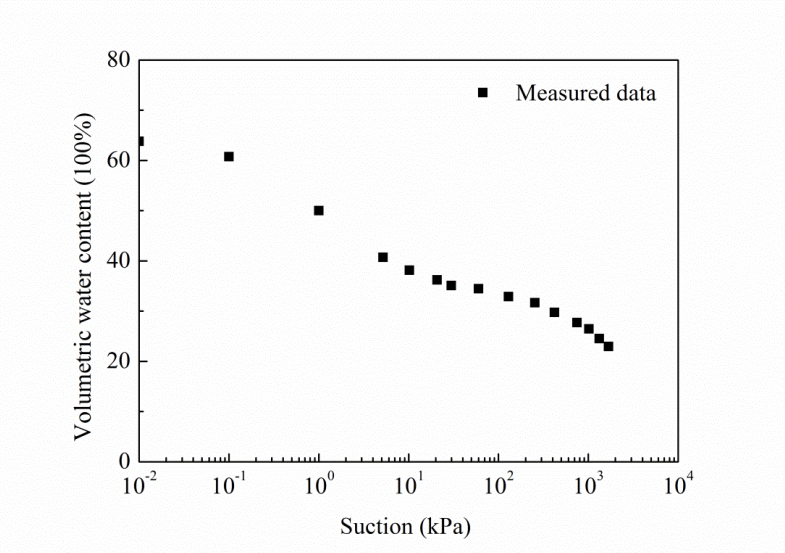

Figure 4.12 Measured soil water characteristic curve data for 2460

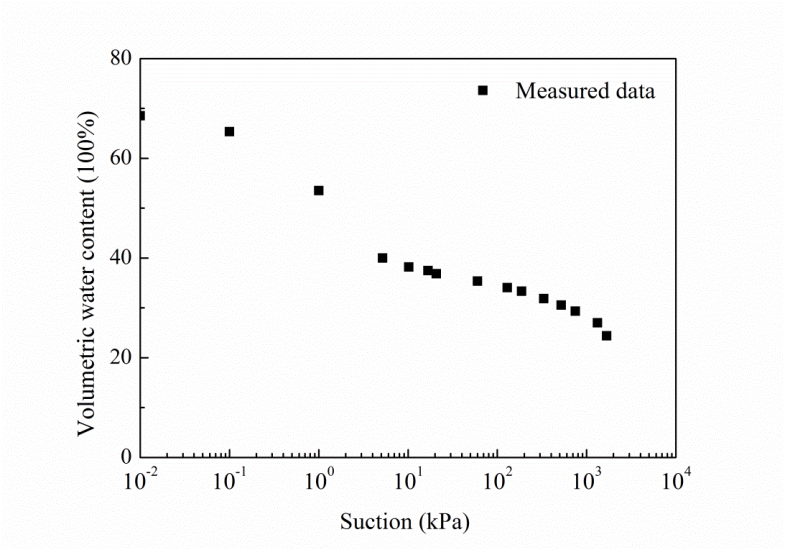

Figure 4.13 Measured soil water characteristic curve data for 1424

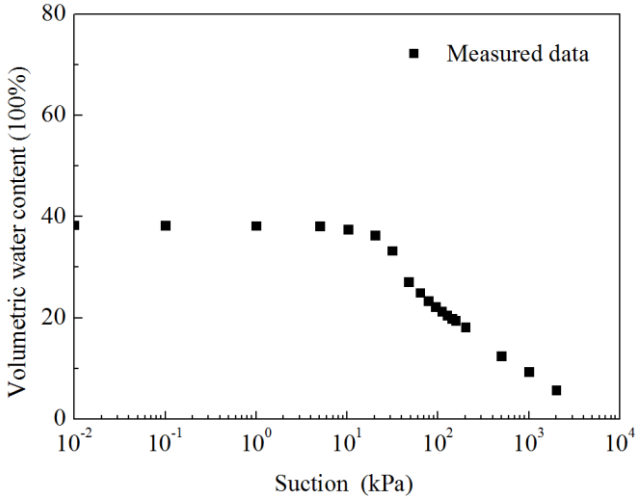

Figure 4.14 Measured soil water characteristic curve data for K7 sand

4.4 SUMMARY

In this chapter, the basic properties of the dual-porosity soils used in the laboratory experiments are presented. The pore geometry of dual-porosity soils has been studied using scanning electron microscopy and mercury intrusion porosimetry. The soil water characteristic curves of four sizes of processed diatomaceous earth and zeolites pellets were measured using a combination of methods to cover a wide range of suctions. The measured soil water characteristic curves for the pelletized diatomaceous earth and zeolites are bimodal and reflect two distinct pore size distributions associated with the microscopic and macroscopic portions of the total porosity of the specimens. Inner structure increase water holding capacity of dual-porosity soils. Raw diatomite and zeolite may be as sand amendments in drylands.

REFERENCES

Armbruster, T., and Gunter, M.E. 2001 Crystal structures of natural zeolites, In: D. L. Bish and D. W. Ming, (ed.) Natural zeolites: Occurrence, properties, applications, Vol. 45. Mineralogical Society of America, Washington, pp. 1-57.

Chen, J. and Gabelman., W. H. 1990 A sand zeolite culture system for simulating plant acquisition of potassium from soils. Plant and Soil, 126(2), 169-176.

Day, R.W. 1995 Engineering properties of diatomaceous fill. Journal Geotechnical Engineering, 121 (12), 908-910.

Durner, W. 1994 Hydraulic conductivity estimation for soils with heterogeneous pore structure. Water Resource Research, 30(2), 211-223.

Hey, M. 1930 Studies on zeolites: part I. general review. Mineralogical Magazine, 22(131), 422-437.

Khilnani, K., and Capik, M.L. 1989 Diatomaceous soils: a new approach. Civil Engineering, 59(2), 68-70.

Kouteren, S.V., 1994 Filters and absorbents. In Carr, D.D. (ed.), SMME, Colorado, USA, pp. 497-507.

Lange, K.P. 1983 Removal of giardia lamblia cysts and other substances by diatomaceous earth filtration. M.S. thesis, Colorado State University, Fort Collins, Colo.

Li, D., Joo, Y.K. Christians, N.E. and Minner, D.D. 2000 Inorganic soil amendment effects on sand-based sports turf media. Crop Science, 40(4), 1121-1125.

Lukasik, J., Farrah, S.R., Truesdail, S., and Shah, D.O. 1996 Adsorption of microorganisms to sand and diatomaceous earth particles coated with metallic hydroxides. Kona, 14, 87-91.

Mallants, D., Tseng, P.H., Toride, N., Timmerman, A., and Feyen, J. 1997 Evaluation of multimodal hydraulic functions in characterizing a heterogeneous field soil. Journal of Hydrology, 195 (1), 172-199.

Othmer, H., Diekkruger, B., and Kutilek, M. 1991 Bimodal porosity and unsaturated hydraulic conductivity. Soil Science, 152 (3), 139-149.

Peters, R.R., and Klavetter, E.A. 1988 A continuum model for water movement in an unsaturated fractured rock mass. Water Resources Research, 24(3), 416-430.

Pruess, K., Wang, J.S.Y., and Tsang, Y.W. 1990 On thermohydrologic conditions near high-level nuclear wastes emplaced in partially saturated fractured tuff. 2. Effective con-tinuum approach. Water Resources Research, 26(6), 1249-1261.

Smettem, K.R.J., and Kirby, C. 1990 Measuring the hydraulic properties of a stable aggregated soil. Journal of Hydrology, 117 (1-4), 1-13.

Stavnes, S., Yorke, C.A., and Thompson. L. 1996 In situ bioremediation of petroleum in tight soils using hydraulic fracturing. In Proceedings of the HazWaste World/Superfund 17th Conference, Washington, D.C.

Sundine Enterprises, Inc. 1996 Isolite product literature. Sundine Enterprises, Inc., Arvada, Colo.

Tanaka, H., and Locat, J. 2000 A microstructural investigation of Osaka Bay clay: The impact of microfossils on its mechanical behavior. Canadian Geotechnical Journal, 36(3), 439-508.

Tateishi, Y. 1997 Geotechnical properties of diatomaceous soils and stability of surface layer for the cut slop. Doctoral dissertation, Saga Univ., Saga, Japan.

Waltz F.C. Jr, Quisenberry V.L. and McCarty L.B. 2003 Physical and hydraulic properties of root zone mixes amended with inorganics for golf putting green. Agronomy Journal, 95(2), 395-404.

Wang, J.S.Y., and Narasimhan, T.N. 1985 Hydrologic mechanisms governing fluid flow in a partially saturated, fractured, porous medium. Water Resources Research, 21(12), 1861-1874.

Wang, J.S.Y., and Narasimhan, T.N. 1990 Fluid flow in partially saturated, welded–nonwelded tuff units. Geoderma, 46(1-3), 155-168.

Williams, K. A. and Nelson, P. V. 1997 Using precharged zeolite as a source of potassium and phosphate in a soilless container medium during potted chrysanthemum production. Journal of the American Society for Horticultural Science, 122(5), 703-708.

Wilson, G.V., Jardine, P.M., and Gwo, J.P. 1992 Modeling the hy-draulic properties of a multiregion soil. Soil Science Society of America Journal, 56(6), 1731-1737.

Zhang, X., Liu, X., Meng, G., 2005. Sintering kinetics of porous ceramics from natural diatomite. Journal of The American Ceramic Society, 88(7), 1826-1830.

CHAPTER 5

5. BIMODAL DESCRIPTIONS OF SOIL WATER CHARACTERISTIC CURVES FOR DUAL-POROSITY STRUTURAL SOILS

5.1 INTRODUCTION

Modeling water flow and solute transport through the vadose zone requires knowledge of the relationship between moisture and suction. The soil water characteristic curves (SWCCs), also known as the water retention curves (WRCs), constitutes a basic relationship between moisture and suction used for prediction of the hydraulic behavior of unsaturated porous materials.

Numerous unimodal functions (e.g. Brooks and Corey, 1964; van Genuchten, 1980; Fredlund and Xing, 1994; Kosugi, 1994) have been developed to describe SWCCs. These functions were generally derived from idealized pore space models that assume a unimodal pore size distribution. Nevertheless, evidences have been shown that the pore size distributions of some soils are often bimodal or multimodal (Othmer et al., 1991; Durner, 1994; Spohrer et al. 2006; Zhang and Li, 2010). For example, the structural soils consist of interconnected networks of structural (inter-aggregate) and matrix (intra-aggregate) pores forming two (or more) distinct pore spaces (Kutílek, 2004). Typically, spaces of sizes in the order of 10^{-4} to 10^{-2} m are associated with structural pores, while the porous matrix contains smaller pore sizes in the range of 10^{-7} to 10^{-5} m (Tuller and Or, 2002). The existences of two vastly different pore domains resulting in pore size distributions of structural soils are often bimodal. In such soils the independent draining of the structural and matrix pores frequently results in two distinct air-entry values, which any single unimodal function does not reproduce adequately (Othmer et al., 1991; Durner, 1994). To encounter these problems, in the last decades several approaches have been developed to describe bimodal or multimodal SWCCs. Peters and Klavetter (1988) first proposed the

superposition of two unimodal pore systems to represent the bimodal pore size distributions. This approach was generalized by Othmer et al. (1991), Wilson et al. (1992), and Durner (1994) to consider multimodal pore size distributions, each of which is characterized by its own SWCC function. In these approaches the SWCC function of the whole porous medium has been described by linearly overlapping functions of the same form or of different forms (Coppola, 2000). Durner (1994) extended the unimodal van Genuchten functions (van Genuchten 1980) to fit bimodal and multimodal SWCCs by introducing weighting factors for combining individual functions. Burger and Shackelford (2001a, b) proposed piecewise-continuous forms of the Brooks-Corey (1964), van Genuchten (1980), and Fredlund-Xing (1994) SWCC functions to fit the bimodal experimental SWCCs for diatomaceous earth (DE) and sand-DE mixtures. Although above approaches were successfully applied to structural soils, they are lack of a physical basis for their parameters due to the fact that the unimodal SWCC functions they extended were known as empirical equations.

The primary objective of this study was to propose a physical basis SWCC model for structural soils with two distinct pore spaces. The specific objectives were: (i) derivation of SWCC function for structural soils based on pore size distribution; and (ii) simple tests of the proposed model using available datasets. The hysteretic nature of the SWCC can significantly influence water flow and solute transport in unsaturated porous media (Šimůnek et al., 1999). In this paper the proposed model only performs on the drying curves, because if successfully captures the bimodal shape of drying curves it also fit for the bimodal wetting curves.

5.2 METHODS

5.2.1 Theoretical analysis of dual-porosity structural soils

Assume that ideal dual-porosity structural soils consist of uniform sphere aggregates packed in simple cubic structure and intra-aggregates also have same structure (shows in Figure 5.1). There are two major pore series, i.e. structural pores (i.e. inter-aggregate pores) and matrix pores (i.e. intra-aggregate pores). Two pore series in the soil are assumed to be connected. Therefore, the suctions in the two characteristic

pore series are the same. The SWCC of ideal dual-porosity structural soil is shown in Figure 5.2 (a). The soil remains saturated before suctions reach the air entry value (stage 1). The air entry value is controlled by the routing radius (RR_1) (i.e. the radius of the largest sphere that can pass through the porous medium) of structural pores, which is related to the packing structure and the sphere diameter. As the suctions reach the air entry value (stage 2), all the bulk water in the structural pores (BW_1) will drain without additional suction. After all the bulk water in the structural pores (BW_1) has drained, a small amount of water (i.e., the water-pendular rings (RW_1)) around aggregate-to-aggregate contact points remains and drains slowly while the matric suction increases rapidly (stage 3). Further, when the suction increases to the starting-drainage-suction of bulk water stored in the matrix pores, the bulk water stored in the matrix pores (BW_2) will drain (stage 4). After the suction reaches the end-of-drainage-suction of bulk water stored in the matrix pores (BW_2), the water-pendular rings in the matrix pores (RW_2) starts to drain (stage 5). Hence, the volume proportion of water-pendular rings in the matrix pores (RW_2) determines the residual soil water content.

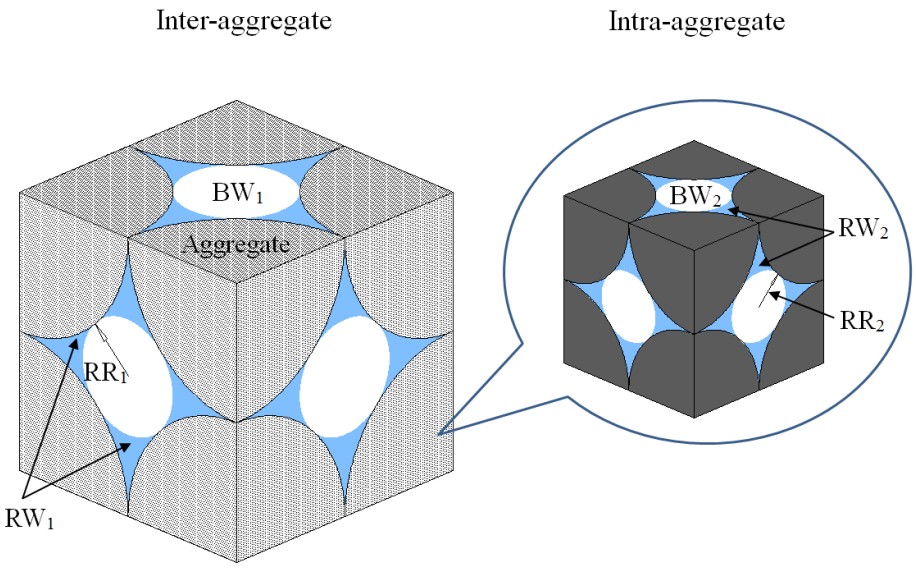

Figure 5.1 Schematic of 3D simple cubic packing of ideal dual-porosity structural soil

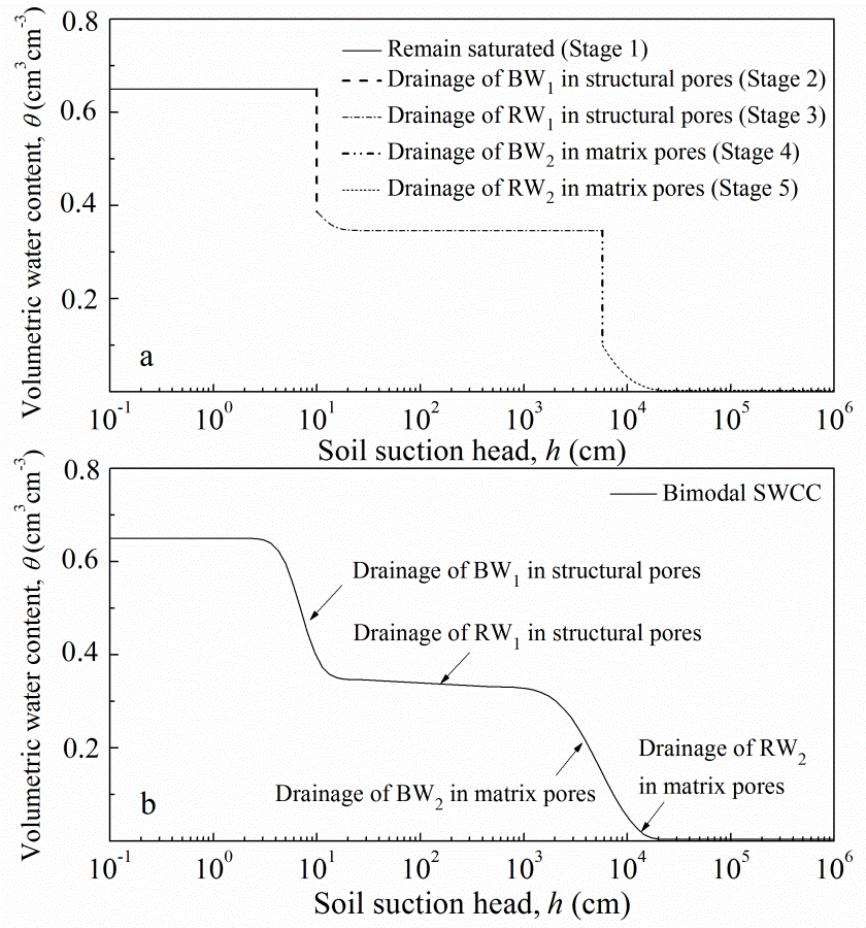

Figure 5.2 Theoretical bimodal SWCC for (a) simple cubic packing geometry, and (b) random packing geometry

In random packing geometry of aggregates, the bulk water is stored in pores with different routing radius. Then the drainage process of bulk water (stage 2) continues from the drainage suction of the largest bulk water spheres to the drainage suction of the smallest bulk water spheres. After the bulk water drains, the water-pendular rings will drain (stage 3) continues from the drainage suction of the largest pendular rings to the drainage suction of the smallest pendular rings. The same is true for random packing geometry of intra-aggregate. Random packing geometry results in the SWCC of dual-porosity soils more smoothly (shows in Figure 5.2 (b)).

5.2.2 Bimodal SWCC function

Brutsaert (1966) studied four models of pore size distribution, among them the lognormal distribution in relation to SWCCs. A more detailed analysis was presented by Kosugi (1994), who assumed the lognormal pore probability density function for

pore radii, $g(r)$ as

$$g(r)=\frac{\theta_s-\theta_r}{\sqrt{2\pi}\sigma r}\exp\left\{-[\ln(r/r_m)]^2/2\sigma^2\right\} \tag{5-1}$$

where r, the pore radius (cm), obeys the lognormal distribution; θ_s and θ_r, the saturated and residual volumetric water content (cm^3cm^{-3}), respectively; $r_{m,}$ the median pore radius (cm), and σ denotes the standard deviation of $\ln(r)$. Based on this assumption, the SWCC function can be expressed as (Kosugi, 1994):

$$S_e=(\theta-\theta_r)/(\theta_s-\theta_r)=F_n\left[\ln(h/h_m)/\sigma\right] \tag{5-2}$$

where S_e, the effective saturation; θ, the volumetric water content (cm^3cm^{-3}); h_m, the median matric head (cm) component with r_m; and $F_n(x)$, the complementary normal distribution function defined as

$$F_n(x)=\frac{1}{\sqrt{2\pi}}\int_x^\infty \exp(-t^2/2)dt \tag{5-3}$$

where t is a dummy variable. For the dual-porosity structural soils, there are two continual pore series: structural pores and matrix pores. Probability density functions for two pore series are assumed as lognormal distribution and can be superposed to obtain the overall probability density function of the structural soils. Follow Durner (1994) combined two continual pore series by introducing weighting factors to describe volumetric percentage of each pore fraction, the pore probability density function of the dual-porosity structural soil as the following form

$$\begin{aligned} &g(r)=\sum_{i=1}^{k}\phi_i g_i(r)=\sum_{i=1}^{k}\phi_i\frac{\theta_s-\theta_r}{\sqrt{2\pi}\sigma_i r}\exp\left\{-[\ln(r/r_{m_i})]^2/2\sigma_i^{\,2}\right\} \\ &0<\phi_i<1 \text{ and } \sum_{i=1}^{k}\phi_i=1 \end{aligned} \tag{5-4}$$

where k, the number of pore series (k=2 for the dual-porosity structural soils); $g_i(r)$, the pore probability density function (cm^{-1}) for the ith pore series; ϕ_i, the volumetric percentage of the soil components with the ith pore series; r_{m_i}, the median pore radius (cm) for the ith pore series; σ_i denotes the standard deviation of $\ln(r)$ associated with the ith pore series. And SWCC function for the dual-porosity structural soil as a cumulative curve of Eq. (5-4)

$$S_e = \sum_{i=1}^{k} \phi_i F_n \left[\ln(h / h_{m_i}) / \sigma_i \right]$$
$$0<\phi_i<1 \text{ and } \sum_{i=1}^{k} \phi_i = 1 \qquad (5\text{-}5)$$

where h_{m_i}, the median matric head (cm), components with the *i*th pore series. Figure 5.3 (a) shows the superposition of two hypothetical pore size distributions which define a bimodal pore series according to Eq. (5-4). The dot line can be interpreted as structural pores distribution, with $\ln(r_{m_1})$ is -3.64, σ_1 is equal to 0.47 and maximum pore size density around r =3×10^{-2} cm, whereas the red dash line can be seen as matrix pores distribution with $\ln(r_{m_2})$ is -10.17, σ_2 is equal to 0.72 and its maximum density in the range of r = 4×10^{-5} cm. Fig. 3 (b) shows the bimodal SWCC (solid line) corresponding two hypothetical pore size distributions, unimodal SWCC for structural pores with volumetric percentage ϕ_1 is 0.54 (dot line) and matrix pores with ϕ_2 is equal to 0.46 (red dash line).

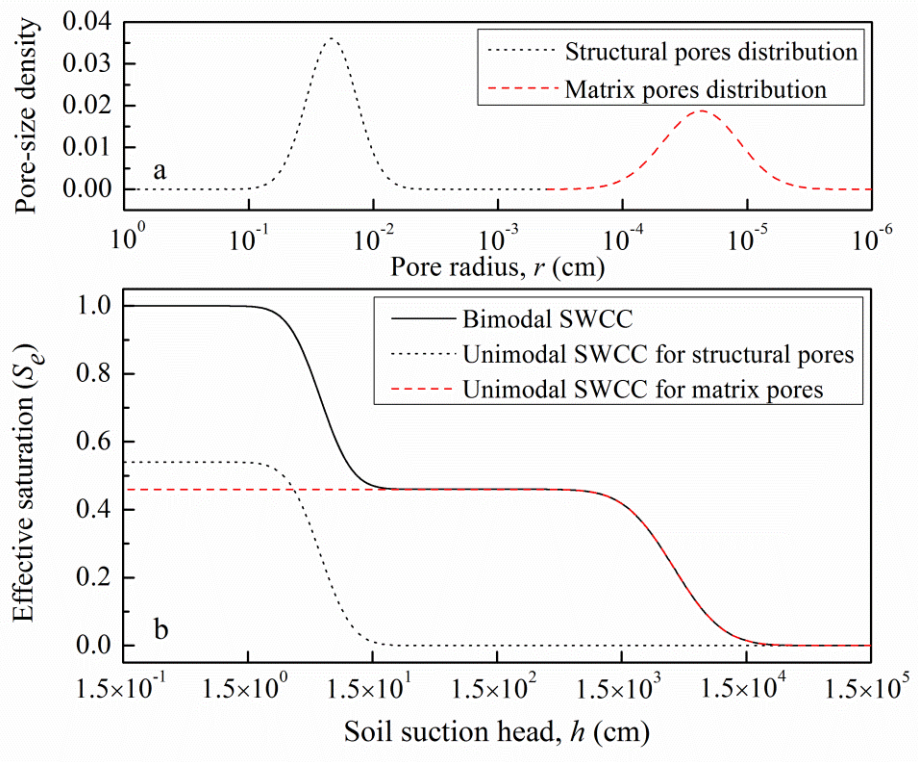

Figure 5.3 Construction of a bimodal SWCC function. (a) Pore size distribution of structural pores (dot line), and matrix pores (red dash line). (b) Bimodal SWCC (solid line), unimodal SWCC for structural pores (dot line) and matrix pores (red dash line)

Eq. (5-5) is derived on the basis of there exist two combined lognormal pore radius density curve in the structural soil, hereafter referred to as bimodal lognormal (BLN) model. In the case of k=n (n>2), there exist multiple pore series in the soil and Eq. (5-5) becomes the multimodal lognormal (MLN) SWCC function.

5.2.3 Evaluation of the bimodal SWCC model

We evaluated proposed bimodal SWCC model by applying them to various soils. First, proposed bimodal model was compared with unimodal model. Four diatomaceous earth and zeolites samples in Chapter 4 and other six soil samples include loam and silt loam were selected for this purpose (shows in Table 5.1). These six soil samples were obtained from the Unsaturated SOil hydraulic DAtabase (UNSODA) (Nemes et al., 2001) which contains of SWCC, hydraulic conductivity and water diffusivity data as well as pedological information of some 790 soil samples from around the word. The unimodal lognormal (ULN) SWCC model based on theoretical considerations and can be simplified to the currently used expressions of van Genuchten or other empirical models (Kosugi et al., 2002). For these reasons, all comparisons were performed with respect to the ULN model only. In this evaluative procedure, the parameter θ_s was set at its measured value and θ_r was assumed to be zero. For soils that did not provide porosity or θ_s value, the first point of the experimental SWCC data that corresponds to the lowest suction head was used as θ_s (Chan and Govindaraju, 2004).

Further evaluations were performed for 14 artificial soils (shows in Table 2) cited from Burger and Shackelford (2001a, b), which were also used by Zhang and Chen (2005) for verification of functions they proposed. The SWCCs were measured for two commercial DE (CG1 and CG2) and 12 different mixtures of CG1 pellets with Sand 20-60, CG2 pellets with Sand 20-60, and CG2 pellets with Sand 10-20 at four different percentages of DE ranging from 4 to 30% by dry weight. Burger and Shackelford (2001a, b) also proposed piecewise-continuous forms of the Brooks-Corey (1964), van Genuchten (1980), and Fredlund-Xing (1994) SWCC functions to fit the bimodal experimental SWCCs. Their fitted results shown that

bimodal van Genuchten function (BvG) visually fitted the data the best. Therefore our proposed BLN function was compared with BvG function. In this case, θ_s was considered as a fitting parameter to verify the effectiveness of the BLN model and θ_r was assumed to be zero.

In this study, the root mean square error (RMSE) of the measured and simulated volumetric water content θ, and coefficients of determination (R^2) were used as measure of the goodness-of-fit.

5.3 RESULTS AND DISCUSSION

5.3.1 ULN and BLN models fitted results

Fitted parameters and corresponding RMSE values for ULN and BLN functions are showed in Table 5.1. For all soils, the RMSEs for the measured and simulated variables show improvement when BLN model is used rather than the ULN model. The good fit of the proposed BLN model is indicated by the lower values of RMSE. Table 5.1 shows that all the materials are successfully described by the BLN model with coefficients of determination, $R^2 > 0.98$. Such high values of R^2 indicate the effectiveness of the BLN model in describing measured data.

In all related soils, the volumetric percentage of the structural pores (ϕ_1) in a range of 14-36%, in other words the matrix pores occupy the majority of total pores. Table 1 also shows that the median suction head in ranges between 10.50 cm to 69.66 cm for the structural pores (h_{m_1}) and from 7242.66 cm to 18990.28 cm for the matrix pores (h_{m_2}). It infers that the median pore radii are from 2.14×10^{-3} cm to 1.42×10^{-2} cm for structural pores and from 7.85×10^{-6} cm to 2.06×10^{-5} cm for matrix pores (h_m and r_m is inversely proportional). The classification systems of soil pores by Tuller and Or (2002) is questionable when consider our results. As pointed out by Kutílek et al. (2006), our results support the belief that the classification systems of soil pores based upon fixed boundaries between pore size categories is not appropriate.

Figures 5.4-5.13 displays the fitted curves of the related soil samples obtained by ULN and BLN functions. All soils are show a clearly structural behavior that is captured fairly well by BLN function, while the poor fit offered by the ULN function is evident. As Durner (1994) proposed that a good description of the SWCC is the

basis for more accurate prediction of the soil's unsaturated hydraulic conductivity function across the entire soil water content range. Our proposed approaches can potentially be used as effective tool for predicting hydraulic porosities in the medium with structures.

Table 5.1 ULN and BLN models curve-fit parameters for the materials

Soil		Fitted	Structural pores			Matrix pores				
			ϕ_1	h_{m_1}	σ_1	ϕ_2	h_{m_2}	σ_2	*RMSE*	R^2
Code	Texture	model	(%)	(cm)		(%)	(cm)			
#3000	DE	ULN	-	0.29	2.98	-	-	-	0.089	0.944
		BLN	90.61	0.51	1.50	9.39	4536.92	2.08	0.004	1.000
RC417	DE	ULN	-	33.92	7.19	-	-	-	0.130	0.921
		BLN	35.93	1.13	1.63	64.07	1085.13	1.30	0.008	0.998
2460	ZE	ULN	-	0.84	10.31	-	-	-	0.217	0.959
		BLN	37.19	1.18	2.00	62.81	4124.39	1.89	0.003	1.000
1424	ZE	ULN	-	1.57	9.71	-	-	-	0.189	0.946
		BLN	47.44	1.12	1.55	52.56	5164.93	2.16	0.010	0.998
2530	Loam	ULN	-	2100.49	3.71	-	-	-	0.024	0.895
		BLN	25.17	69.66	0.47	74.83	11163.94	3.11	0.003	0.998
2601	Loam	ULN	-	2943.43	4.37	-	-	-	0.021	0.964
		BLN	33.21	37.99	1.10	66.79	18438.87	2.28	0.001	1.000
2604	Loam	ULN	-	1395.24	4.27	-	-	-	0.019	0.957
		BLN	35.22	33.39	1.10	64.78	13917.31	3.08	0.002	0.999
2750	Loam	ULN	-	2214.74	4.51	-	-	-	0.019	0.977
		BLN	28.87	22.15	1.20	71.13	12353.47	2.81	0.006	0.996
2751	Sandy loam	ULN	-	11849.58	4.39	-	-	-	0.012	0.977
		BLN	18.22	23.46	1.09	81.79	18990.28	2.15	0.002	0.999
2753	Sandy loam	ULN	-	4239.51	3.53	-	-	-	0.017	0.971
		BLN	13.98	10.50	0.94	86.02	7242.66	2.16	0.008	0.991

DE: diatomaceous earth; ZE: zeolite.

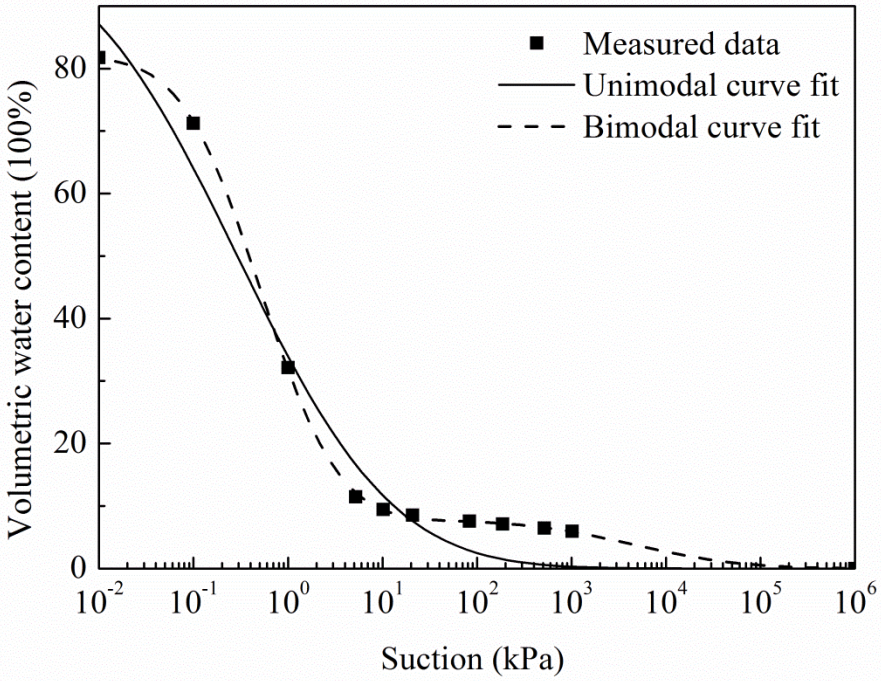

Figure 5.4 Fitted SWCC for #3000 based on ULN and BLN model

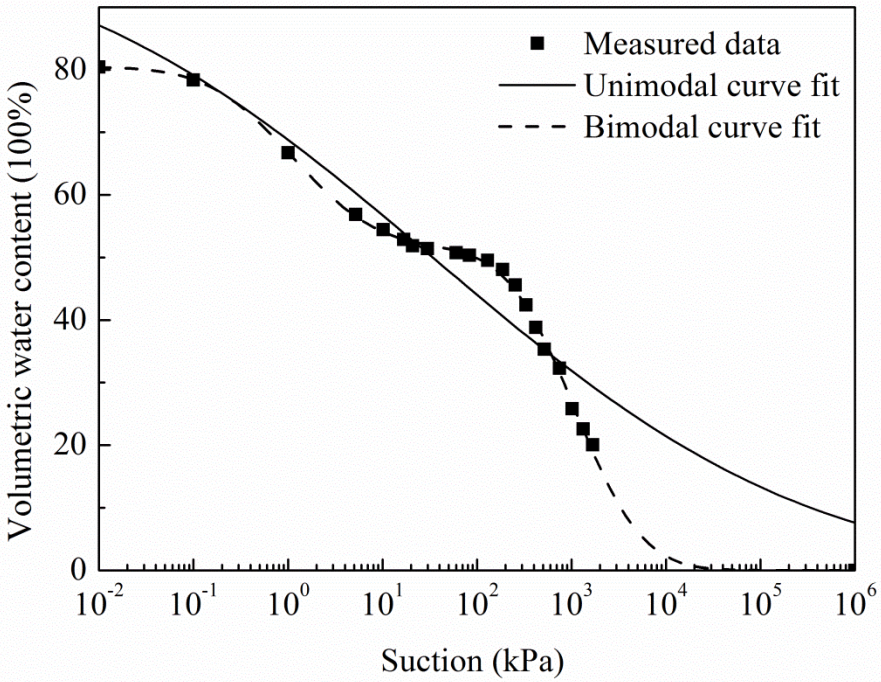

Figure 5.5 Fitted SWCC for RC417 based on ULN and BLN model

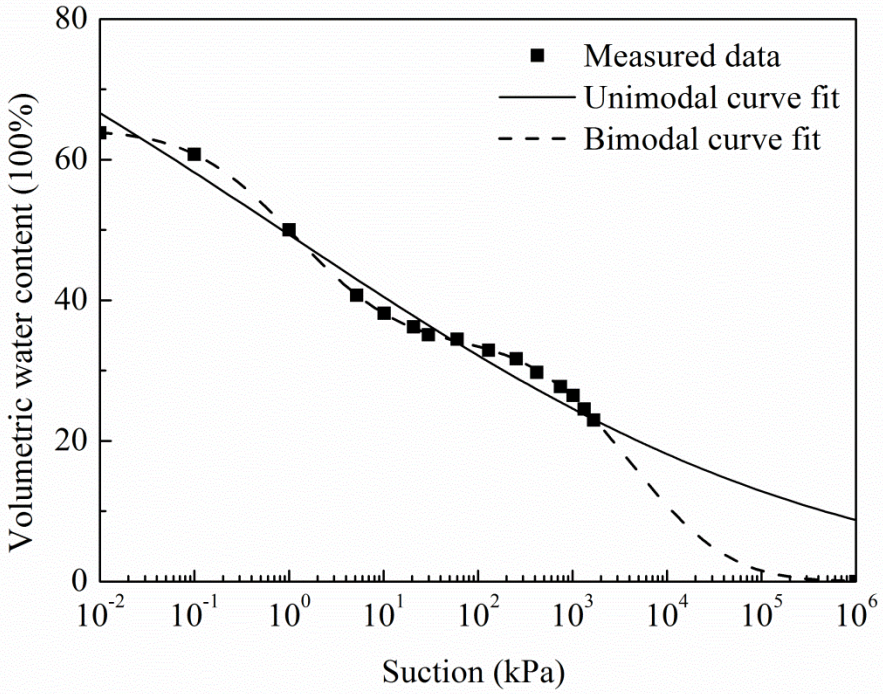

Figure 5.6 Fitted SWCC for 2460 based on ULN and BLN model

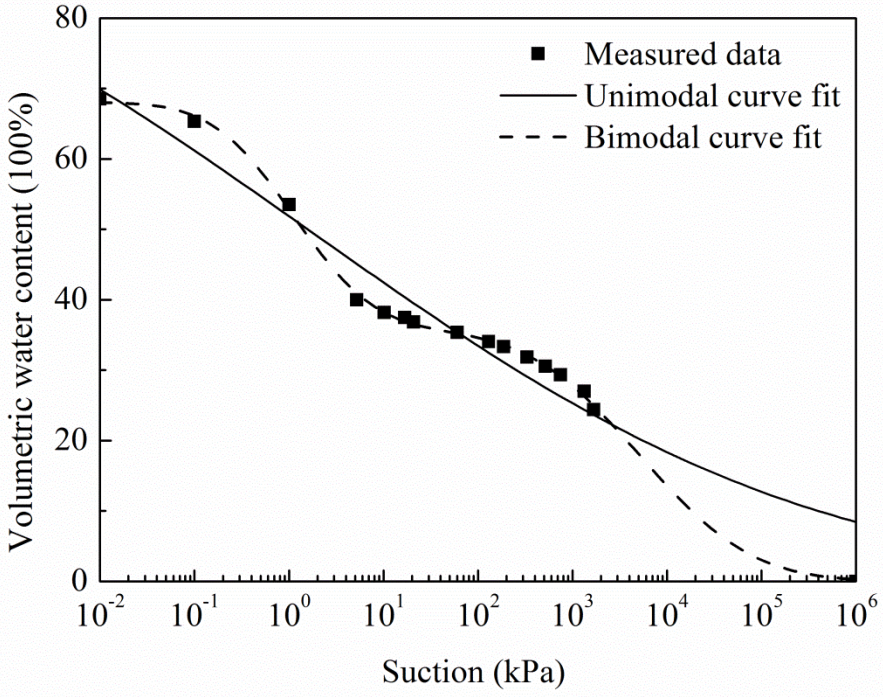

Figure 5.7 Fitted SWCC for 1424 based on ULN and BLN model

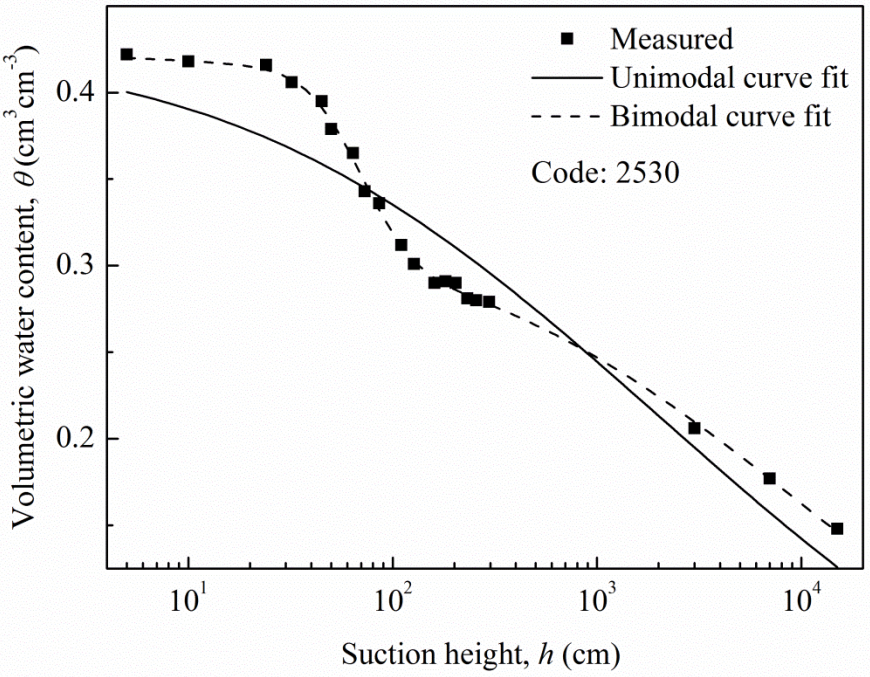

Figure 5.8 Fitted SWCC for 2530 based on ULN and BLN model

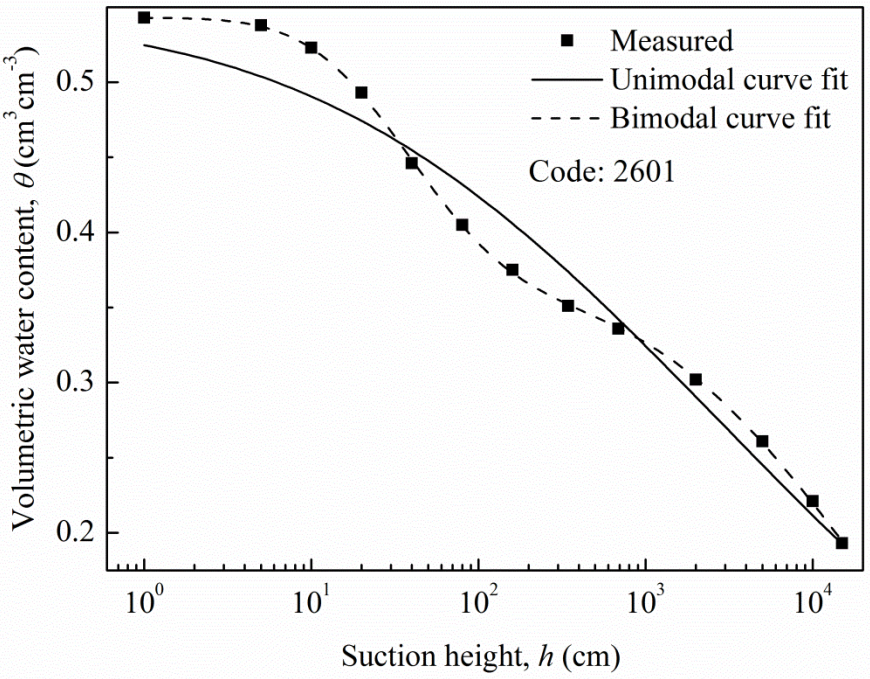

Figure 5.9 Fitted SWCC for 2601 based on ULN and BLN model

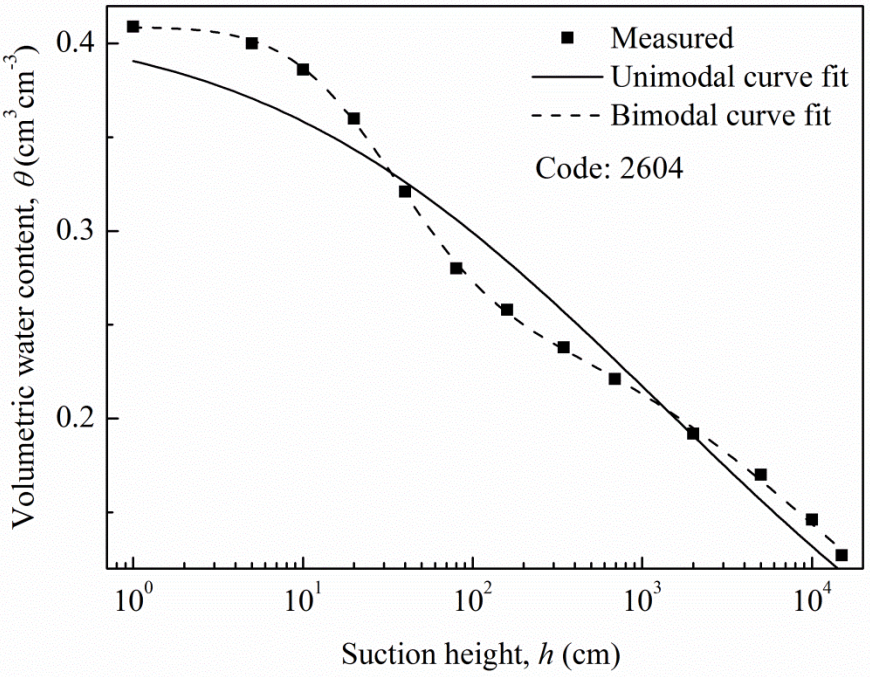

Figure 5.10 Fitted SWCC for 2604 based on ULN and BLN model

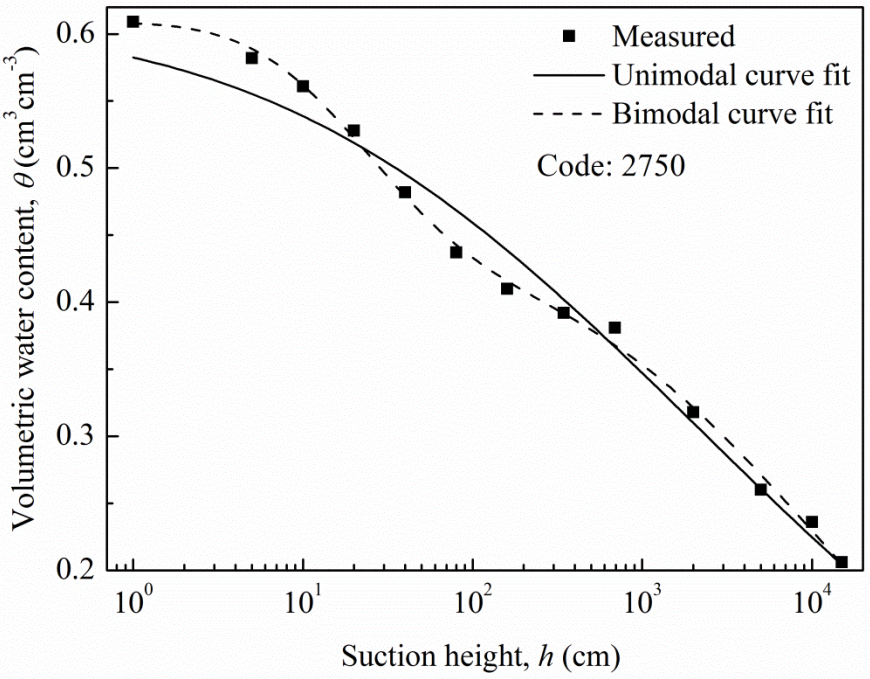

Figure 5.11 Fitted SWCC for 2750 based on ULN and BLN model

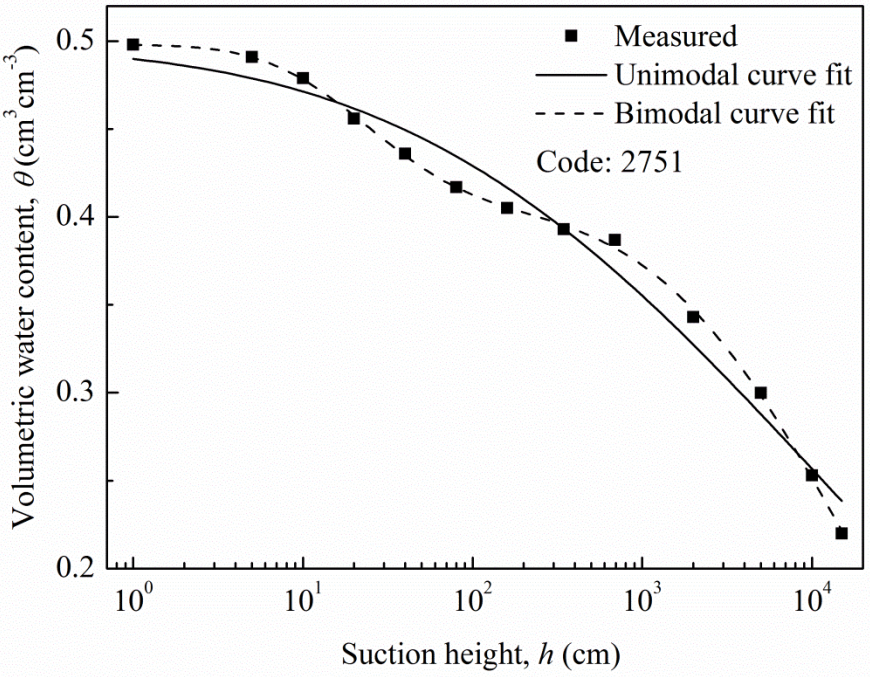

Figure 5.12 Fitted SWCC for 2751 based on ULN and BLN model

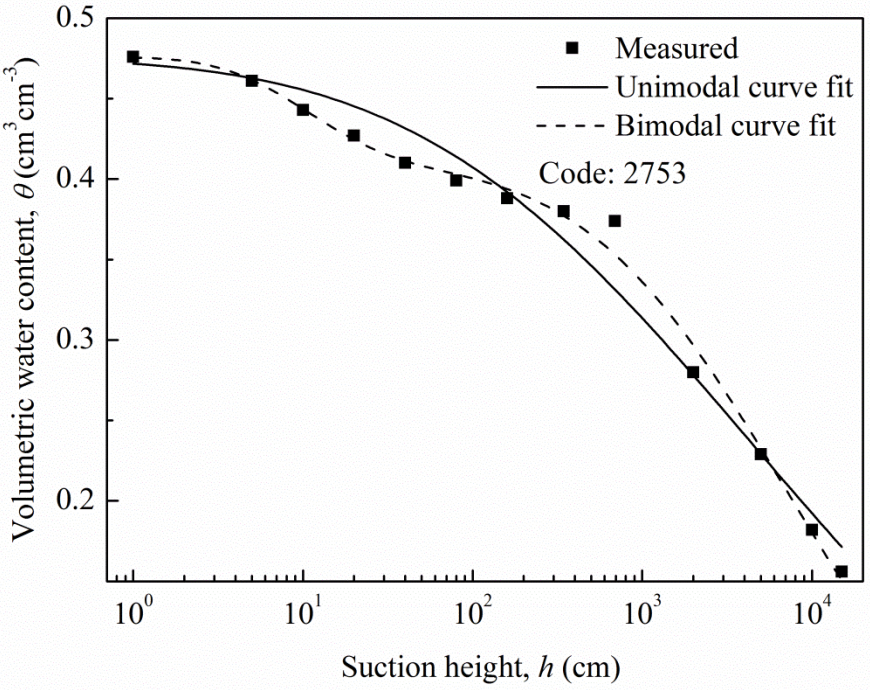

Figure 5.13 Fitted SWCC for 2753 based on ULN and BLN model

5.3.2 BvG and BLN models fitted results

The fitted results for 14 artificial soils using the BLN function are shown in Table 5.2 and Figures 5.14-5.16. The BvG function fitted results were shown in Table 7 and Fig.7 of Burger and Shackelford (2001b).

Table 5.2 BLN model curve-fit parameters for the materials

			Structural pores			Matrix pores			
Materials	DE (%)	θ_s (%)	ϕ_1 (%)	h_{m_1} (cm)	σ_1	ϕ_2 (%)	h_{m_2} (cm)	σ_2	R^2
CG1	100	76.01	54.44	5.67	0.47	45.56	3872.87	0.72	0.978
CG2	100	70.26	47.98	3.81	0.17	52.02	2263.39	0.88	0.974
CG1 and Sand 20-60	4.1	47.50	88.68	14.02	0.60	11.32	12028.85	0.48	0.999
	8.7	50.00	80.57	13.55	0.54	19.43	10517.67	1.34	0.999
	14.1	52.00	77.35	13.05	0.63	22.65	7016.37	1.29	0.989
	27.6	61.21	69.23	8.38	0.82	30.77	6138.04	1.49	0.999
CG2 and Sand 20-60	4.4	47.00	88.04	13.88	0.56	11.96	5871.32	1.60	0.999
	9.4	49.01	83.50	12.32	0.69	16.50	7530.38	0.47	0.999
	15.2	52.00	78.15	11.73	0.64	21.86	10094.76	0.65	0.998
	29.4	58.03	66.97	10.9	0.73	33.03	5202.23	1.24	0.999
CG2 and Sand 10-20	3.6	41.36	91.78	6.13	0.76	8.22	11520.75	0.35	1.000
	7.8	43.01	83.99	6.70	0.55	16.01	3128.64	1.06	0.997
	12.7	49.68	82.76	4.58	0.99	17.24	6099.25	1.40	0.999
	25.3	55.98	72.08	6.54	0.94	27.92	3360.98	0.98	1.000

DE: diatomaceous earth.

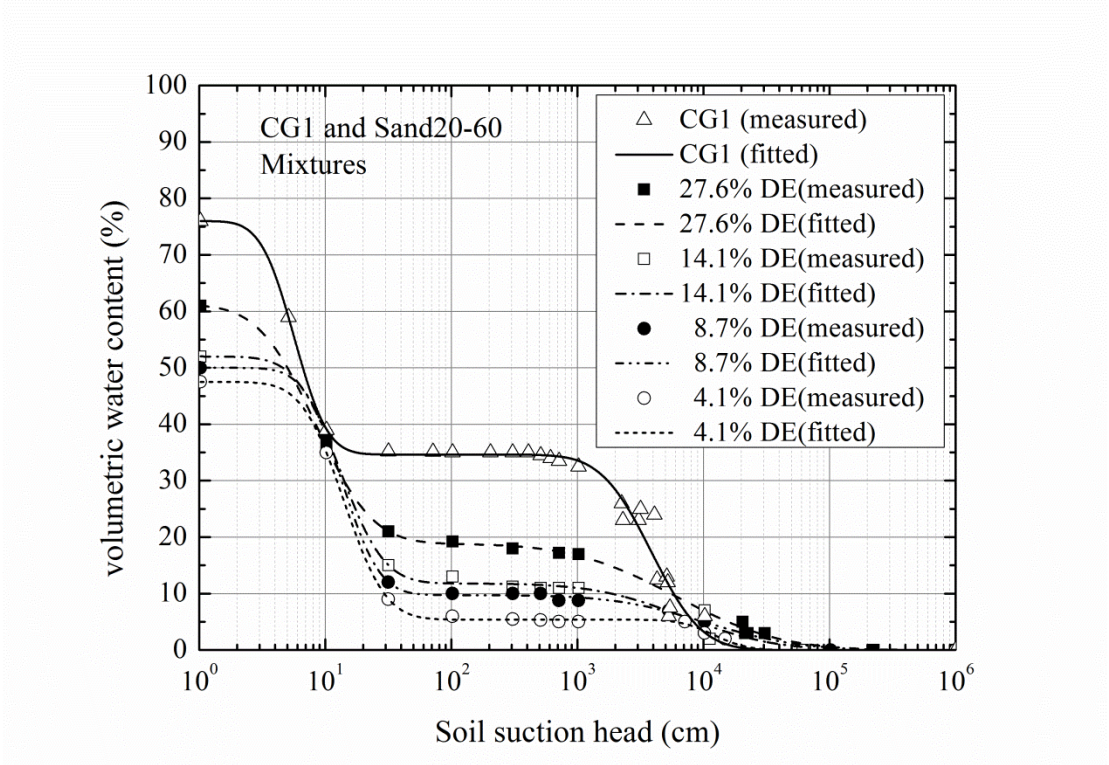

Figure 5.14 Fitted SWCC for CG1 and Sand 20-60 mixtures based on BLN fitting function

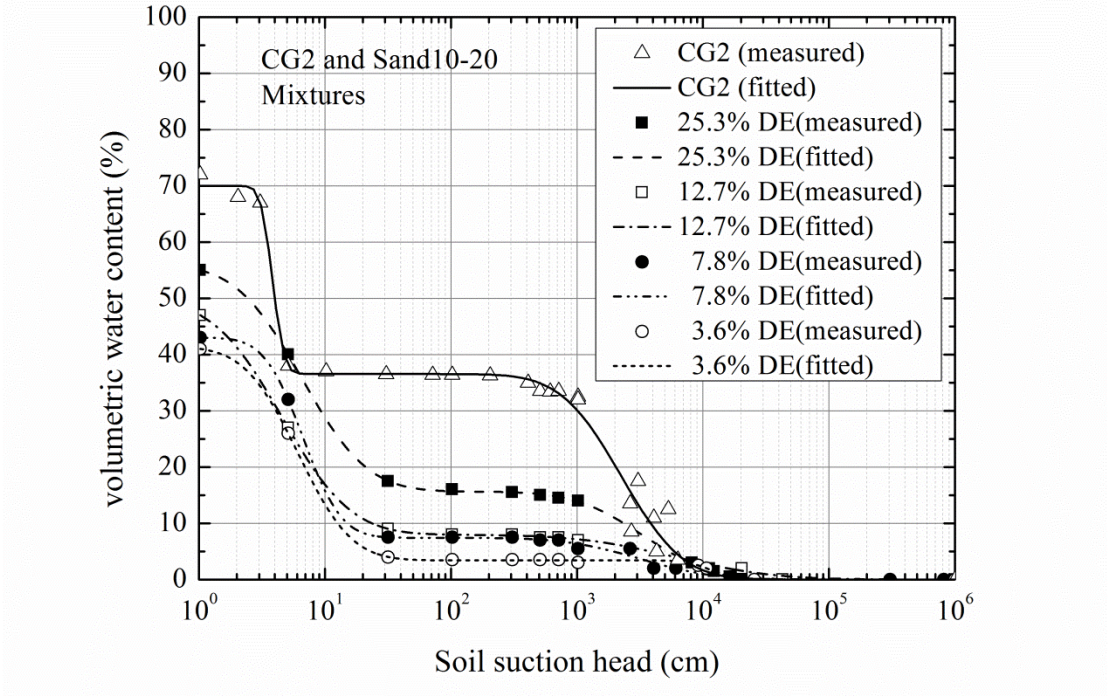

Figure 5.15 Fitted SWCC for CG2 and Sand 10-20 mixtures based on BLN fitting function

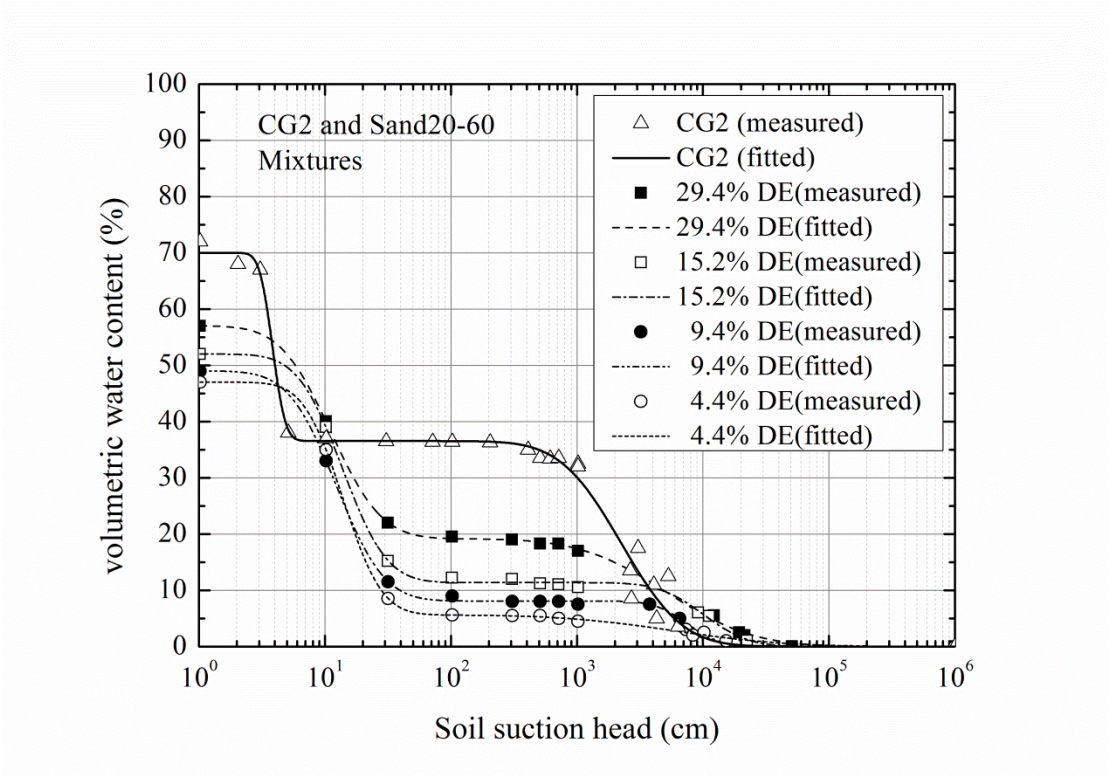

Figure 5.16 Fitted SWCC for CG2 and Sand 20-60 mixtures based on BLN fitting function

It is worth to noting that the high values of R^2 confirm again the good ability of the proposed BLN model to describe experimental data. The low difference between the measured and simulated θ_s (RMSE=0.010), also indicate the effectiveness of the BLN model in describing measured data.

For mixture of the three groups, the saturated volumetric water content (θ_s) increase along with DE increase in the mixtures. It infers that DE can increase the total porosity of the mixtures. Furthermore, the volumetric percentage of the structural pores (ϕ_1) is decreasing with the increase of DE. In contrast, the value of ϕ_2 increases along with the DE growth. These phenomena all illustrate that DE have inner structure and increases DE can increase the water holding capacity of the mixtures. Table 2 also shows that the median suction head (h_{m_1}) of the structural pores for the groups CG1 and Sand 20-60, CG2 and Sand 20-60, decrease as the amount of DE increase. It infers that the median pore radius of the structural pores (r_{m_1}) is increasing with increase of DE (h_{m_1} and r_{m_1} is inversely proportional). The result may be due to the particle size of CG1 and CG2 are bigger than Sand 20-60 (Fig.2 of Burger and Shackelford, 2001b). For CG2 and Sand 10-20 group this phenomenon is

not shown clearly due to their similar particle size distributions. The median suction head (h_{m_2}) of the matrix pores is not regular. The reason may be attributed to the fact that the measured data of the high suction portions are scatter, which can be proved by the standard deviation σ_2.

The BvG method also successfully fitted measure data. However, it was derived empirically and fitting parameters did not have physical significances, complicated process and artificial selection of the junction point somewhat arbitrarily. All these shortcomings limit its application. Unlike the BvG model, fitting procedure of BLN model is easier and all parameters have the physical significances which can be related to physical properties of the materials. These physically based parameters could more intuitively analyze the measured data. And after comparing the coefficients of determination (R^2) of two methods, it can be concluded that BLN function fitting more accurate than BvG function.

5.4 SUMMARY

In this chapter, mathematical functions for both bimodal and mutimodal SWCCs have been proposed. The proposed equations are defined by parameters that have physical significances which can be related to the properties of the materials. Experimental datasets fitting and parametric analyses were used to illustrate the fitting capability of the proposed equations. The proposed approaches make the treatment of SWCC data easier and resulted in well agreement between measurement and simulation. These functions can potentially be used as effective tool for indentifying hydraulic porosities in the medium with structures.

REFERENCES

Brooks, R., and Corey, A. 1964 Hydraulic properties of porous medium. Hydrology Paper No. 3, Colorado State Univ., Fort Collins,Colo.

Brutsaert, W. (1966). Probability laws for pore size distributions. Soil Science, 101(2), 85-92.

Burger, C. A., and Shackelford, C. D. 2001a Evaluating dual porosity of pelletized diatomaceous earth using bimodal soil water characteristic curve functions. Canadian Geotechnical Journal, 38(1), 53-66.

Burger, C. A., and Shackelford, C. D. 2001b Soil water characteristic curves and dual porosity of sand-diatomaceous earth mixtures. Journal of Geotechnical and Geoenvironment Engineering, 127(9), 790-800.

Chan, T.P., and Govindaraju, R.S. 2004 Soil water retention curves from particle-size distribution data based on polydisperse sphere systems. Vadose Zone Journal, 3(4), 1443-1454.

Coppola, A. 2000 Unimodal and bimodal descriptions of hydraulic properties for aggregated soils. Soil Science Society of America Journal, 64(4), 1252-1262.

Durner, W. 1994 Hydraulic conductivity estimation for soils with heterogeneous pore structure. Water Resource Research, 30(2), 211-223.

Fredlund, D. G., and Xing, A. 1994 Equations for the soil water characteristic curve. Canadian Geotechnical Journal, 31(4), 521-532.

Spohrer, K., Herrmann, L., Ingwersen, J., and Stahr, K. 2006 Applicability of Uni- and Bimodal Retention Functions for Water Flow Modeling in a Tropical Acrisol. Vadose Zone Journal, 5(1), 48-58.

Kosugi, K. 1994 Three-parameter lognormal distribution model for soil water retention. Water Resource Research, 30(4), 891-901.

Kosugi, K., Hopmans, J.W., and Dane, J.H. 2002 Parametric models. In: J.H. Dane and G.C. Topp (ed.) Methods of soil analysis. Part 4. Physical methods. SSSA Book Ser. 5. SSSA, Madison, WI, pp. 739-757.

Kutílek, M. 2004 Soil hydraulic properties as related to soil structure. Soil Tillage

Research, 79(2), 175-184.

Kutílek, M., Jendele, L., Panayiotopoulos, K. P. 2006 The influence of uniaxial compression upon pore size distribution in bi-modal soils. Soil Tillage Research, 86(1), 27-37.

Nemes, A., Schaap, M.G., Leij., F.J. 2001 Description of the unsaturated soil hydraulic database UNSODA version 2.0. Journal of Hydrology, 251(3), 151-162.

Othmer, H.B., Diekkrüger, B., and Kutílek, M. 1991 Bimodal porosity and unsaturated hydraulic conductivity. Soil Science, 152(3), 139-150.

Peters, R.R., and Klavetter, E.A. 1988 A continuum model for water movement in an unsaturated fractured rock mass. Water Resource Research, 24(3), 416-430.

Šimůnek, J., Kodešová, R., M. Gribb, M., van Genuchten, M. Th. 1999 Estimating hysteresis in the soil water retention function from cone permeameter experiments. Water Resource Research, 35(5), 1329-1345.

Tuller, M., and Or, D. 2002 Unsaturated hydraulic conductivity of structured porous media: A review of liquid configuration-based models. Vadose Zone Journal, 1(1), 14-37.

van Genuchten, M.Th. 1980 A closed-form equation for predicting the hydraulic conductivity of unsaturated soils. Soil Science Society of America Journal, 44(5), 892-898.

Wilson, G.V., Jardine, P.M., and Gwo, J.P. 1992 Modeling the hydraulic properties of a multiregion soil. Soil Science Society of America Journal, 56(6), 1731-1737.

Zhang, L.M., and Chen, Q. 2005 Predicting Bimodal Soil water characteristic curves. Journal of Geotechnical and Geoenvironment Engineering, 131(5), 666-670.

Zhang, L.M., and Li. X. 2010 Microporosity structure of coarse granular soils. Journal of Geotechnical and Geoenvironment Engineering, 136(10), 1425-1436.

CHAPTER 6

6. PHYSICALLY BASED CLOSED-FORM EXPRESSION FOR THE BIMODAL UNSATURATED HYDRAULIC CONDUCTIVITY FUNCTION

6.1 INTRODUCTION

Simulation of flow and contaminant transport through the vadose zone requires knowledge of the soil hydraulic properties. These properties are the soil water characteristic curve (SWCC) relating the volumetric water content, θ (cm^3cm^{-3}), to the matric head, h (cm), and the hydraulic conductivity curve giving the hydraulic conductivity K (cm/s) as a function of θ or h (Coppola, 2000). Although hydraulic conductivity may be obtained by direct measurements, it is still time-consuming, labour intensive and expensive. However, alternative theoretical approaches based on statistical distribution models of pore size allow reasonably accurate estimates of conductivity to be obtained through the use of more easily measured SWCC data (Mualem, 1986).

The equation proposed by van Genuchten (1980) for the SWCC is widely adopted and generally coupled with Mualem's (1976) expression for predicting hydraulic conductivity. The van Genuchten–Mualem model has produced satisfactory results in soils with a unimodal pore size distribution. Nevertheless, the pore size distributions of some soils is often bimodal or multimodal (Durner, 1994; Zhang and Chen, 2005; Spohrer *et al*. 2006; Zhang and Li, 2010). For example, structural soils consist of interconnected networks of matrix (inter-aggregate) and structural (intra-aggregate) pores forming two (or more) distinct pore spaces (Kutílek, 2004). The existence of two vastly different pore domains results in pore size distributions of structural soils that are often bimodal. In such soils the independent draining of the structural and matrix pores frequently results in two distinct air-entry values, which any single

unimodal function does not reproduce adequately (Othmer *et al*., 1991; Durner, 1994). To counter these problems, several approaches have been developed to describe bimodal or multimodal SWCCs in the past decades. Peters and Klavetter (1988) first proposed the superposition of two unimodal pore systems to represent bimodal pore size distributions. This approach was generalized by Othmer *et al*. (1991), Durner (1994) and Zhang and Chen (2005) to consider multimodal pore size distributions, each of which is characterized by its own SWCC function. Recently, Liu *et al*. (2012) proposed a more physically based SWCC model by superposing the unimodal lognormal model of Kosugi (1994). Superposition of the unimodal SWCC model has also been used for modelling the hydraulic conductivity of structured soils. Priesack and Durner (2006) derived a closed-form expression for the multimodal unsaturated conductivity function by combining the multimodal representation of van Genuchten's SWCC function (van Genuchten, 1980) with the conductivity representation model of Mualem (Mualem, 1976). Spohrer *et al*. (2006) investigated the applicability of unimodal and bimodal representations of van Genuchten's SWCC functions for modelling water flow in a tropical acrisol. A physically based approach to represent the hydraulic properties of structured porous media was proposed by Tuller and Or (2002), which considered equilibrium liquid configurations in bimodal pore space. However, the derived functions of this approach are rather complex (Priesack and Durner, 2006). Kutílek (2004) also proposed a physically based hydraulic model for structural soils using the lognormal hydraulic model of Kosugi (1994) and partitioned the structural and matrix pore domains by the air-entry value of the matrix pore.

The primary objective of this study was to develop a physically based closed-form expression for the bimodal unsaturated hydraulic conductivity function of soils with bimodal pore size distribution. The specific objectives were: (i) to derive a bimodal closed-form unsaturated lognormal hydraulic conductivity function by combining the bimodal lognormal SWCC model (Liu *et al*. 2012) with Mualem's hydraulic model (Mualem, 1976); (ii) to demonstrate the applicability of the proposed functions using

experimental data for the representation of bimodal SWCCs and corresponding conductivity curves .

6.2 METHODS

6.2.1 Bimodal equations of soil hydraulic functions

1) Bimodal SWCC function

Brutsaert (1966) studied four models of pore size distribution, among them the lognormal distribution in relation to SWCC. A more detailed analysis was presented by Kosugi (1994), who assumed the lognormal pore probability density function for pore radii, $g(r)$ as:

$$g(r) = \frac{\theta_s - \theta_r}{\sqrt{2\pi}\sigma r} \exp\left\{-[\ln(r / r_m)]^2 / 2\sigma^2\right\} \tag{6-1}$$

where r, the pore radius (cm), obeys the lognormal distribution; θ_s and θ_r, the saturated and the residual volumetric water content (cm^3cm^{-3}), respectively; r_m denotes the median pore radius (cm), and σ denotes the standard deviation of $\ln(r)$. For dual-porosity structural soils, there are two continual pore series: structural pores and matrix pores. Liu *et al*. (2012) assumed the probability density functions for each pore series obey lognormal distribution and could be superposed to obtain the overall probability density function of the structural soils. Two continual pore series were combined by introducing weighting factors to describe the volumetric percentage of each pore fraction, the pore probability density function of the dual-porosity structural soil proposed by Liu *et al*. (2012) has the following form:

$$\begin{aligned} g(r) &= \sum_{i=1}^{k} \phi_i g_i(r) = \sum_{i=1}^{k} \phi_i \frac{\theta_s - \theta_r}{\sqrt{2\pi}\sigma_i r} \exp\left\{-[\ln(r / r_{m_i})]^2 / 2\sigma_i^2\right\} \\ 0 &< \phi_i < 1 \text{ and } \sum_{i=1}^{k} \phi_i = 1 \end{aligned} \tag{6-2}$$

where k, the number of pore series (k = 2); $g_i(r)$, the pore probability density function (cm^{-1}) for the ith pore series; ϕ_i, the volumetric percentage of the soil components with the ith pore series; r_{m_i}, the median pore radius (cm) for the ith pore series; σ_i denotes the standard deviation of $\ln(r)$ associated with the ith pore series. Based on

bimodal lognormal pore size distribution, Liu *et al*. (2012) proposed the bimodal SWCC function for the structural soil as follows:

$$S_e = (\theta-\theta_r)/(\theta_s-\theta_r) = \sum_{i=1}^{k} \phi_i F_n\left[\ln(h/h_{m_i})/\sigma_i\right]$$
$$0<\phi_i<1 \text{ and } \sum_{i=1}^{k}\phi_i=1 \quad (6\text{-}3)$$

where S_e, the effective saturation; θ, the volumetric water content (cm^3cm^{-3}); h denotes the suction head (cm); h_{m_i}, the median matric head (cm) of ith pore series associates with r_{m_i} by the capillary equation ($h_{m_i} = A/h_{m_i}$, constant value of A = 0.149 cm^2); $F_n(x)$, the complementary normal distribution function is defined as:

$$F_n(x) = \frac{1}{\sqrt{2\pi}}\int_x^{\infty} \exp(-t^2/2)dt \quad (6\text{-}4)$$

where t is a dummy variable. Eq. (6-3) is derived on the basis of there being two combined lognormal pore radius density curves in the structural soil. In the case of k = n (n > 2), there are multiple pore series in the soil and Eq. (6-3) becomes the multimodal lognormal SWCC function.

2) Bimodal unsaturated hydraulic conductivity function

With the assumption of pore continuity and connectivity, Burdine (1953) and Mualem (1976) proposed approaches for unsaturated hydraulic conductivity. A generalized form of the model for predicting the relative hydraulic conductivity K_r from SWCC is written as (Hoffmann-Riem *et al*., 1999):

$$K_r = K/K_s = S_e^{\lambda}\left(\int_0^{S_e}\frac{dS_e}{h^{\beta}}\Big/\int_0^{1}\frac{dS_e}{h^{\beta}}\right)^{\gamma} \quad (6\text{-}5)$$

where K_s and K are the saturated and unsaturated hydraulic conductivities (cms^{-1}), respectively. The parameters λ, β as tortuosities and pores connectivity for γ (subject to $\lambda \geqslant 0$, $\beta > 0$, and $\gamma > 1$). These parameters determine the shape of the hydraulic conductivity function K. The integral in Eq. (6-5) is transformed as follows:

$$\int_0^{S_e}\frac{dS_e}{h^{\beta}} = \frac{1}{A^{\beta}(\theta_s-\theta_r)}\int_0^{r} r^{\beta}g(r)dr \quad (6\text{-}6)$$

Substituting Eq. (6-2) into Eq. (6-6) leads to:

$$\int_0^{S_e} \frac{dS_e}{h} = \frac{1}{\sqrt{2\pi}A^{\beta}} \sum_{i=1}^{k} \frac{\phi_i}{\sigma_i} \int_0^{r} r^{\beta-1} \exp\left\{-[\ln(r / r_{m_i})]^2 / 2\sigma_i^2\right\} dr \tag{6-7}$$

Substitution of $y_i = \ln(r/r_{m_i})$ into Eq. (6-7) yields:

$$\int_0^{S_e} \frac{dS_e}{h} = \frac{1}{\sqrt{2\pi}A^{\beta}} \sum_{i=1}^{k} \frac{\phi_i r_{m_i}^{\beta}}{\sigma_i} \int_0^{\ln(r/r_{m_i})} \exp\left(\beta y_i - y_i^2 / 2\sigma_i^2\right) dy_i \tag{6-8}$$

Substituting $z_i = (\sigma_i^2 - y_i)/\sqrt{2}\sigma_i$ into Eq. (6-8) leads to:

$$\int_0^{S_e} \frac{dS_e}{h} = \frac{1}{-\sqrt{\pi}A^{\beta}} \sum_{i=1}^{k} \phi_i r_{m_i}^{\beta} \exp\left(\frac{\beta^2\sigma_i^2}{2}\right) \int_{\infty}^{[\sigma_i^2 - \ln(r/r_{m_i})]/\sqrt{2}\sigma_i} \exp\left(-z_i^2\right) dz_i$$

$$= \sum_{i=1}^{k} \frac{\phi_i}{h_{m_i}^{\beta}} \exp\left(\frac{\beta^2\sigma_i^2}{2}\right) F_n\left[\frac{\ln(r_{m_i}/r)}{\sigma_i} + \beta\sigma_i\right]$$

$$= \sum_{i=1}^{k} \frac{\phi_i}{h_{m_i}^{\beta}} \exp\left(\frac{\beta^2\sigma_i^2}{2}\right) F_n\left[\frac{\ln(h/h_{m_i})}{\sigma_i} + \beta\sigma_i\right] \tag{6-9}$$

Substitution of $S_e = 1$ into Eq. (6-9) yields:

$$\int_0^{1} \frac{dS_e}{h} = \sum_{i=1}^{k} \frac{\phi_i}{h_{m_i}^{\beta}} \exp\left(\frac{\beta^2\sigma_i^2}{2}\right) \tag{6-10}$$

Substituting Eq. (6-9) and Eq. (6-10) into Eq. (6-5) obtains:

$$K_r = S_e^{\lambda} \left(\frac{\sum_{i=1}^{k} \frac{\phi_i}{h_{m_i}^{\beta}} \exp\left(\frac{\beta^2\sigma_i^2}{2}\right) F_n\left[\frac{\ln(h/h_{m_i})}{\sigma_i} + \beta\sigma_i\right]}{\sum_{i=1}^{k} \frac{\phi_i}{h_{m_i}^{\beta}} \exp\left(\frac{\beta^2\sigma_i^2}{2}\right)} \right)^{\gamma} \tag{6-11}$$

Eq. (6-11) is the bimodal lognormal unsaturated hydraulic conductivity function when $k = 2$. In the case of k = n (n > 2), Eq. (6-11) becomes the multimodal lognormal unsaturated hydraulic conductivity function. The cases of the Burdine's and Mualem's conductivity model are obtained by setting $\lambda = 1$, $\beta = 2$, $\gamma = 1$ and $\lambda = 0.5$, $\beta = 1$, $\gamma = 2$ in Eq. (6-11), respectively. In this study, we adopted Mualem's model to predict unsaturated hydraulic conductivity, Eq. (6-11) becomes:

$$K_r = S_e^{0.5}\left(\frac{\sum_{i=1}^{k}\frac{\phi_i}{h_{m_i}}\exp\left(\frac{\sigma_i^2}{2}\right)F_n\left[\frac{\ln(h/h_{m_i})}{\sigma_i}+\sigma_i\right]}{\sum_{i=1}^{k}\frac{\phi_i}{h_{m_i}}\exp\left(\frac{\sigma_i^2}{2}\right)}\right)^2 \quad (6\text{-}12)$$

6.2.2 Evaluation of the bimodal hydraulic model

The proposed bimodal hydraulic model (bimodal SWCC and unsaturated hydraulic conductivity functions) was evaluated by applying it to various soils. The bimodal lognormal soil hydraulic (hereafter referred to as BLN) model was compared with the unimodal lognormal soil hydraulic (ULN) model proposed by Kosugi (1996) and the bimodal van Genuchten–Mualem soil hydraulic (BvG) model proposed by Priesack and Durner (2006). Six soil samples were selected for this purpose (shown in Table 1). Three examples used the soil hydraulic property data cited from Smettem and Kirkby (1990), Mohanty *et al*. (1997) and Kutílek (2004). Further evaluations were performed for three soils cited from the UNSODA database (Nemes *et al*., 2001). In all cases, parameter θ_s was set at its measured value and θ_r was assumed to be zero because no clear information about residual water content was available for the soils we considered. In this evaluative procedure, the root mean square error (RMSE) of the measured and simulated variables was used as measure of the goodness-of-fit.

6.3 RESULTS AND DISCUSSION

6.3.1 Soil water characteristic curve function

The soil hydraulic parameters and corresponding RMSE values for all soil samples are reported in Table 6.1. Comparisons among the RMSE (S_e) values in Table 6.1 for all soil samples show that the fit results of the BLN model and BvG model are almost same, and always better than the ULN function. The best fit to the available SWCC data occurred for the example of Kutílek (2004), with RMSE (S_e) values of 0.002. In nearly all cases, using the bimodal models yielded RMSE (S_e) values that are about one order of magnitude lower than using the unimodal model. In terms of parameters of the BLN model, the median suction head ranges between 2.20 cm to 1214.15 cm for the structural pores (h_{m_1}) and from 119.04 cm to 18990.27 cm for the matrix pores (h_{m_2}). This implies that the median pore radii are from 1.23×10^{-4} cm to 6.79×10^{-2} cm for structural pores and from 7.85×10^{-6} cm to 1.25×10^{-3} cm for

matrix pores (h_m and r_m are inversely proportional). The classification system of soil pores by Tuller and Or (2002) is questionable when considering our results. Our results support the belief that the classification systems of soil pores based upon fixed boundaries between pore size categories is not appropriate, as pointed out by Kutílek et al. (2006). The BvG model also successfully fit measured SWCC data. However, it was derived empirically and fitting parameters α_1, n_1, α_2 and n_2 do not have physical significance. Although the ULN model parameters have physical significance, they were, however, unable to describe the bimodal behavior of structural soils.

Table 6.1 Comparison of the fitted and predicted capability of ULN, BvG and BLN models

Example	Soil taxon	Model	Parameter and values						RMSE (S_e)	RMSE (K_r)
		ULN		h_m (cm)	σ					
		BvG	ϕ_1	α_1	n_1	ϕ_2	α_2	n_2		
		BLN	ϕ_1	h_{m_1}(cm)	σ_1	ϕ_2	h_{m_2}(cm)	σ_2		
Smettem and Kirkby (1990)	Typic Haploxeroll	ULN	-	25.42	3.24	-	-	-	0.058	0.325
		BvG	0.52	0.56	2.07	0.48	0.01	2.01	0.010	0.246
		BLN	0.49	2.86	0.98	0.51	254.85	1.09	0.009	0.091
Mohanty *et al.* (1997)	Typic Torrifluvent	ULN	-	111.14	0.78	-	-	-	0.029	0.415
		BvG	0.07	0.85	1.77	0.93	0.01	2.83	0.012	0.323
		BLN	0.06	2.20	0.44	0.94	119.04	0.69	0.011	0.095
Kutilek (2004)	Aquic Hapludalf	ULN	-	821.83	4.23	-	-	-	0.030	0.292
		BvG	0.31	0.16	2.16	0.70	0.00	1.28	0.002	0.069
		BLN	0.26	8.42	0.87	0.74	3171.25	2.51	0.003	0.050
UNSODA Code: 2751	-	ULN	-	11849.58	4.39	-	-	-	0.022	0.458
		BvG	0.22	0.08	1.75	0.79	0.00	1.32	0.002	0.338
		BLN	0.18	23.46	1.09	0.82	18990.28	2.15	0.002	0.304
UNSODA Code: 2752	-	ULN	-	5510.85	3.92	-	-	-	0.025	0.179
		BvG	0.19	0.20	1.58	0.81	0.00	1.32	0.007	0.160
		BLN	0.15	9.93	1.26	0.85	9533.20	2.26	0.007	0.154
UNSODA Code: 4672	Typic Hapludalf	ULN	-	10172.07	3.45	-	-	-	0.015	0.585
		BvG	0.56	0.02	1.14	0.44	0.00	1.20	0.009	0.543
		BLN	0.57	1214.15	2.31	0.43	17454.59	0.12	0.008	0.444

Comparisons between the measured SWCC data points and the fitted unimodal and bimodal curves are shown in Figures 6.1-6.6. The BvG and BLN model fitted curves almost coincide and fairly well fit the measured data, while the poor fit offered by ULN model is evident. Figures 6.1-6.6 clearly show that the ULN model is unable to capture the typical features of structural behaviours.

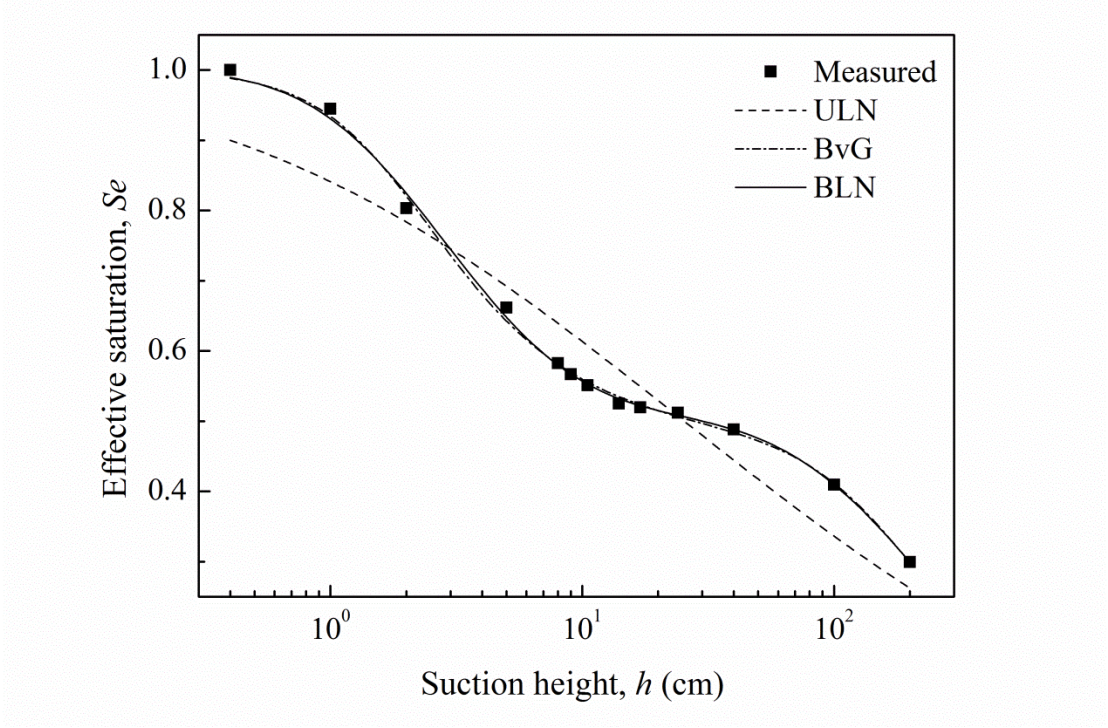

Figure 6.1 Fitted SWCC for sample from Smettem and Kirkby (1990) based on ULN, BvG and BLN functions

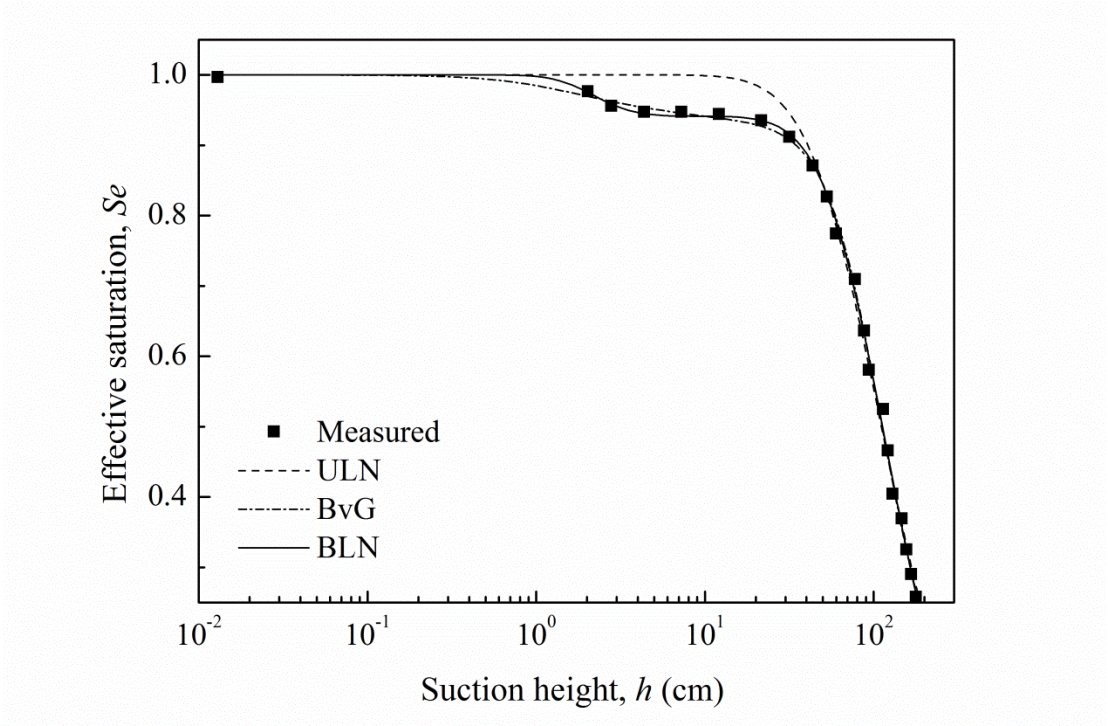

Figure 6.2 Fitted SWCC for sample from Mohanty *et al*. (1997) based on ULN, BvG and BLN functions

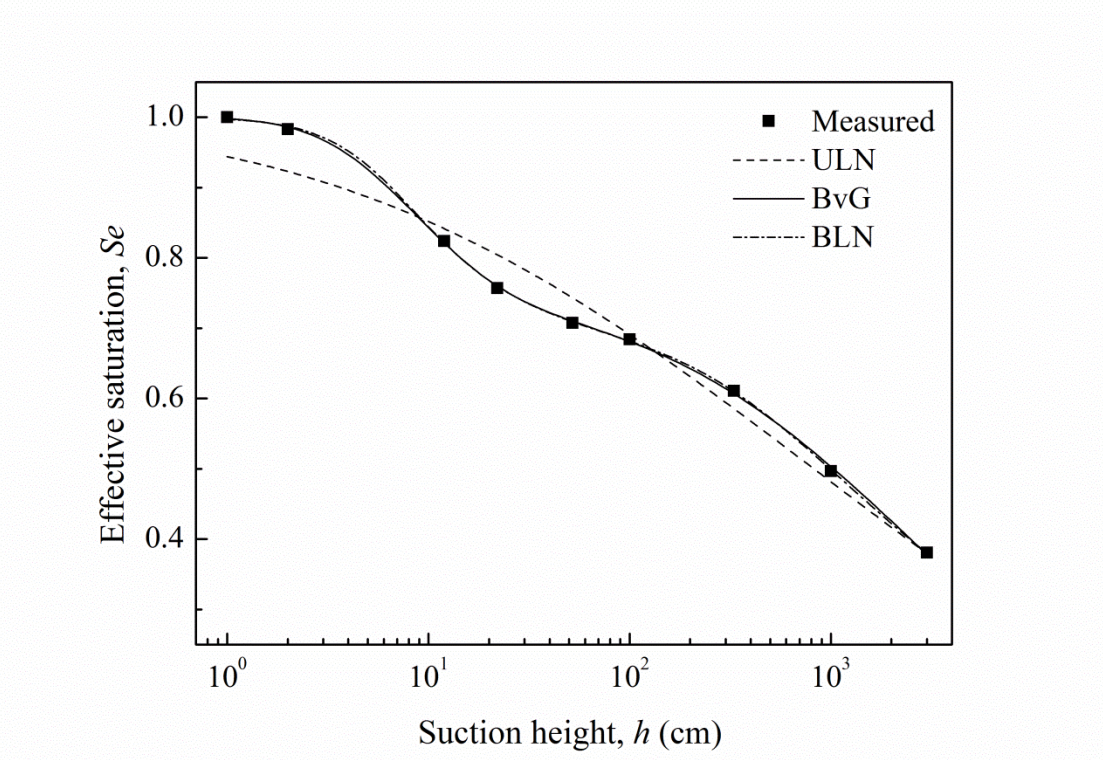

Figure 6.3 Fitted SWCC for sample from Kut Ɨek (2004) based on ULN, BvG and BLN functions

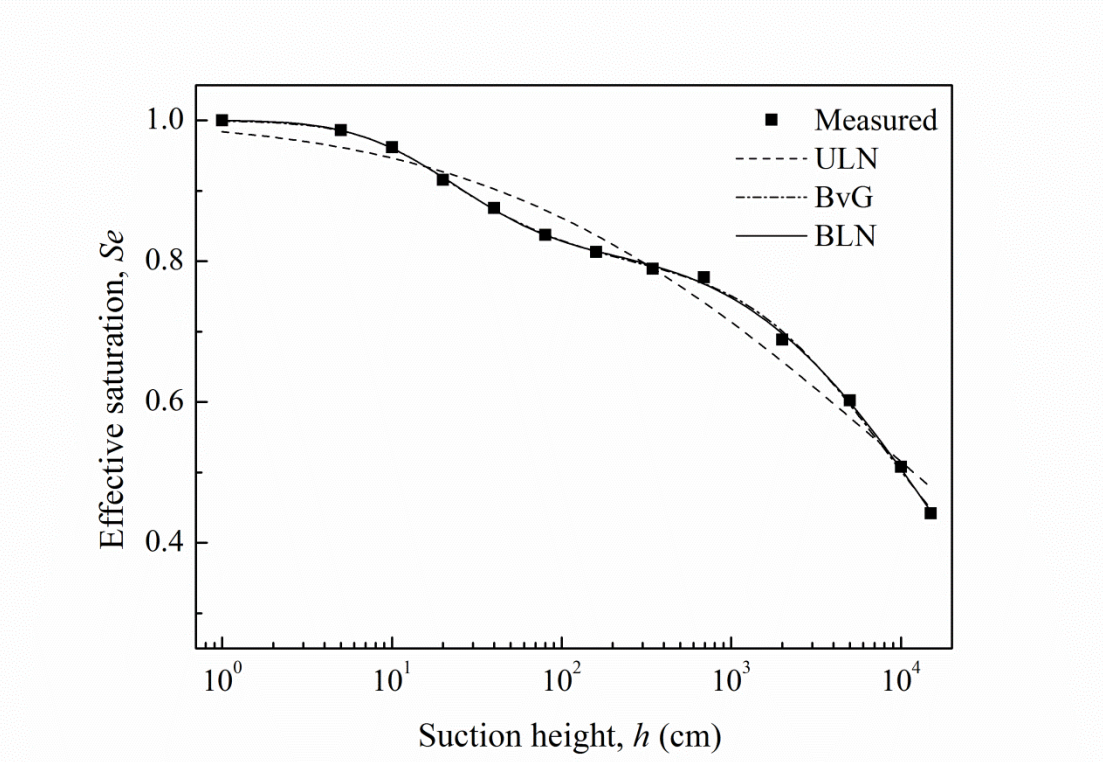

Figure 6.4 Fitted SWCC for sample from UNSODA (2751) based on ULN, BvG and BLN functions

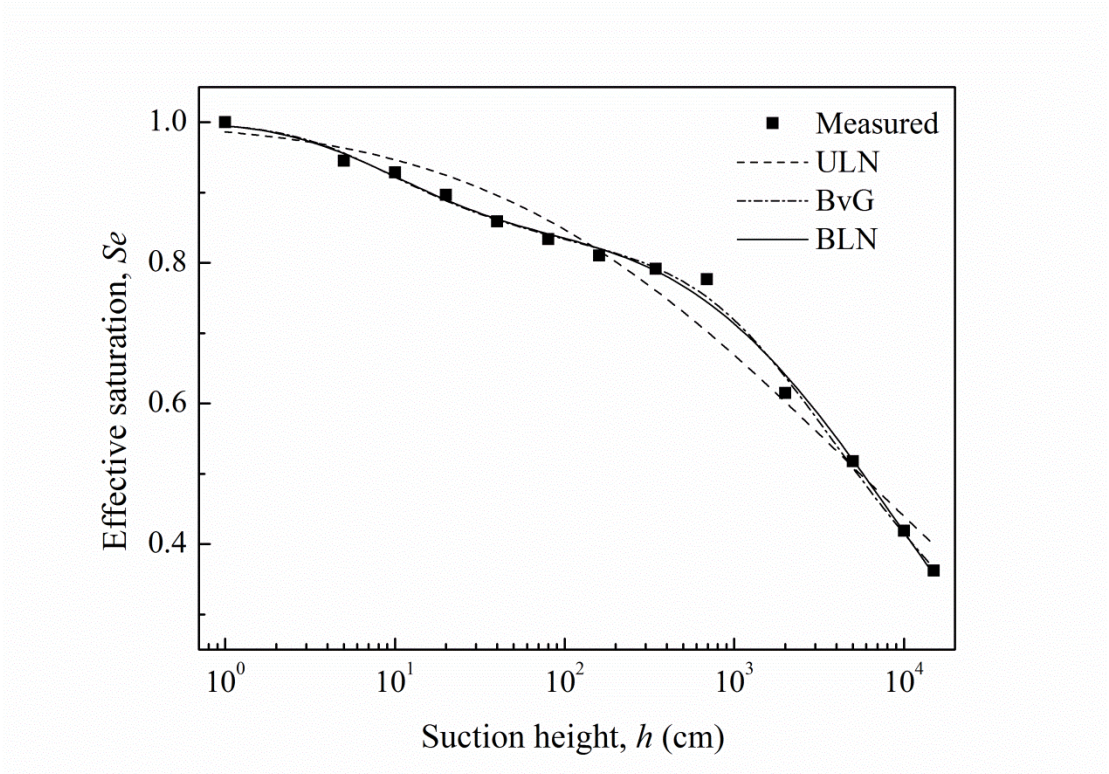

Figure 6.5 Fitted SWCC for sample from UNSODA (2752) based on ULN, BvG and BLN functions

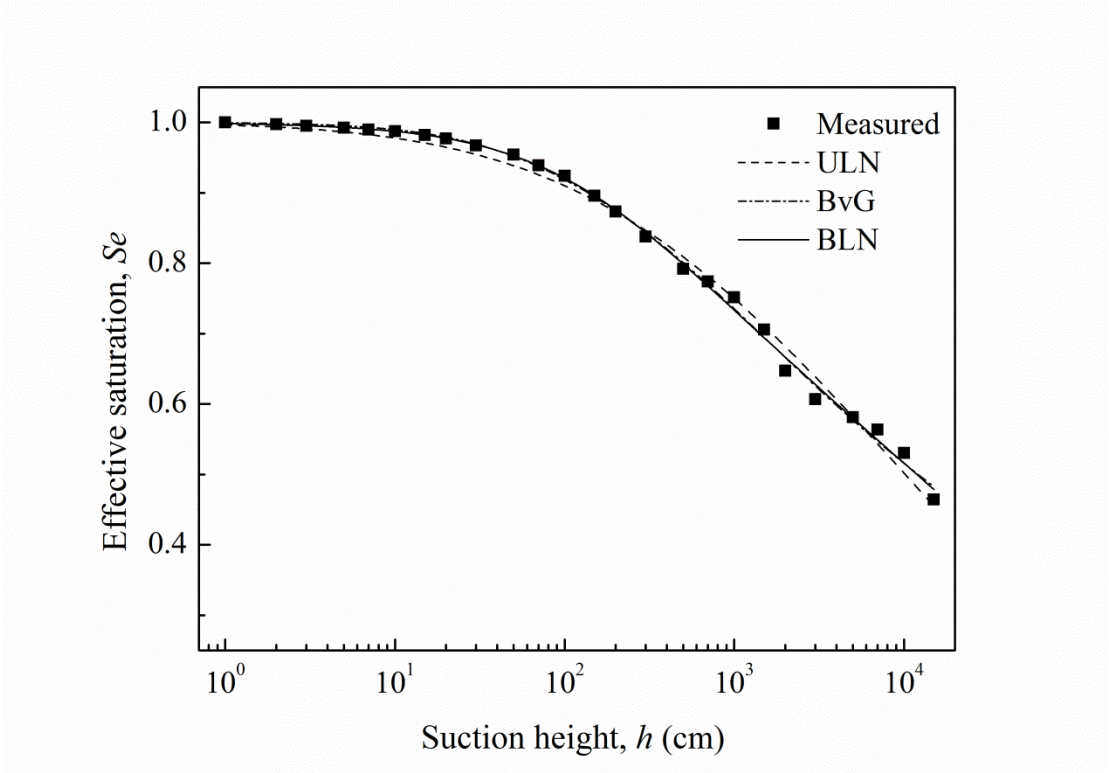

Figure 6.6 Fitted SWCC for sample from UNSODA (4672) based on ULN, BvG and BLN functions

6.3.2 Unsaturated hydraulic conductivity functions

Table 6.1 shows that the RMSE (K_r) values decreased when the BLN model was used and this model was always better than the ULN and BvG models. In terms of predicting the unsaturated hydraulic conductivity, the examples of Smettem and Kirkby (1990), Mohanty *et al*. (1997) and Kutílek (2004) seem to have benefitted more from adopting the proposed BLN model. The ULN model was unable to describe the typical features of structural behaviour, which largely affected the prediction of the unsaturated hydraulic conductivity for the soil samples considered. Although the BvG model reasonably described the SWCC data, it does not perform well as BLN model for predicting the unsaturated hydraulic conductivity. This may partly be due to the larger flexibility of the BLN model. The measured $K_r(h)$ data points and the predicted results using ULN, BvG and BLN models for soil samples are shown in Figures 6.7-6.12. Comparisons between the measured $K_r(h)$ data and the predicted relative hydraulic conductivity curves highlight the good agreement of the proposed BLN model with the measured data. From Figure 2 and Figure 3 we conclude that the BvG model, which gives a reasonable description of the SWCC, does not necessarily imply a good prediction of the unsaturated hydraulic conductivity behaviours. Table 1 and Figures 6.7-6.12 demonstrate that the proposed BLN model improved the ability of representations of the hydraulic curves to simulate water flow in structural soils. It is worth mentioning that the application of the BLN model to UNSODA 2752 and UNSODA 4672 resulted in inadequate representation of the conductivity curve, although the fit of the SWCC data was rather good (Figures 6.5 and 6.6). The main reason for the discrepancy between the predictions and the measured data sets is in the use of fixed values of parameters λ, β and γ, where according to the rigid model $\lambda = 0.5$, $\beta = 1$, $\gamma = 2$. Future research should focuson the appropriate evaluation of all three parameters in the $K_r(h)$ function on the basis of soil micromorphological features.

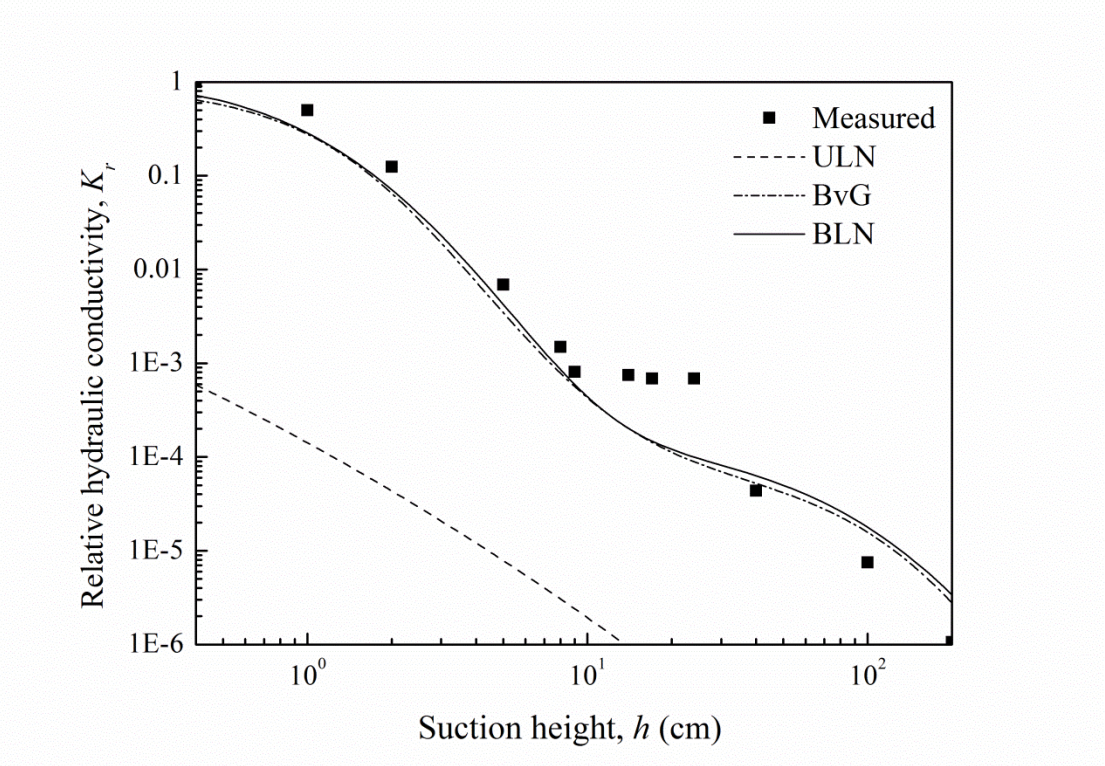

Figure 6.7 Predicted hydraulic conductivity curve for sample from Smettem and Kirkby (1990) based on ULN, BvG and BLN models

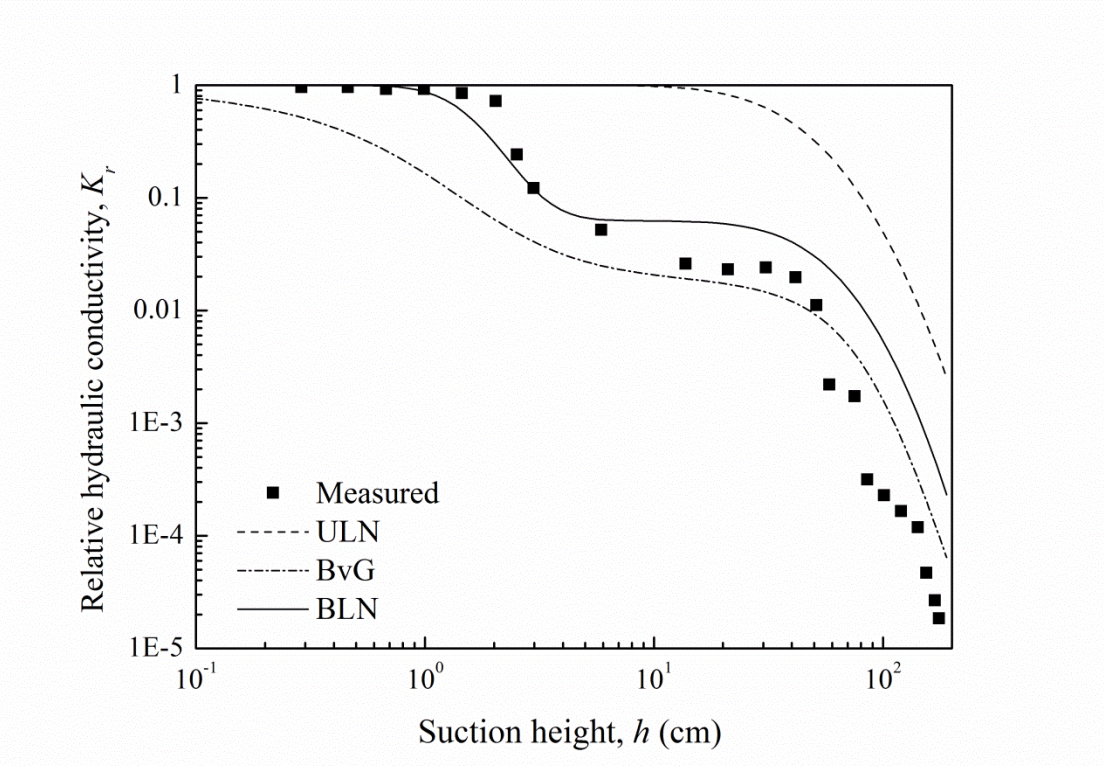

Figure 6.8 Predicted hydraulic conductivity curve for sample from Mohanty *et al*. (1997) based on ULN, BvG and BLN models

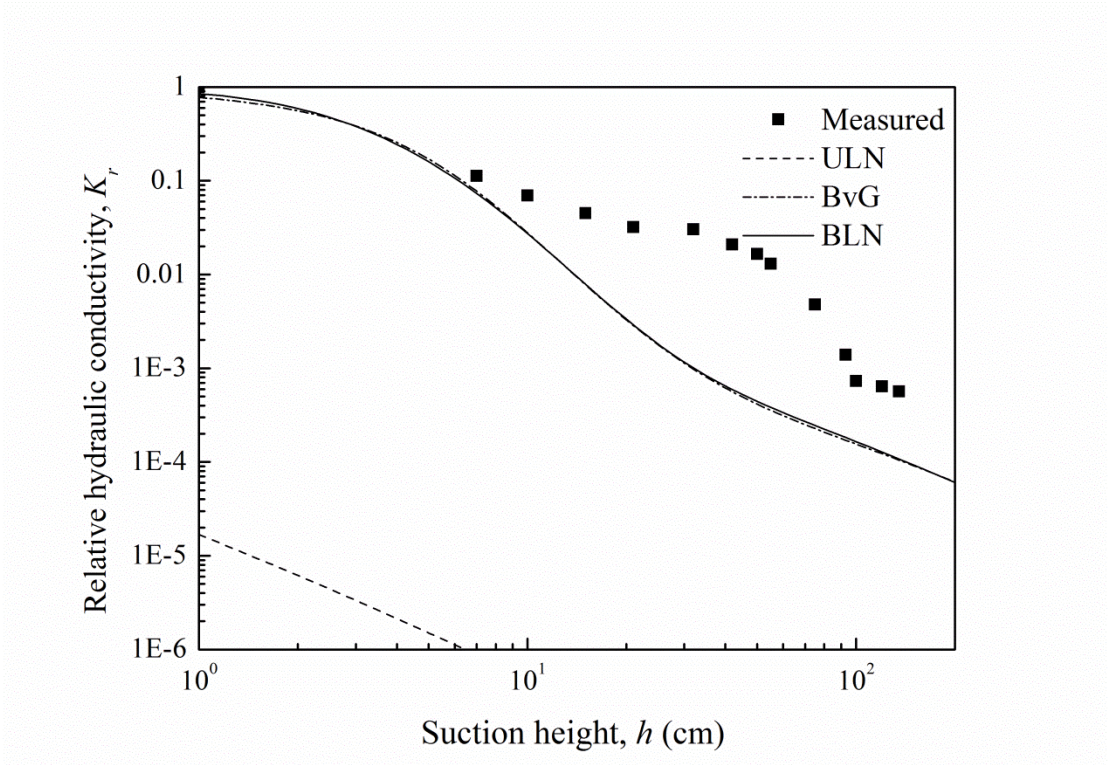

Figure 6.9 Predicted hydraulic conductivity curve for sample from Kut ĺek (2004) based on ULN, BvG and BLN models

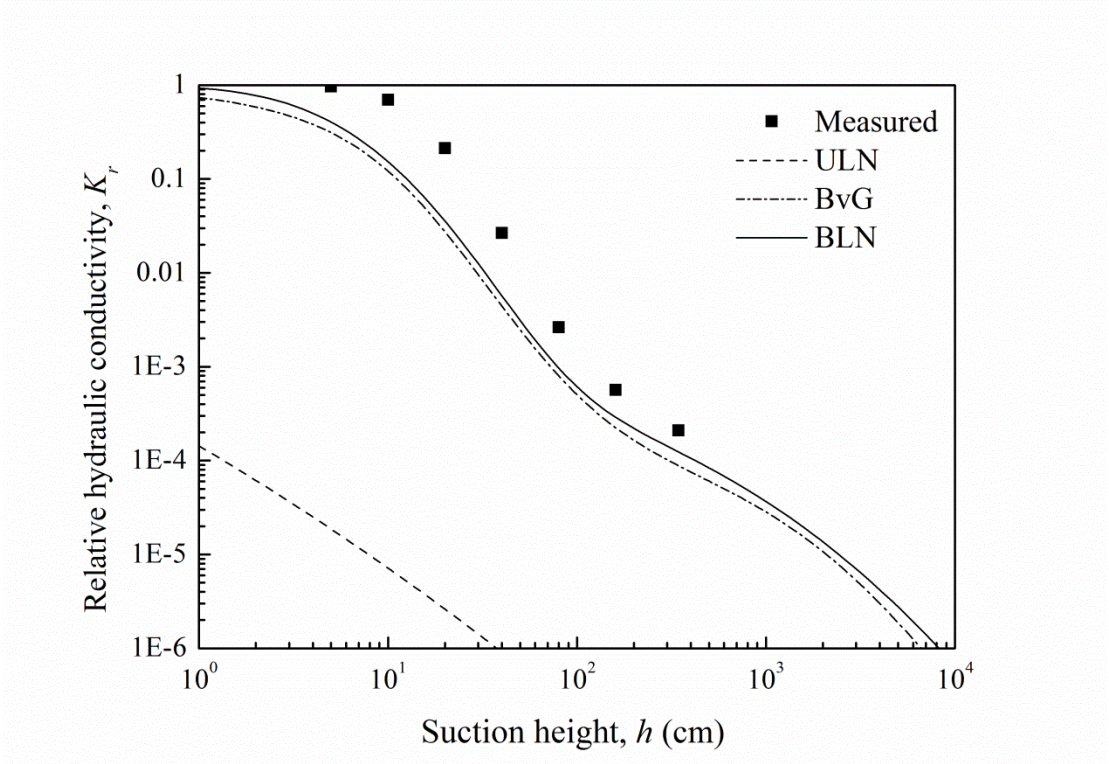

Figure 6.10 Predicted hydraulic conductivity curve for sample from UNSODA (2751) based on ULN, BvG and BLN models

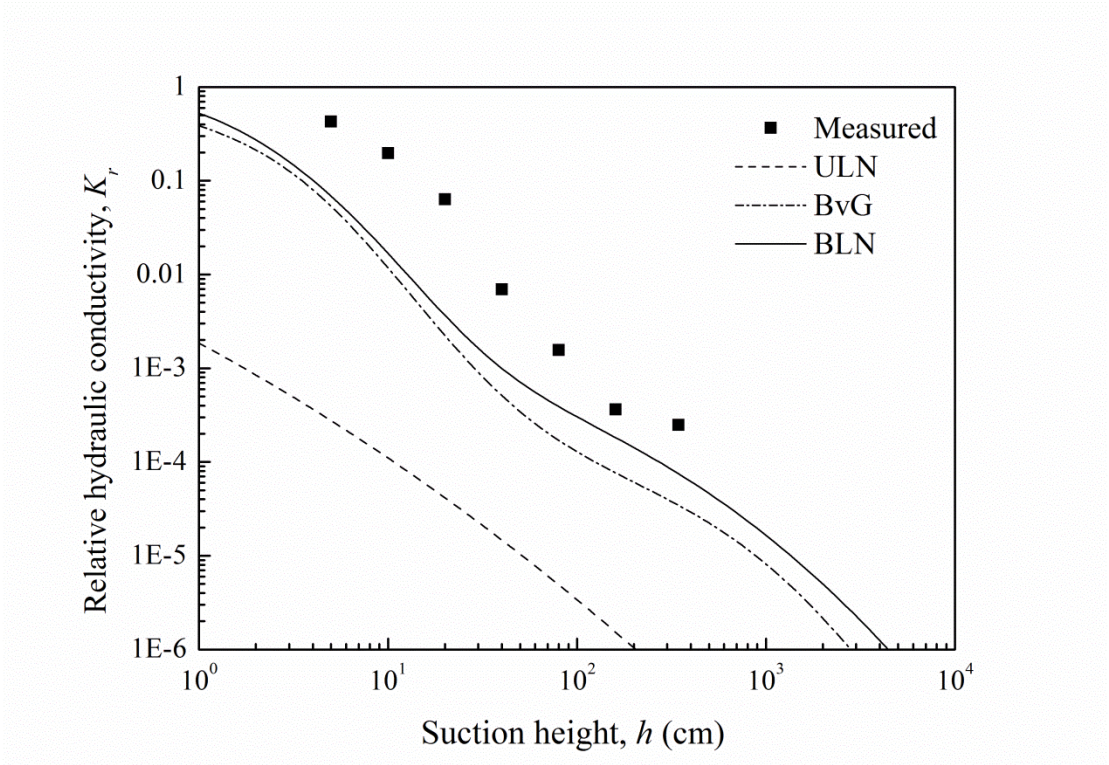

Figure 6.11 Predicted hydraulic conductivity curve for sample from UNSODA (2752) based on ULN, BvG and BLN models

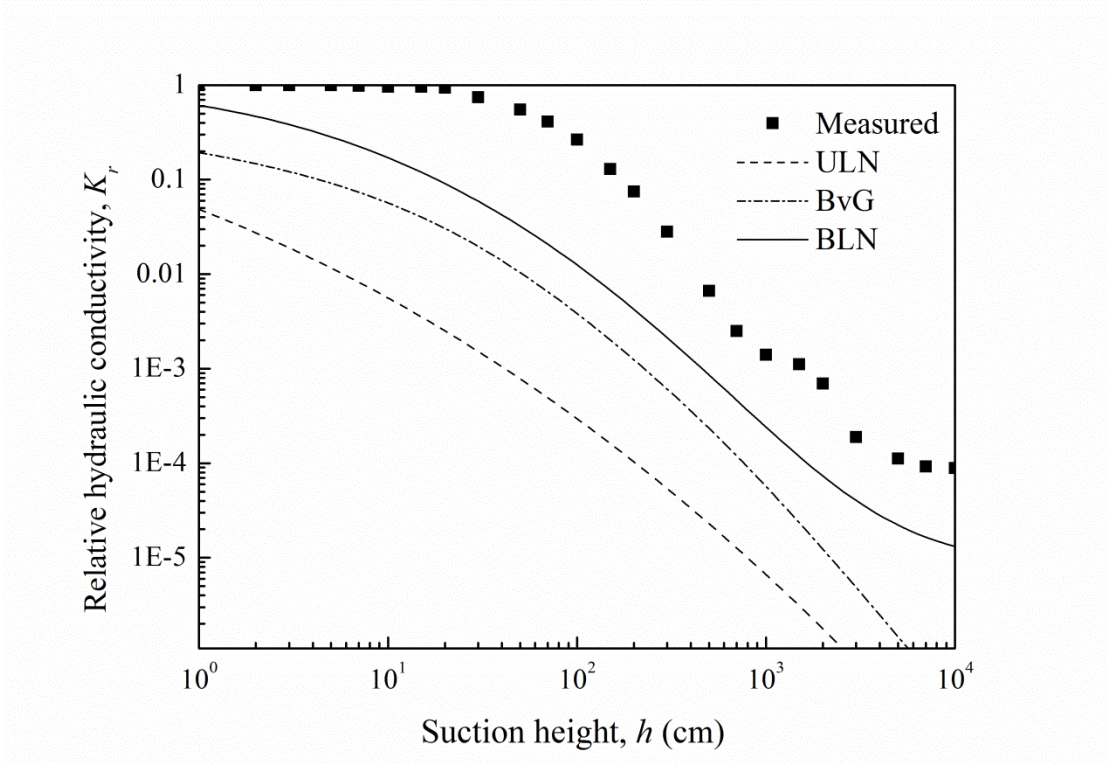

Figure 6.12 Predicted hydraulic conductivity curve for sample from UNSODA (4672) based on ULN, BvG and BLN models

6.4 SUMMARY

In this chapter, a physically based closed-form expression for the bimodal unsaturated hydraulic conductivity function was proposed for soils with bimodal pore size distribution. By assuming a lognormal pore size distribution for each pore domains and using weighting factors combined individual functions. The proposed equations are defined by parameters that have physical significances which can be related to the properties of the materials. Experimental data verification and parametric analyses were undertaken to demonstrate the fit and predicting capability of the proposed equations. The proposed BLN model improved capability of representations of the hydraulic curves to simulate water flow in structural soils. These functions can potentially be used as an effective tool for identifying hydraulic porosities in structural soils.

REFERENCES

Brutsaert, W. 1966 Probability laws for pore size distributions. Soil Science, 101(2), 85–92.

Burdine, N.T. 1953 Relative permeability calculation from size distribution data. Journal of Petroleum Technology, 5(3), 71–78.

Coppola, A. 2000 Unimodal and bimodal descriptions of hydraulic properties for aggregated soils. Soil Science Society of America Journal, 64(4), 1252–1262.

Durner, W. 1994 Hydraulic conductivity estimation for soils with heterogeneous pore structure. Water Resource Research, 30(2), 211–223.

Hoffmann-Riem, H., van Genuchten, M.Th. and Fluhler, H. 1999 A general model of the hydraulic conductivity of unsaturated soils. pp. 31–42. In: van Genuchten, M.Th. et al. (ed.) Proc. Int. Workshop, Characterization And Measurements Of The Hydraulic Properties Of Unsaturated Porous Media, 22–24 October 1997. University of California, Riverside.

Kosugi, K. 1994 Three-parameter lognormal distribution model for soil water retention. Water Resource Research, 30(4), 891–901.

Kosugi, K. 1996 Lognormal distribution modal for unsaturated soil hydraulic properties. Water Resource Research, 32(9), 2697–2703.

Kutílek, M. 2004 Soil hydraulic properties as related to soil structure. Soil Tillage Research, 79(2), 175–184.

Kut ĭek, M., Jendele, L. & Panayiotopoulos, K. P. 2006 The influence of uniaxial compression upon pore size distribution in bi-modal soils. Soil Tillage Research, 86(1), 27–37.

Liu, S. Y., Yasufuku N., Liu, Q., Omine, K. & Hemanta, H. 2013 Bimodal and multimodal descriptions of soil water characteristic curves for structural soils. Water Science and Technology, 67(8), 1740–1747.

Mohanty, B. P., Bowman, R. S., Hendrickx, J. M. H. & van Genuchten., M.Th. 1997 New piecewise-continuous hydraulic functions for modeling preferential flow in an intermittent-flood-irrigated field. Water Resource Research, 33(9), 2049–2063.

Mualem, Y. 1976 A new model for predicting the hydraulic conductivity of unsaturated porous media. Water Resource Research, 12(3), 513–522.

Mualem, Y. 1986 Hydraulic conductivity of unsaturated soils: prediction and formulas. In: A. Klute (ed.) Methods of Soil Analysis. Part 1. 2nd ed. Agron. Monogr. 9. ASA and SSSA, Madison, WI. pp. 799–823.

Nemes, A., Schaap, M. G. & Leij., F. J. 2001 Description of the unsaturated soil hydraulic database UNSODA version 2.0. Journal of Hydrology, 251(3), 151–162.

Othmer, H. B., Diekkrüger, B. & Kut ŀek, M. 1991 Bimodal porosity and unsaturated hydraulic conductivity. Soil Science, 152(3), 139–150.

Peters, R. R. & Klavetter, E. A. 1988 A continuum model for water movement in an unsaturated fractured rock mass. Water Resource Research, 24(3), 416–430.

Priesack, E. & Durner, W. 2006 Closed-form expression for the multi-modal unsaturated conductivity function. Vadose Zone Journal, 5(1), 121–124.

Schaap, M.G. 2005. Models for indirect estimation of soil hydraulic properties. pp. 1145–1150. In M.G. Anderson (ed.) Encyclopedia of hydrological sciences. John Wiley & Sons, New York.

Smettem, K. R. J. & Kirkby, C. 1990 Measuring the hydraulic properties of a stable aggregated soil. Journal of Hydrology, 117(1–4), 1–13.

Spohrer, K., Herrmann, L., Ingwersen, J. & Stahr, K. 2006 Applicability of uni- and bimodal retention functions for water flow modeling in a tropical acrisol. Vadose Zone Journal, 5(1), 48–58.

Tuller, M., and Or, D. 2002 Unsaturated hydraulic conductivity of structured porous media: A review of liquid configuration-based models. Vadose Zone Journal, 1(1), 14–37.

van Genuchten, M.Th. 1980 A closed-form equation for predicting the hydraulic conductivity of unsaturated soils. Soil Science Society of America Journal, 44(5), 892–898.

Zhang, L. M. & Chen, Q. 2005 Predicting bimodal soil water characteristic curves. Journal of Geotechnical and Geoenvironmental Engineering, 131(5), 666–670.

Zhang, L. M. & Li, X. 2010 Microporosity structure of coarse granular soils. Journal of Geotechnical and Geoenvironmental Engineering, 136(10), 1425–1436.

CHAPTER 7

7. CONCLUSIONS AND FUTURE WORK

7.1 Conclusions

Simulation of flow and contaminant transport through the vadose zone requires knowledge of the soil hydraulic properties. These properties are the soil water characteristic curve (SWCC) relating the volumetric water content, θ (cm^3cm^{-3}), to the matric head, h (cm), and the hydraulic conductivity curve giving the hydraulic conductivity K (cm/s) as a function of θ or h. Although hydraulic properties may be obtained by direct measurements, it is still time-consuming, labour intensive and expensive. In this study, alternative theoretical approaches used to estimate hydraulic properties through the use of more easily measured data.

The following major conclusions can be drawn:

(1) The physically based scaling technique was extended to the Arya and Paris model to predict soil water characteristic curve for single-porosity soils from particle-size distribution. Experimental soil data that representing wide range of textures that include sand, sandy loam, loam, silt loam, and clay, were selected for this purpose. In addition, other soil samples with different textures were used to test this method. Results showed that the physically based scaling technique improved the Arya and Paris estimation and outperformed other approaches. Especially, when applied the physically based scaling technique approach to soils with similar texture. The study can clearly demonstrate the potential capability to apply the physically based scaling technique for estimating the soil water characteristic curve is a robust method in soil hydrologic studies.

(2) The basic properties of the dual-porosity soils used in the laboratory experiments were presented. The pore geometry of dual-porosity soils has been studied using

scanning electron microscopy and mercury intrusion porosimetry. The soil-water characteristic curves of dual-porosity soils were measured using a combination of methods to cover a wide range of suctions. The measured soil water characteristic curves for dual-porosity soils are bimodal and reflect two distinct pore size distributions associated with the microscopic and macroscopic portions of the total porosity of the specimens.

(3) A mathematical functions for both bimodal and mutimodal SWCCs have been proposed. The proposed equations are defined by parameters that have physical significances which can be related to the properties of the materials. Experimental datasets fitting and parametric analyses were used to illustrate the fitting capability of the proposed equations. The proposed approaches make the treatment of SWCC data easier and resulted in well agreement between measurement and simulation. These functions can potentially be used as effective tool for indentifying hydraulic porosities in the medium with structures.

(4) A physically based closed-form expression for the bimodal unsaturated hydraulic conductivity function was proposed for soils with bimodal pore size distribution. By assuming a lognormal pore size distribution for each pore domains and using weighting factors combined individual functions. The proposed equations are defined by parameters that have physical significances which can be related to the properties of the materials. Experimental data verification and parametric analyses were undertaken to demonstrate the fit and predicting capability of the proposed equations. The proposed BLN model improved capability of representations of the hydraulic curves to simulate water flow in structural soils. These functions can potentially be used as an effective tool for identifying hydraulic porosities in structural soils.

7.2 Future work

(1) Capillary rise of dual-porosity soils.

Experimental data on the capillary rise test for single-porosity soils have been reported, and many ideas have also been reported. However, a constitutive model

for predicting capillary rise height for dual-porosity soils has still not been established. A theoretical model for predicting capillary rise height for dual-porosity soils should be developed and calibrated with experimental data.

(2) Measurement of permeability for dual-porosity soils at low suctions.

The experimental data of permeability of dual-porosity soils at low suctions (around 1 kPa) are still rather limited. A steep slope is considered to be present on the permeability function in that zone for dual-porosity soils with high coarse fractions. Difficulties in measuring the permeability at low suctions include dealing with spatial variations of permeability, accurate controlling of the soil density, considering different sample preparation methods, and dealing with the suction difference along sample height. An accurate measurement of permeability at low suctions is of great value for understanding flow in porous media and is essential for an accurate seepage analysis.

(3) Evaluate performances of dual-porosity soils as soil amendments in drylands.

Raw diatomite and zeolite can be used as soil amendment to retain water and plant nutrients in root zone. The high porosity associated with the inner structure of these materials allows them to retain much water. In order to evaluate performances of dual-porosity soils as soil amendments, the field experiments will be conduct in drylands.

(4) Develop a program for fitting and estimating hydraulic properties of unsaturated soils.

The proposed models can potentially be used as an effective tool for identifying hydraulic properties in porous media. In order to make it more convenient to use, a program will be developed for fitting and estimating hydraulic properties of unsaturated soils.